UNIVERSIDADE ESTADUAL DE CAMPINAS

FACULDADE DE ENFERMAGEM

CARLOS JORGE POBLETE JARA

AVALIAÇÃO DO TRATAMENTO TÓPICO COM O COMPLEXO FIBRINOGÊNIO-FIBRONECTINA NO PROCESSO DE CICATRIZAÇÃO DE FERIDAS

CAMPINAS

2021

CARLOS JORGE POBLETE JARA

AVALIAÇÃO DO TRATAMENTO TÓPICO COM O COMPLEXO FIBRINOGÊNIO-FIBRONECTINA NO PROCESSO DE CICATRIZAÇÃO DE FERIDAS

Tese apresentada à Faculdade de Enfermagem da Universidade Estadual de Campinas como parte dos requisitos exigidos para a obtenção do título de Doutor em Ciências da Saúde na Área de Concentração: Cuidado e Inovação Tecnológica em Saúde e Enfermagem.

ORIENTADOR: PROF(a). DR(a). ELIANA PEREIRA DE ARAÚJO

ESTE EXEMPLAR CORRESPONDE À VERSÃO
FINAL DA TESE DEFENDIDA PELO
ALUNO CARLOS JORGE POBLETE JARA, E ORIENTADO PELA
PROF(a). DR(a). ELIANA PEREIRA DE ARAÚJO

CAMPINAS

2021

FICHA CATALOGRÁFICA

Ficha catalográfica
Universidade Estadual de Campinas
Biblioteca da Faculdade de Ciências Médicas
Maristella Soares dos Santos - CRB 8/8402

P75a

Poblete, Carlos, 1983-
Avaliação do tratamento tópico com o complexo fibrinogênio-fibronectina no processo de cicatrização de feridas / Carlos Jorge Poblete Jara. – Campinas, SP : [s.n.], 2021.

Orientador: Eliana Pereira de Araujo.
Tese (doutorado) – Universidade Estadual de Campinas, Faculdade de Enfermagem.

1. Fibrinogênio. 2. Cicatrização. 3. Receptor de fibronectina. 4. Enfermagem. I. Araujo, Eliana Pereira de, 1965-. II. Universidade Estadual de Campinas. Faculdade de Enfermagem. III. Título.

Informações para Biblioteca Digital

Título em outro idioma: Evaluation of topical treatment with the fibrinogen-fibronectin complex in the wound healing process
Palavras-chave em inglês:
Fibrinogen
Wound healing
Fibronectin receptor
Nursing
Área de concentração: Cuidado e Inovação Tecnológica em Saúde e Enfermagem
Titulação: Doutor em Ciências da Saúde
Banca examinadora:
Eliana Pereira de Araujo [Orientador]
Sylvia Stuchi Maria-Engler
Andréa Monte Alto Costa
Maria Helena de Melo Lima
Gabriela Freitas Pereira de Souza
Data de defesa: 26-05-2021
Programa de Pós-Graduação: Enfermagem

Identificação e informações acadêmicas do(a) aluno(a)
- ORCID do autor: https://orcid.org/0000-0001-5444-721X
- Curriculo Lattes do autor: http://lattes.cnpq.br/8247689654006061

BANCA EXAMINADORA DA DEFESA DE DOUTORADO

CARLOS JORGE POBLETE JARA

ORIENTADOR: PROFA. DRA. ELIANA PEREIRA DE ARAÚJO

MEMBROS:

1. PROFA. DRA. ELIANA PEREIRA DE ARAÚJO

2. PROFA. DRA. SYLVIA STUCHI MARIA-ENGLER

3. PROFA. DRA. ANDRÉA MONTE ALTO COSTA

4. PROFA. DRA. MARIA HELENA DE MELO LIMA

5. PROFA. DRA. GABRIELA FREITAS PEREIRA DE SOUZA

Programa de Pós-Graduação em Enfermagem da Faculdade de Enfermagem da Universidade Estadual de Campinas.

A ata de defesa com as respectivas assinaturas dos membros da banca examinadora encontra-se no Sistema de Fluxo de Dissertação/Tese e na Secretaria de Pós-graduação da Faculdade de Enfermagem.

DATA DA DEFESA: 26/05/2021

DEDICATÓRIA

Dedico nosso trabalho à minha mãe, que me ensinou preencher meu destino, com um sorriso no rosto.

AGRADECIMENTOS

Agradeço a Professora Eliana Pereira de Araújo, por ter estimulado e acompanhado minha transformação para me tornar um pesquisador, pela parceria, por ouvir, pelos conselhos, por estar aí, e pela amizade, muito obrigado.

Agradeço ao Jose Luís Saavedra por ter sido minha família no Brasil, e por adoçar meus dias com a sua paz, muito obrigado.

Agradeço a Bruno Souza e sua mãe Senhora Idione por ter cuidado de mim quando eu precisei, e por ter sido minha família no Brasil, muito obrigado.

Agradeço a Vanessa Bobbo, pela amizade e por ter sido minha família no Brasil, muito obrigado.

Agradeço ao Alex Ferrante, pelas comidas, carinho, e por ter sido minha família no Brasil, muito obrigado.

Agradeço a Professora Roberta Cunha por ter me escolhido no 2014, muito obrigado.

Agradeço a Paulina Bravo e Monica Valenzuela, por ter sido minha família no Chile, muito obrigado.

Agradeço a Valeria Povoa, Beatriz de Andrade, Natália Mendes, Rodrigo Carraro, Erika Anne, Joseane Morari, Gerson Ferraz e Marcio Cruz pelo apoio técnico. Agradeço ao Saulo Saad e Leticia Zanotto, que fizeram de burocracia administrativa, vários momentos agradáveis de diálogo. Agradeço a Senhora Cintia da FEnf e Senhora Carmen do OCRC, auxiliares de serviços que doaram gentilmente vários minutos de interessantes conversas, muito obrigado.

Agradeço ao Professor Lício Velloso, pelos 6 anos de formação em pesquisa, muito obrigado.

Agradeço ao David Sidarta, por ter me ensinado trabalhar com transcriptômica, muito obrigado.

Agradeço a Jaqueline Ramirez por ter me permitido lhe ajudar no seu trabalho, e ter permitido destinar horas ao meu lazer, muito obrigado.

Agradeço a Gladys Paredes pela amizade, muito obrigado.

Agradeço a Professora Inês Monteiro por me permitir imaginar futuros diferentes, muito obrigado.

Agradeço ao Professor Bill Velander, por ter me ajudado no projeto, muito obrigado.

Agradeço a Carina Sólon, por ter sido sempre gentil comigo, muito obrigado.

Agradeço a Luz Campos, trabalhadora social de Curico, agradeço a Maria Cecilia Carvacho, trabalhadora social da PUC Chile, Agradeço a Prof. Mirian Rubio, por destinado seu tempo em me apoiar, muito obrigado.

Agradeço a Thais Paulinho Prado pela parceria e amizade, muito obrigado.

Agradeço ao Jonathan Ferreira Campos pela amizade, muito obrigado.

Agradeço ao Bruno Mantoni pela amizade, muito obrigado.

Agradeço ao Patrick Turiano pela amizade, muito obrigado.

Agradeço ao Jaime Espinosa pela amizade, muito obrigado.

Agradeço a Alejandra Reyes Oyanadel pela amizade, muito obrigado.

Agradeço a Erika Torres por ter me apoiado quando eu precisei, muito obrigado.

Agradeço Prof. Pankaj Karande da Engenharia Química e Biológica do Rensselaer Polytechnic Institute que gentilmente forneceu a infraestrutura e apoio financeiro para financiar nossa pesquisa, muito obrigado.

Agradeço a República Federativa do Brasil, que gentilmente forneceu a infraestrutura, recursos humanos e apoio financeiro para que esta pesquisa tenha sido desenvolvida. Agradeço também a unidade Federativa, Estado de São Paulo, pelos recursos financeiros e infraestrutura na qual grande parte de esta pesquisa foi desenvolvida, muito obrigado.

Agradeço a Organização dos Estados Americanos, por ter fornecido a oportunidade, o apoio financeiro inicial e ter acreditado no meu projeto e desenvolvimento profissional, muito obrigado.

Agradeço aos desenvolvedores da plataforma *App Inventor* Hal Abelson e Mark Friedman do Instituto de Tecnologia de Massachusetts, que permitiram a criação do aplicativo Labinsane, muito obrigado.

Esta pesquisa especificamente, foi apoiada pela Universidade de Nebraska, Lincoln, Biomedical Seed Grant; Investigação Médica do Exército dos EUA (W81XWH-05- 1-0527, Velander); Departamento de Defesa, EUA (W81XWH-BAA-11-1 ERMS No.10091006, Carlson e Velander). Imagens de microscópio confocal foram feitas no Centro de Pesquisa de Microscopia de Morrison na Universidade de Nebraska, Lincoln e O Laboratório Central de Tecnologias de Alto Desempenho em Ciências da Vida (LaCTAD). Também apoio da manutenção financeira do pesquisador principal da Coordenação de Aperfeiçoamento de Pessoal de Nível Superior (CAPES Código de Financiamento 001), como também aportes da Fundação de Pesquisa de São Paulo (FAPESP #2013/08293-7 e #2013/07607-8.) – através do projeto CEPID-OCRC - Centro de Comorbidades de Obesidade. A Faculdade de Enfermagem da Unicamp junto com todos os discentes, docentes e funcionários que me acompanharam neste muito grato período, muito obrigado.

Finalmente, agradeço à Rosa Jara, minha querida mãe, por me ensinar a ser tudo aquilo que hoje eu conheço como eu, por me estimular para ser eu mesmo, sem cobranças e com um sorriso no meu rosto, muito obrigado. Agradezco a mi mamá, Rosa Jara, por enseñarme a ser yo mismo y ser todo aquello que hoy conozco como yo. Agradezco a mi mamá también, por haberme permitido ser yo, sin cobranzas, y con una sonrisa en mi rostro, muchas gracias, mamá

RESUMO

A cicatrização é um processo complexo no qual orquestram-se vários tipos celulares assim como proteínas estruturais. O Fibrinogênio (F1), proteína principal da matriz provisória na ferida, é responsável por ocluir a área lesionada, dando início ao processo cicatricial. A Fibronectina (FN) é uma proteína que se liga ao F1 e assim, estabiliza-se a matriz na área da ferida. Uma vez estabilizada, ocorrem processos de migração celular ao leito da lesão como também ligação do F1 ao colágeno da pele ilesa circundante. No entanto, a maioria dos estudos descrevem que a ligação do F1 a FN acontece apenas em situações patológicas como infecções ou doenças inflamatórias, embora, um estudo recente descreveu a purificação do complexo de F1 ligado FN a partir de plasma humano de indivíduos saudáveis.

Este trabalho trata-se de estudo *in vitro* e *in vivo*, no qual foi avaliada a velocidade de cicatrização, morfologia da ferida, modulação de genes envolvidos no processo de cicatrização, proliferação e migração celular em animais, tratados diariamente por via tópica com o Fibrinogenio (F1) e Fibronectina (FN). Também avaliamos o uso das matrizes de F1 e FN em modelos *in vitro* de cicatrização. As feridas foram foto documentadas sistematicamente e as amostras foram extraídas nos dias 2, 6 e 11 após a excisão. Estas amostras foram analisadas por meio de PCR em tempo real, imunofluorescência, microscopia óptica e de luz polarizada. Nossos resultados mostraram que o complexo γγ′F1: pFN acelera significativamente o proceso cicatricial, formação de tecido de granulação, e estimula a reepitelização em feridas na pele de camundongos. Além disso, o uso da mistura de F1 e FN em feridas feitas em pele humana equivalente também estimulou o proceso cicatrizial. Para análise estatística, os grupos foram comparados utilizando test t student para dois grupos e 2-way ANOVA com o teste Bonferroni para três grupos ou mais. O nível de significância adotado foi de $p<0,05$. Os dados foram expressos como médias, erro-padrão, sendo indicado o número de experimentos independentes.

Linha de Pesquisa: Tecnologia e Inovação no Cuidado de Enfermagem e Saúde.

Palavras-chave: Fibrinogênio; Cicatrização; Receptor de Fibronectina; Enfermagem.

ABSTRACT

The healing process is a complex multi-steps process in which several cell types and structural proteins are orchestrated. Fibrinogen (F1), the main protein of the provisional matrix in the wound, is responsible for occluding the injured area, initiating the healing process. Fibronectin (FN) is a protein that binds to F1 and thus stabilizes the matrix in the injured area. Once stabilized, macrophage aggregation processes, cell migration to the wound bed, as well as binding of F1 to the collagen of the surrounding unhealthy skin occur. However, most studies describe that F1 binding to FN occurs only in pathological situations such as infections or inflammatory diseases. A recent study described the purification of the F1-bound FN complex from human plasma from healthy individuals.

This work is an experimental study in animals and in vitro, in which the healing speed, wound morphology, modulation of genes involved in the healing process, proliferation and cell migration in animals with acute wound model, will be evaluated by a daily topically application of Fibrin and Fibrinogen. We will also evaluate the use of F1 and FN matrices for in vitro healing models. The wounds will be systematically documented, and the samples will be extracted on days 2, 6 and 11 after excision. Our results showed that the complex γγ′F1: pFN significantly accelerates the healing process, formation of granulation tissue, how to potentiate reepithelization in mice skin wounds and in human equivalent 3D skin wounds. These samples will be analyzed using real-time PCR, optical microscopy, and polarized light. For statistical analysis, the groups were compared using test t student when comparing two groups and 2-way ANOVA with the Bonferroni test when comparing three groups or more. The level of significance adopted will be $p < 0.05$. The data will be expressed as means, standard error, indicating the number of independent experiments.

Keywords: Fibrinogen; Wound Healing; Nursing; Receptors, Fibronectin

LISTA DE ILUSTRAÇÕES

LISTA DE ABREVIATURAS E SIGLAS

AKT	Proteína Quinase B
CTL	Grupo controle, não tratado com o complexo FF
DM	Diabetes Mellitus
DM2	Diabetes Mellitus tipo 2
MEC	Matriz Extracelular
ERK	Quinases Reguladoras da Sinalização Extracelular
EPH	Pele Humana Equivalente
FN	Fibronectina
F1	Fibrinogênio
FLRT2	Proteína transmembrana 2 rica em Fibronectina e Leucina
FGF-2	Fator de Crescimento de Fibroblasto 2
IGF-1	Fator de Crescimento Semelhante à Insulina 1
IL-1	Interleucina 1
IL-1β	Interleucina 1 Beta
IL-6	Interleucina 6
IL-10	Interleucina 10
Itga5	Integrina alfa 5
KDa	Kilo Dalton
MCP1	Proteína Quimiotática de monócitos 1
MIT	Instituto de Tecnologia de Massachusetts
MMP-1	Metaloproteinases 1
MMP-2	Metaloproteinases 2
MMP-9	Metaloproteinases 9

PCR	Reação em Cadeia da Polimerase
pFN	Fibronectina do plasma
pF1	Fibrinogênio do plasma
PDGF	Fator de Crescimento Derivado de Plaquetas
PKB	Proteína Quinase B
Procr	Receptor de Proteína C
Plaur	Receptor de uroquinase
RNAm	Mensageiro do Ácido Ribonucleico
RNA	Ácido Ribonucléico
SDF-1α	Fator 1 Alfa Derivado de Célula Estromal
TIMP-2	Inibidores de Metaloproteinase 2
TNFα	Fator de Necrose Tumoral Alfa
TGF-α	Fator de Crescimento Transformador Alfa
TGF-β	Fator de Crescimento Transformador Beta
HUVECs	Células endoteliais da veia umbilical humana
VEGF	Fator de Crescimento Endotelial Vascular
γγ'F1:pFN	Complexo Gama/gama prima Fibrinogênio do plasma com Fibronectina do plasma
pF1:pFN	Mistura de Fibrinogênio do plasma com Fibronectina do plasma

SUMÁRIO

INTRODUÇÃO

O processo de cicatrização é caracterizado pela formação de novo tecido na área lesionada. Na pele, o reparo tem como objetivo iniciar a estabilização da função de barreira através da formação da Matriz Extracelular (MEC) provisória a qual é substituida finalmente por tecido fibrótico ou cicatricial (1). Este processo pode ser dividido didaticamente em quatro fases seriadas, embora ocorram em paralelo: inicialmente a homeostase, seguida da resposta inflamatória, proliferação-migração celular e finalmente a remodelação do novo tecido (2-5).

Em feridas cutâneas, imediatamente após a lesão, inicia-se o processo de hemostasia, com o objetivo de interromper a perda de fluidos (6). O Fibrinogênio ou Fator de coagulação I (F1) é o componente principal do sistema hemostático (7). O fibrinogênio e a fibronectina (FN) (10:1 Molar no sangue) são polimerizados pela trombina e estabilizados pelo fator XIII (FXIII) para formar o tampão de fibrina estabilizado (8-10). As plaquetas e os leucócitos polimorfonucleares aglomeram-se no coágulo para logo secretar fatores que amplificam a agregação de outras plaquetas, processo conhecido como ativação plaquetária (11). As plaquetas aderidas ao coágulo, proporcionam um sistema de armazenamento e transporte de fibrinogênio, como também de fatores inflamatórios e de crescimento, entre eles o Fator de Crescimento Derivado de Plaquetas (PDGF), Fator de Crescimento Transformador (TGF) e o Fator de Crescimento Endotelial Vascular (VEGF) (12, 13). A estabilização da matriz de fibrina é secundária à formação do complexo fibrina-fibronectina (F1:FN) (14). Macrófagos circulantes ligam-se à matriz de F1:FN, liberando inicialmente, citocinas inflamatórias (15, 16). Estas citocinas, mais peptídeos produto da clivagem do fibrinogênio solúvel em insolúvel, como também a

Proteína Quimioatratora de Monócitos-1 (MCP-1), atraem outros monócitos e macrófagos, marcando a seguinte etapa, a fase inflamatória (3, 17).

Na fase inflamatória, logo após a formação do coágulo de fibrina, leucócitos no local da ferida eliminam bactérias por meio da fagocitose, e monócitos atraídos na lesão, diferenciam-se em macrófagos ativados os quais, liberam citocinas inflamatórias como TNF-α IL1-β, IL-6, Procr e Plaur (18-20). Além disso, leucócitos no local da ferida junto as plaquetas, secretam fatores de crescimento que iniciam a formação do tecido de granulação (3). Entre os fatores de crescimento secretados nessa fase estão o TGF- α/β, VEGF e o PDGF, que por um lado participam da formação da nova matriz extracelular e angiogênese, como também estimulam a ativação de fibroblastos das bordas da lesão. Estes últimos são capazes de secretar Interleucina-1 (IL-1) e Fator de Crescimento Semelhante à Insulina (IGF-I) que em conjunto com macrófagos, darão início a fase proliferativa (3).

Na fase proliferativa, novos macrófagos são ativados e aumenta a secreção de TGF-β, MCP-1, PDGF, IGF-1 e o Fator de Crescimento de Fibroblastos-2 (FGF-2). A matriz de F1:FN começa a ser substituída por um tecido mais resistente e estável (21). Macrófagos transdiferenciados em fibroblastos representam a vasta maioria das células produtoras de colágeno (20). Progressivamente, a matriz de F1:FN e substituída pelo colágeno, sendo degradada pela Plasmina ativa, protease específica contra a fibrina, (17, 22), dando início a fase de remodelação, etapa final do processo de reparo tecidual. É nesse período que a cicatriz adquire sua máxima resistência, assim como uma intensa deposição e concentração de colágeno. Inicialmente o colágeno tipo III é depositado, o qual forma uma estrutura flexível para logo depois, ser substituído parcialmente pelo

colágeno do tipo I com fibras dispostas de forma organizada e reticuladas, com menor porosidade e menor quantidade de vasos sanguíneos, dando o aspecto característico da cicatriz (21).

Fibrinogênio e Fibronectina (F1:FN)

O Fibrinogênio é uma glicoproteína circulante de 340 kDa, sintetizada principalmente por hepatócitos e constituído por duas moléculas simétricas, cada uma composta por um conjunto de três cadeias polipeptídicas diferentes denominadas alfa (α), beta (β) e gama (γ). Esta molécula é altamente heterogênea devido ao *splicing* alternativo, à modificação pós-transdução extensiva e à degradação proteolítica (9). O Fibrinogênio apresenta duas classes de cadeias gama: 1) *gama* e 2) *gama'* (gama prima), que diferem uma da outra por às suas sequências *COOH* terminais. Quando o Fibrinogênio polimerizado pela trombina e estabilizado na presença do Fator de Coagulação XIII ativado (FXIIIa) e o Ca2 +, forma-se dois tipos de dímero gama (Figura 1): 1) *gama - gama* e 2) *gama - gama '* (23). Em torno de 10% da fibrina possui uma subpopulação γ'. A ligação da trombina ao Fibrinogênio ocorre em dois locais, sendo um deles na cadeia gama prima (24). O Fibrinogênio heterodimérico (γ / γ') apresenta várias atribuições funcionais únicas decorrentes dos seus 25 aminoácidos adicionais no terminal carboxílico da cadeia gama (25). Esses 25 novos aminoácidos do fibrinogênio *gama'* apresentam lugares de ligação extras tanto para a trombina quanto para o fator XIII (24).

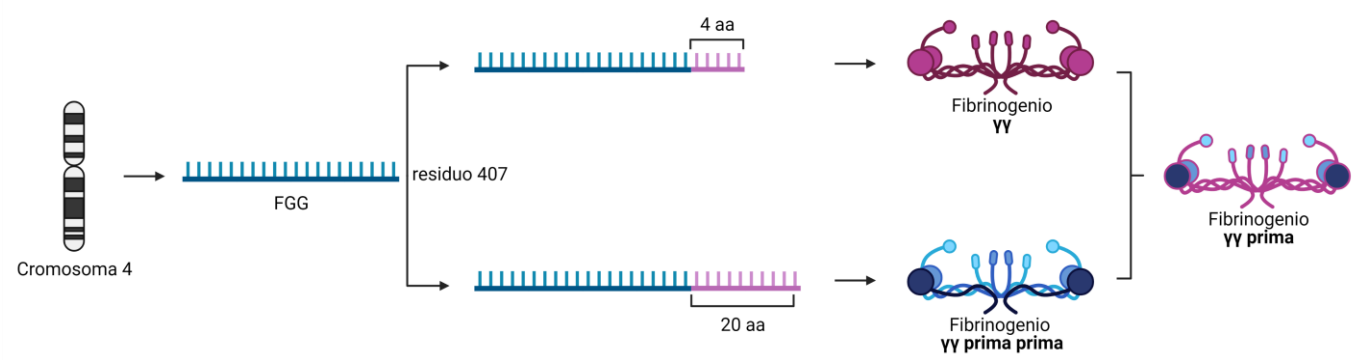

Figura 1: diferentes variantes do fibrinogênio à modificação pós-transdução. Figura construída pelo autor.

Uma das proteínas capaz de interagir com o Fibrinogênio (F1) é a Fibronectina (FN) (22). No humano, há duas formas de FN, a Fibronectina Plasmática (pFN) sintetizada por hepatócitos e a Fibronectina Celular (cFN) sintetizada por fibroblastos, células endoteliais, macrófagos e algumas células epiteliais (26).

A ligação da FN ao F1 é chamada de ligação de Reboque ou *Passo a Passo*. No primeiro passo acontece a interação não covalente na qual a FN liga-se de forma reversível ao F1. No segundo, o FXIIIa estabiliza a interação não covalente mediando a reticulação covalente, também conhecida como ligação cruzada (27, 28). De fato, a deficiência de FXIII foi extensivamente estudada usando camundongos *knockout* os que apresentam cicatrização de feridas prejudicada (29).

Estudos da década dos 80 forneceram importantes informações sobre a função e estrutura da FN. Grinnell e Feld (1981), em um estudo *in vitro*, descobriram que a FN está distribuída ao longo de filamentos de fibrina dos coágulos de sangue

(30). Um ano após, o mesmo grupo de pesquisadores identificou que a FN também faz parte do coágulo formado durante o processo de cicatrização (31). Eles concluíram que os coágulos sanguíneos formados são um complexo de fibrina-fibronectina e que há uma camada contínua de FN sobre os coágulos responsáveis por proporcionar a estabilidade mecânica necessária para o início da cicatrização (30). Estudos posteriores demonstraram que a FN ligada ao F1 age como substrato para migração celular pois esse complexo adota uma conformação desdobrada que resulta na exposição dos domínios de ligação para as células (integrinas). As integrinas são uma família de receptores de superfície celular heterodiméricos, capazes de ligar-se à F1 e FN e interagir com esses domínios de ligação. Especificamente, a integrina alfa 5 (ou Itga5, α5β1, ou receptor alfa de fibronectina) é altamente e somente expressa na papila migratória de células epiteliais em contato direto com a matriz F1:FN da ferida (19). Demostrou-se que a interação da integrina Itga5 da membrana celular dos queratinócitos com a fibronectina contribui para a proliferação, além de facilitar a adesão e a migração através da matriz F1:FN destas células (32). Além disso, a adesão de fibroblastos à matriz F1:FN durante a cicatrização de feridas também é mediada via integrina Itga5 (3).

No entanto, estudos têm demonstrado que o complexo F1:FN existe apenas no plasma de pacientes com doenças inflamatórias, infecciosas como no plasma de pacientes com artrite reumatoide (33-37). Devido a este fato, nosso parceiro da Universidade de Nebraska nos Estados Unidos, tem trabalhado com o objetivo de purificar esse complexo, devido às perspectivas do seu uso para tratamento de feridas.

Ismail e colaboradores (38), isolaram o complexo F1:FN a partir de plasma humano de indivíduos saudáveis utilizando uma sequência de

crioprecipitação com sulfato de amônio e cromatografia em gel. Em uma segunda cromatografia com gelatina, o grupo demonstrou que o componente F1 plasmático, o qual liga-se à FN plasmático, é composto exclusivamente pelo heterodímero γγ'. Os autores identificaram também que o complexo Fibrinogênio plasmático γγ' (γγ'F1) associado a Fibronectina (pFN) do plasma (γγ'F1:pFN) purificado é termicamente estável quando comparado com as preparações de plasma que não contêm FN, como também é estável em pH fisiológico. Além disso, este grupo demonstrou *in vitro* que na matriz formada a partir do complexo γγ'F1:pFN houve aumento significativo da força de resistência do coágulo e do tempo de coagulação quando comparado com outras combinações (F1 e FN), ou de F1 e FN isoladamente (38).

Feridas e complicações relacionadas

Em algumas situações de doenças o processo de reparo tecidual torna-se prejudicado, como por exemplo, na presença de biofilmes (39), úlceras vasculares (40) e feridas do pé diabético (41). Nesses casos ocorre inflamação prolongada (42), pobre angiogênese e uma menor deposição de colágeno na MEC (43). Além disso, em Diabetes Mellitus (DM), ocorre diminuição significativa de alguns dos importantes fatores de crescimento como o IGF-1, TGF-β e VEGF como também aumento de enzimas capazes de destruir a MEC como as Metaloproteinases 1 e 2 (MMP-1 e MMP-2) e a redução dos Inibidores de Metaloproteinase-2 (TIMP-2) que são inibidores endógenos dessas enzimas que degradam MEC (44). Especificamente, as feridas crônicas contêm proteases que digerem a fibronectina e interferem na polimerização do Fibrinogenio (45-50).

Uma das principais limitações na cicatrização de feridas em pacientes com feridas crônicas é a insuficiência circulatória devida, entre outros, à rigidez dos

microvasos. Nesse sentido, pesquisas anteriores têm desenvolvido matrizes de fibrina com alta capacidade de estimular o crescimento de células endoteliais *in vitro* e *in vivo* (10) e assim, estimular o crescimento de vasos no contexto de feridas crônicas. Matrices formadas exclusivamente por Fibrinogenio gama prima, permitiram que células endoteliais criassem estruturas estáveis dentro da matriz (51). Por outro lado, pacientes com feridas crônicas apresentam uma diminuição da quantidade assim como da atividade da Proteina quinase B (AKT) e Quinases reguladas por sinal extracelular (ERK) fosforiladas, proteínas chaves da sinalização de insulina (52). A FN apresenta um domínio de adesão celular que estimula a ativação de ERK1/2 (53). A FN interage com outras proteínas da matriz extracelular e através de integrinas de superfície celular (54). Além disso, a diminuição da Akt1 em fibroblastos resulta numa adesão e migração à fibronectina prejudicadas, sendo a FN um dos principais ligantes da integrina Itga5 (55).

Modelo de feridas *in vitro* em Pele humana equivalente

O uso de animais experimentais em testes de toxicidade e irritabilidade, tem mostrado alta variabilidade nos seus resultados tanto dentro quando entre laboratórios (56). Por esse motivo, desde a década dos 70, foram desenvolvidos métodos alternativos ao uso animal que conseguiram diminuir a variabilidade dos resultados e assegurar uma determinada reprodutibilidade (57). Estes modelos *in vitro* de pele humana equivalente têm sido validados como testes alternativos de irritação cutânea (57-60), gerando diretrizes mundiais descritas pela Organização Internacional de Normalização (ISO 10993-23:2021). Porém, até hoje, não há um modelo *in vitro* que recapitule ou esteja validado para reproduzir todas ou parte das fases do processo de cicatrização animal. Nesse sentido, grandes avanços têm sido realizados para mimetizar em parte cada uma das fases do processo de reparo

cutânea animal, desde modelos *in vitro* em duas dimensões (61, 62) até o uso de Pele humana equivalente em três dimensões. Até hoje, os modelos *in vitro* disponíveis têm demostrado ser capazes de reproduzir algumas das características do processo de cicatrização. Embora, em todos estes modelos, a imitação da matriz inicial de Fibrinogênio e Fibronectina fisiológica foi ignorada (63-70).

HIPÓTESE

Nossa hipótese se baseia em que células epidérmicas e dérmicas identificam a matriz de Fibrina e Fibronectina como um estímulo vectorial concêntrico de proliferação e de migração. Este biomaterial pode facilitar o processo de cicatrização fisiológico, por ser uma cobertura instantânea, com baixo risco de rejeição, e baixos efeitos colaterais, por ser um composto formado por substâncias endógenas. Este componente transitório acelular, comporta-se como uma matriz natural, biocompatível e reabsorvível que ajudará na oclusão instantânea da ferida, permitirá uma rápida migração de queratinócitos, como também estimulará a proliferação celular em modelos *in vivo* e *in vitro* de cicatrização de pele.

JUSTIFICATIVA

Trocas frequentes de coberturas, que utilizam materiais não reabsorvíveis, muitas vezes traumatiza e afetam negativamente o processo cicatricial. Desse modo, nosso trabalho se justificou em utilizar coberturas advindas de materiais bioabsorvíveis (71), que diminuam a iatrogenia secundária ao ato de troca do curativo. O nosso trabalho se justificou também pela importância de desenvolvermos substâncias biocompatíveis, não imunogênicas, reabsorvíveis e que possam dar suporte estrutural ao crescimento celular (72). Nesse sentido, a

compreensão aprofundada do efeito do complexo γγ'F1:pFN e a mistura de F1 com FN no processo de cicatrização em modelos *in vivo* e *in vitro* é importante para dar sustentação às futuras investigações da utilização deste complexo em seres humanos. Nesse sentido, este trabalho se justifica também na importância da enfermagem como ciência, no desenvolvimento de novos conhecimento e de novas tecnologias para finalmente estas, consigam ser transladadas ao trabalho de enfermeiros clínicos.

OBJETIVOS

Geral

Avaliar os efeitos do uso tópico do Complexo yy'F1:pFN e mistura F1 e FN no processo de cicatrização de feridas em camundongos e pele humana equivalente.

Específicos

Determinar o tempo de cicatrização e aspectos morfológicos da ferida;

Avaliar crescimento de células de resposta imunológicas e células epiteliais;

Avaliar a expressão gênica e protêica de citocinas, quimosinas, fosfatases e fatores de crescimento envolvidos com o processo cicatricial como TNF-α, IL-6, IL-1β, IL-10, TGF, IGF, VEGF, FGF, MCP-1, Plaur, Procr, Itga5, FLRT2 e MMP9;

MÉTODOS

Trata-se de um estudo experimental, no qual foi investigada a evolução de feridas cutâneas provocadas na região dorsal de camundongos (73) e pele humana equivalente.

O complexo fibrinogênio-fibronectina plasmático (γγ'F1:pFN), VEGF, FII como o rFXIIIa foi gentilmente cedido pelo Prof. Dr. William H. Vellander da Universidade de Nebraska (EUA). Este foi derivado de 1000 unidades de plasma sanguíneo humano testado e avaliado livre de patógenos específicos, doado de soldados voluntários saudáveis aprovado pela Forças Armadas dos Estados Unidos através do Departamento de Defesa dos Estados Unidos de América.

DESENHO EXPERIMENTAL

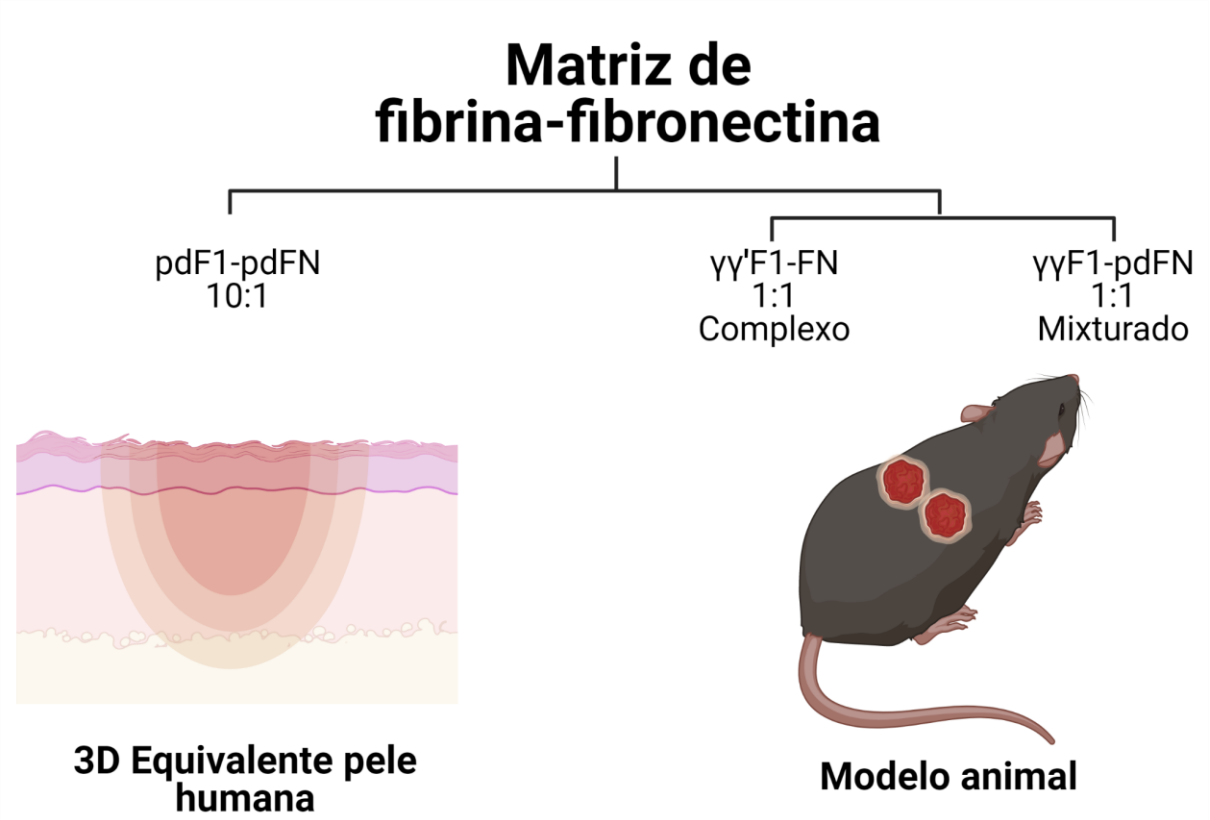

Figura 2: desenho experimental do uso da matriz de fibrina-fibronectina no modelo de pele humana equivalente e no modelo animal. Figura construída pelo autor.

Foram utilizados Camundongos Isogênicos *Mus musculus* C57BL/6J (CEUA aprovado, número 4467-1/2017, Anexo 1) machos com 08 semanas de idade recebidos com quatro semanas de vida, provenientes do Centro de Bioterismo da UNICAMP (CEMIB) e mantidos em caixas individuais desde 1 semana antes do início do experimento. Os camundongos foram alimentados e hidratados com ração padrão para roedores (Purina) e água *"ad libitum"* sob condição padronizada de iluminação (ciclo de 12 horas claro/escuro) e temperatura de 22 ± 2ºC.

Os animais foram separados aleatoriamente em 03 grupos:

01- Grupo que recebeu o complexo γγ'F1:pFN (*Complexo* para abreviar);

02- Grupo que recebeu a mistura de pF1 e pFN (*Mistura* para abreviar);

03- Grupo que recebeu soro ringer (*Controle* ou CTL);

As amostras de pele humana equivalente 3D foram separadas aleatoriamente em 03 grupos:

01- Grupo pele 3D que recebeu a mistura de pF1 e pFN com feridas de 7 milímetros;

02- Grupo pele 3D que recebeu a mistura de pF1 e pFN com feridas de 4 milímetros;

03- Grupo de animais que recebeu soro ringer (Controle ou CTL);

Realização das Feridas no modelo animal

Com 8 semanas de idade, as feridas foram confeccionadas com um perfurador de biopsia de 6 mm de diâmetro em camundongos anestesiados, excisando a pele e o *panniculus carnosus* subjacente, seguindo o Modelo de Feridas Excicionais como descrito na literatura (74, 75). Cada animal foi anestesiado com cloridrato de ketamina (100 mg/kg) e cloridrato de xylazina (10 mg/kg) intraperitoneal usando o aplicativo para plataforma Android, *Labinsane* (2017), desenvolvido para este projeto, para este propósito. Este aplicativo calcula uma mistura mestre de anestésico baseado no peso total de todos os animais, para depois, identificar os microlitros individuais para cada animal dependendo do peso/massa de este (76) disponível no Google Play Store (Dados não publicados, manuscrito em revisão em Frontier Veterinary Surgery and Anesthesiology). 10-15 minutos depois de conferida a perda do reflexo córneo e pedioso, foi efetuada a tricotomia e depilação dorsal,

para o dia seguinte, a excisão da pele. As feridas foram cobertas e a cicatrização ocorreu por segunda intenção (74). Os animais foram tratados com Tramadol 20 mg/kg administrada por via intraperitoneal 15-20 min após o início da cirurgia e continuaram, duas vezes por dia, durante 48 h como analgesia (77) usando o aplicativo *Labinsane* para o cálculo analgésico individual.

Realização das Feridas no modelo de Pele humana equivalente 3D

As *feridas* foram confeccionadas com perfuradores de biopsia de 7mm e 4mm de diâmetro no centro de cada Equivalente de Pele Humana (EPH) dia 11 após da sua criação. Cada EPH foi transladado para uma placa de Petri seca após o tratamento com 10 ml de inibidor de tripsina: HEPES (1:1) por 1 min para remover restos de meio de cultura. Realizamos o ferimento com um rápido e único movimento perpendicular, para depois realizar um movimento rotatório e assim liberar o tecido lesionado do EPH. A ferida no centro do EPH foi imediatamente preenchida com a mistura de F1-FN e trombina e transladada na incubadora 37 °C, 5% CO2 para sua polimerização.

Tratamento da ferida

As feridas dos animais foram tratadas nos dias 0, 2, 4, 6 e 9 após sua excisão e supervisadas até a cicatrização completa. As feridas nas peles humanas reconstituídas foram tratadas uma única vez no dia 0, imediatamente depois da confecção da ferida.

Avaliação macroscópica da ferida

O processo de cicatrização foi avaliado através de fotografias realizadas com câmera digital Nikon D610® (Japão). As fotografias foram feitas pelo mesmo avaliador, cada dois dias até o fechamento completo utilizando um tripé apropriado.

Para capturar as imagens, cada animal foi anestesiado com cloridrato de ketamina (70 mg/kg) e cloridrato de xylazina (7 mg/kg) intraperitoneal usando o aplicativo para plataforma Android *Labinsane*. As imagens foram digitalizadas e a área das feridas, mensurada por meio da utilização do software ImageJ® (National Institutes of Health, Bethesda, MD). O fechamento da ferida foi expresso em porcentagem (%) em relação à área inicial.

Coleta dos tecidos

As amostras dos tecidos foram coletadas nos dias 2, 6 e 11 dias após a excisão no modelo animal e no dia 10 no modelo *in vitro*. As amostras foram fixadas com 4% PFA (pH 7,5; corrigido com NaOH), e incubadas a 4°C durante a noite (pele animal) e 15 minutos 4°C pele in vitro. O PFA foi descartado das amostras, seguido de três lavagens de 15 min cada com PBS 1x.

Teste de adesão 2D em cultura de células

Fibroblastos de prepúcio humano foram cultivados em DMEM com 10% FBS (78, 79). O uso de fibroblastos primários de doadores anônimos com consentimento informado, aprovado pelo *Institutional Review Board* no Centro Médico da Universidade de Nebraska e pelo Comitê de Pesquisa e Desenvolvimento do Centro Médico Omaha, EUA. Foram usadas células nas passagens 4 a 6. As células endoteliais da veia umbilical humana (HUVECs) foram adquiridas da Bioscience Lonza e cultivados no Meio de crescimento de células endoteliais-2 (EGM2). Foram plaqueadas $1x10^4$ em 200 µl de meio em placas de 96 poços. As células aderidas foram documentadas com microscópio de contraste de fases. As células foram fixadas com PFA 4% e coradas com DAPI. Os núcleos foram documentados com microscópio de fluorescência.

Cultura de células 3D dentro das matrizes de fibrina.

Foram preparados 100 µl de matriz de fibrina com $2x10^4$ células em poços individuais de uma placa de formato de 96 poços. 200 µl de meio foram adicionados em cada poço. A morfologia foi registrada por microscopia de contraste de fase. A viabilidade das células dentro do gel foi determinada pelo kit de análise de células *Live/Dead* (Invitrogen) de acordo com as instruções do fabricante.

Microscopia Óptica

Após dissecção, os tecidos de pele fixados por imersão em paraformaldeído foram processados com álcool em concentrações crescentes (70%, 80%, 95% e 100%), xilol e parafina, incluídos em blocos de parafina, seccionados em cortes de 5 μm com o auxílio de micrótomo e fixados em lâminas de microscopia previamente tratadas com polilisina. Para a avaliação da morfologia celular na cicatrização os cortes foram corados com a técnica de hematoxilina e eosina. Os cortes foram incubados 30 segundos com hematoxilina, passados em água destilada e incubados por mais 30 segundos com eosina, seguidos de nova passagem em água destilada e desidratação. As lâminas foram montadas com Entellan® e a seguir analisadas e a imagem digital captada em microscopia óptica.

Imuno-histoquímica

Após fixação com formaldeído 4% durante o período da noite e crio proteção com sacarose 40%, cortes de 30 μ foram realizados usando o criostato CM3050S Leica (Leica Mycrosystems), secados em 24 horas em temperatura ambiente. Os tecidos foram lavados três vezes em PBS durante 3 min e incubados em temperatura ambiente 2 horas com solução bloqueio (5% de BSA, Tween 20 0.5% em PBS 1x). Foram utilizados os anticorpos primários específicos para marcadores de queratinócitos (K14, Abcam, ab7800, diluição 1:200) e Fibronectina (ab23750 diluição 1:1000), Fibrinogênio (ab27913 diluição 1:1000).

Extração de RNA

As amostras foram homogeneizadas em reagente de TRIzol® (InVitrogen, São Paulo, Brasil) por 30 s usando um homogeneizador de tecidos (Polytron-Agrgregate, Kinematica, Littau/Luzern, Switzerland) na velocidade máxima. Em seguida foram centrifugadas a 6.000 g, e o conteúdo total de RNA foi isolado de acordo com as instruções do fabricante e quantificado por espectrofotometria. A integridade do RNA foi verificada por eletroforese em gel de agarose. A síntese de cDNA foi realizada com 2μg do total de RNA usando o Hight-Capacity cDNA Reverse Transcription Kit (Applied Biosystems).

PCR em tempo real

A expressão gênica foi analisada através de PCR em Tempo Real usando o sistema gênico (SABioscience). Foram usados os oligonucleotídeos gene-específicos sintetizadas pelo fabricante (SABiosciences). Os dados foram analisados usando o sistema PCR Data Analysis Software (Excel & Web based) (SABiosciences). Alíquotas de 5,0 ng de RNA foram submetidas à transcrição reversa utilizando-se primers hexaméricos randômicos e Superscrit Maloney MLV transcriptase reversa. As reações de PCR em tempo real foram realizadas utilizando-se o sistema TaqManTM (Applied Biosystems), que é constituído por um par de primers e uma sonda marcada com um fluoróforo. O gene GAPDH (TaqManTM - Applied Biosystems) foi escolhido como controle endógeno da reação, o qual serve para normalizar a expressão do gene de interesse nas diferentes amostras. Após o cálculo das eficiências de amplificação do gene de interesse e do controle endógeno, foi construído um gráfico de dispersão, o qual tem por finalidade definir qual é a amplitude de concentrações para as quais o sistema é eficiente. Para a quantificação relativa do gene em estudo, as reações de PCR em tempo real

foram realizadas em duplicata a partir de: 6,25µL de TaqMan Universal PCR Master Mix 2x, 0,625µL da solução de primers e sonda, 1,625µL de água e 4,0µL de cDNA, sendo que no controle negativo, foi adicionado 4,0 µL de água ao invés do cDNA. As condições de ciclagem foram: 50º C por 2 minutos, 95º C por 10 minutos e 40 ciclos de 95º C por 15 segundos e 60º C por 1 minuto. Primers para genes específicos foram adquiridos de Applied Biosystems e IDT DNA Technology contra TGF-1β (Mm.PT.58.43.479940), TNF-α (Mm00443258_m1), IL-6 (Mm00446190_m1), VEGF-α (Mm.PT.58.14200306), FGF-1 (Mm.PT.56a.41158563), SOX-2 (Mm.PT.58.12958650.g), IGF-1 (Mm.PT.58.5811533), IL-1β n(Mm00434228_m1), MCP-1 (Mm99999056_m1), IL-10 (Mm01288386_m1), SDF-1 (Mm00445553_m1), itga (NM_010577.3), Plaur (ENSG00000011422), MMP9 (ENSG00000100985), Procr (ENSG00000101000) FLRT2 (ENSG00000185070) e GAPDH (4352339E). Os valores da expressão gênica relativa foram obtidos pela análise dos resultados no programa 7500 System SDS Software (Applied Biosystems).

Fator Recombinante XIII.

O Fator XIII recombinante (rFXIII) foi produzido pela equipe do Prof. William H. Velander, de acordo com os métodos descritos por Park (80). Resumidamente, o rFXIII foi purificado a partir de lisados celulares utilizando Ni-IMAC da *GE Healthcare*. A atividade foi determinada usando o kit *Pefa* (Pentapharm, Norwalk, CT). A atividade específica final das preparações de pureza foi > 95% com meia 59 ± 19 unidades/ mg.

Preparação de fibrinogênio e fibronectina

As unidades de plasma humano armazenaram-se em -80°C para depois ser descongelada a 4°C. O plasma foi centrifugado a 4000 rpm durante 20 min. O sobrenadante foi re-congelado e armazenado para subsequente purificação de fibrinogênio e fibronectina e outras proteínas derivadas do plasma. O crioprecipitado foi suspenso em citrato de sódio 45 mM, ácido 6-aminocapróico 100 mM, pH 7,0 a 37°C. Depois a solução foi centrifugada durante 25 minutos, 4000 rpm. O sedimento foi descartado e o sobrenadante teve inativação viral com detergente solvente por adição de 0,15% de Tri(n-butyl) fosfato, 0,5% de Triton 100x à temperatura ambiente e agitado durante 60 min. O sobrenadante foi tratado com o solvente-detergente ajustado a 1M de sulfato de amónio. A amostra foi agitada à temperatura ambiente durante 30 min, e em seguida centrifugadas a 2000 rpm durante 15 min a temperatura ambiente. O pellet foi re-suspenso em citrato de sódio 20 mM e NaCl 100 mM. A amostra foi dialisada à temperatura ambiente durante a noite com o mesmo tampão. A amostra dialisada foi centrifugada a 2000 rpm durante 15 min à temperatura ambiente. Qualquer precipitado resultante foi descartado.

O sobrenadante foi fracionado para isolar o γγF1, γγ'F1 e pFN como descrito por Siebenlist et al (81), utilizando cromatografia de DEAE Sefarose à temperatura ambiente. A amostra foi aplicada uma coluna de DEAE e em seguida, lavada com uma 10 de citrato de sódio 20 mM, NaCl 100 mM, pH 7,4. A fração não absorvida foi descrita como γγF1. Além disso, foi extraído a partir do DEAE uma mistura aproximadamente equimolar de γγ'F1 e pFN. A mistura foi dialisada usando um dispositivo de ultrafiltração de de 10 kDa em 4000 g durante 30 minutos.

Polimerização do fibrinogênio-fibronectina

Foi confeccionada a matriz misturando 40.0 µL do complexo gama-fibrinogênio-fibronectina (6.75 mg/mL), ou mistura fibrinogênio e fibronectina (2.97 mg/mL) com 10.0 µL de FXIIIa (0.216 mg/mL) e fator de coagulação II ativado (25 Unidades/mL) com 1.0 µL de VEGF (0.8ng/µL) e Soro Ringer (2.9 µL), misturado completamente com o uso de vórtex®, durante 10 segundos. Em seguida, 40.0 µL dessa mistura foi aplicado imediatamente sobre a ferida. Os animais controles receberam as mesmas quantidades sem o uso do complexo ou a mistura. Segundo dados do estudo piloto sobre a formação da matriz de F1:FN, escolhemos a concentração de 0,1 mg/ml de rFXIIIa para reticular as fibrinas na concentração de 2,5 mg/ml de γγ'F1 ou F1.

Fibras colágenas

As lâminas para análise das fibras de colágeno e elásticas foram coradas com Picrossírius red a análise foi realizada pela técnica de birrefringência e luz clara respectivamente. A avaliação da organização e maturação de fibras colágenas foi realizada através da tipificação da birrefringência da área da ferida por meio de Picrossírius sob a luz polarizada. As fibras de colágeno foram determinadas de acordo com seu padrão de birrefringência (esverdeado/amarelo-esverdeado ou laranja/laranja-avermelhado), a aparência morfológica e sua deposição (reticular, paralela ou intercalada). As amostras foram coletadas nos 6 e 11 dias após da lesão. As lâminas foram visualizadas utilizando microscópio (ZEISS West Germany) com objetiva de 16X/2, câmera Zeiss Axiocam ICc5 e processadas utilizando software Image Pro-Plus.

Aquisição, filtragem e processamento de dados de sequenciamento de RNA de célula única

As análises *in silico* foram realizadas usando um notebook HP ENVY 17 Leap Motion SE NB PC com 16 GB de RAM e processador Intel i7 de quatro núcleos. Amostras de matrizes de expressão de camundongos foram obtidas do *Gene Expression Omnibus* e *ArrayExpress*: códigos E-MTAB-6583 e GSE113854. As células foram filtradas por seu número total de leituras, por seu número de genes detectados e pela sua porcentagem mitocondrial. Usamos as configurações nFeature_RNA> 100 e <5000, nCount_RNA> 100 e <25000 & percent.mt <6. As amostras foram processadas em Seurat v3.1 usando o fluxo de trabalho Seurat padrão. Para agrupamento e visualização, usamos o padrão do pipeline Seurat e a visualização do gráfico de pontos. Os nomes dos clusters foram anotados de acordo com os tipos de celulares dos artigos originais do Joost e colaboradores, como também do Guerrero-Juarez e colaboradores (82, 83).

Interações receptor-ligante

Para definir possíveis interações entre as células, selecionamos os genes FN1 (Fibronectina), Itga5, Itgb1 e Itgav. foi usado. Para determinar se os receptores e ligantes em duas populações formam pares, usamos *iTALK*, uma abordagem computacional para caracterizar e ilustrar sinais de comunicação intercelular no ecossistema de feridas baseados no ambiente tumoral multicelular usando dados de sequenciamento de RNA de célula única (84).

RESULTADOS

Contents lists available at ScienceDirect

Bioactive Materials

journal homepage: http://www.keaipublishing.com/biomat

Novel fibrin-fibronectin matrix accelerates mice skin wound healing

Carlos Poblete Jara[a,b,1], Ou Wang[c,d,1], Thais Paulino do Prado[a,b], Ayman Ismail[c], Frank Marco Fabian[c], Han Li[c,e], Licio A. Velloso[b], Mark A. Carlson[f,g], William Burgess[c], Yuguo Lei[c,d,g,h,*], William H. Velander[c,**], Eliana P. Araújo[a,b,***]

[a] Nursing School, University of Campinas, Campinas, SP, Brazil
[b] Laboratory of Cell Signaling, University of Campinas, Campinas, SP, Brazil
[c] Department of Chemical and Biomolecular Engineering, University of Nebraska, Lincoln, NE, USA
[d] Biomedical Engineering Program, University of Nebraska, Lincoln, NE, USA
[e] School of Biological Science, University of Nebraska, Lincoln, NE, USA
[f] Department of Surgery, University of Nebraska Medical Center and the VA Nebraska-Western Iowa Health Care System, USA
[g] Mary and Dick Holland Regenerative Medicine Program, University of Nebraska Medical Center, Omaha, NE, USA
[h] Fred & Pamela Buffett Cancer Center, University of Nebraska Medical Center, Omaha, NE, USA

ARTICLE INFO

Keywords:
Fibrin
Fibronectin
Nanoclusters
Wound healing

ABSTRACT

Plasma fibrinogen (F1) and fibronectin (pFN) polymerize to form a fibrin clot that is both a hemostatic and provisional matrix for wound healing. About 90% of plasma F1 has a homodimeric pair of γ chains (γγF1), and 10% has a heterodimeric pair of γ and more acidic γ′ chains (γγ′F1). We have synthesized a novel fibrin matrix exclusively from a 1:1 (molar ratio) complex of γγ′F1 and pFN in the presence of highly active thrombin and recombinant Factor XIII (rFXIIIa). In this matrix, the fibrin nanofibers were decorated with pFN nanoclusters (termed γγ′F1:pFN fibrin). In contrast, fibrin made from 1:1 mixture of γγF1 and pFN formed a sporadic distribution of "pFN droplets" (termed γγF1 + pFN fibrin). The γγ′F1:pFN fibrin enhanced the adhesion of primary human umbilical vein endothelium cells (HUVECs) relative to the γγF1 + FN fibrin. Three dimensional (3D) culturing showed that the γγ′F1:pFN complex fibrin matrix enhanced the proliferation of both HUVECs and primary human fibroblasts. HUVECs in the 3D γγ′F1:pFN fibrin exhibited a starkly enhanced vascular morphogenesis while an apoptotic growth profile was observed in the γγF1 + pFN fibrin. Relative to γγF1 + pFN fibrin, mouse dermal wounds that were sealed by γγ′F1:pFN fibrin exhibited accelerated and enhanced healing. This study suggests that a 3D pFN presentation on a fibrin matrix promotes wound healing.

1. Introduction

Skin wound healing consists of four phases: hemostasis, inflammation, proliferation, and remodeling. After an injury in healthy people, plasma fibrinogen (F1) and plasma fibronectin (pFN) (10:1 at M ratio) are polymerized by thrombin and factor XIII (FXIII) to form a fibrin clot to stop bleeding (i.e., the hemostasis) [1]. In the clot, fibronectins are attached covalently to the fibrin nanofibers [2]. In a material sense, F1 and pFN are both diverse macromolecules that greatly contrast each other in structure. F1 is a linear, hexameric, 340 kDa glycoprotein having two alpha, two beta, and two gamma chains [3–5]. pFN is a 440 kDa globular protein having two chains with cellular binding domains. Both F1 and pFN have cellular binding domains that remain cryptic until crosslinking by activated Factor XIII (FXIIIa) into the fibrin matrix [6]. About 90% of F1 circulates as a homodimeric pairing of γ-chains (γγ F1) while the remaining 10% presents a heterodimeric pairing of γ with a more acidic γ′-chain (γγ′F1)[6]. The γ′-chain occurs from an alternative transcript having 20 additional amino acids at the carboxy-terminal that has been correlated with a pleiotropic impact on vascular health [6–8]. Importantly, pFN and γγ′F1 both occur at about the same concentration in plasma of about 300 μg/mL [7–11] and, therefore, their presence in fibrin clots.

Peer review under responsibility of KeAi Communications Co., Ltd.
* Corresponding author. The University of Nebraska, Lincoln, NE, USA.
** Corresponding author. The University of Nebraska, Lincoln, NE, USA.
*** Corresponding author. The University of Campinas, Brazil.
E-mail addresses: ylei14@unl.edu (Y. Lei), wvelander2@unl.edu (W.H. Velander), earaujo@unicamp.br (E.P. Araújo).
[1] These two authors contributed equally.

https://doi.org/10.1016/j.bioactmat.2020.06.015
Received 25 May 2020; Received in revised form 22 June 2020; Accepted 22 June 2020

The hemostasis begins with thrombin-mediated activation of F1 and FXIII. The activated F1 produces a semi-soluble, viscoelastic fibrin aggregate [3,12,13] containing pFN entrained from plasma. The FXIII is inherently present within the polymerizing fibrin aggregate as a complex with 1 out of every 100 γγ′F1 molecules [7]. It disassociates upon the formation of activated FXIII that enables efficient intra-fibrin cross-linking activity to produce an insoluble fibrin matrix [14–18], and to simultaneously anchor the matrix to the wound surface in about 3 min [7,19]. This clotting process causes protein conformational changes that induce interactions between pFN, fibrin, and also wound healing cells.

After hemostasis, the fibrin clot acts as a provisional matrix for different cell types to heal the wound [20]. Neutrophils and inflammatory (or M1) macrophages first enter the matrix to clear bacteria and tissue debris. Neutrophils secrete anti-microbial peptides, proteases and reactive oxygen species (ROS) to remove bacteria and damaged tissue [21]. These chemicals are toxic to surrounding healthy cells as well [21]. The M1 macrophages phagocytosis bacterial and damaged tissue [22–30]. Both cell types directly bind to fibrin nanofibers via their $\alpha_M\beta_2$ integrin receptors. Once the wound is debrided (takes ~3 days [31]), neutrophils undergo apoptosis, and M1 macrophages switch to the regenerative M2 phenotype that secretes cytokines and growth factors to recruit and stimulate healing cells such as endothelial cells, fibroblasts and keratinocytes to heal the wound (i.e., the proliferation phase) [32–34]. Endothelial cells form new blood vessels, and fibroblasts deposit new extracellular matrix proteins to form a granulation tissue (takes ~7 days) [32–34]. Keratinocytes migrate on the granulation tissue to form a new epidermis to close the wound (i.e., re-epithelization) [33]. Healing cells adhere to the fibrin matrix by binding to fibronectins with their integrin receptors [32–35]. The binding also triggers downstream signalings that are required for these cells to migrate, proliferate, and repair the wound [32–36]. Fibronectins also bind, enrich, protect, orientate, and present growth factors locally to potentiate their functions [37–48]. In short, the fibrin-based provisional matrix is the central stage for cells to heal a wound, and fibronectins are essential for adhering and stimulating the healing cells. Consequently, insufficient provisional matrix or fibronectins or fibronectin-induced cell signalings lead to pathological wound healings [32–35,37]. For instance, small wounds can heal in about 14 days, while large wounds take much longer time to heal partially due to the insufficient fibrin-fibronectin provisional matrix.

We hypothesize that increasing the pFN content or FN-cell interaction in the fibrin matrix will promote wound healing via enhancing the migration, proliferation, and function of healing cells. The natural fibrin matrix only contains 10% (molar ratio) fibronectins [1]. Previously, we reported a novel method to increase the pFN content up to 50% (molar ratio) in the fibrin matrix and to present the pFN as nanoclusters on the fibrin nanofibers [8]. In this report, we showed that this novel pFN: γγ′F1 fibrin enhanced the adhesion, proliferation, and morphogenesis of healing cells *in vitro*, and accelerated re-epithelization and granulation tissue formation in mouse dermal wounds. This engineered fibrin sealant has attributes useful to both hemostasis and to promote faster wound healing, including improvement of granulation tissue quality.

Fibrin sealants using fibrinogen purified from human plasma are commercially available for various biomedical applications such as hemostat, tissue sealant, and tissue adhesive [49,50]. They are also widely used for tissue engineering, and drug and cell delivery. However, studies on using purified fibrin sealant alone to enhance wound healing are limited [51–54]. The outcomes are positive but inconsistent and limited. Research showed cells did not infiltrate the topically applied fibrin sealant in rodent skin wounds [55]. Instead, cells migrated underneath the sealant. The limited success may because fibrin sealants typically use high fibrinogen concentrations (e.g., > 25 mg/mL). The resultant fibrin matrices have large and dense fibrin fibers that prevent cell infiltration and proliferation [56]. Additionally, the fibronectin content and presentation in the matrices are not defined. Some studies use fibronectin-deprived sealants. Others use sealants that contain small amounts of fibronectin (1 fibronectin per 10 fibrinogens). Our sealant is novel and different from these commercial fibrin sealant. First, it has low protein concentrations (< 9 mg/mL), and the resultant matrix has similar micro- and nano-structures to the natural fibrin provisional matrix. Second, it contains high fibronectin content (e.g., 1 fibronectin per 10 fibrinogens). Third, fibronectins are presented as nanoclusters on the fibrin fibers.

2. Methods

2.1. Materials

All reagents were obtained from Sigma Chemical Company (St. Louis MO) unless otherwise noted. Human source plasma was provided by the U.S. Army Materials Command (Fort Detrick, MD.). Recombinant human thrombin was purchased from ZymoGenetics (Seattle, WA). DEAE Sepharose fast flow, Superose 6, and Gelatin Sepharose were purchased from GE Healthcare (Uppsala, Sweden). 4–12% NuPage Bis-Tris SDS polyacrylamide gels, Colloidal Blue stain, and See Blue molecular weight markers were from Invitrogen (Carlsbad, CA). Polyclonal antibody (GMA-034) for human fibrinogen was purchased from Green Mountain Antibodies (Burlington, VT). Antibody (ab2413) for human fibronectin was from Abcam.

2.2. Production of recombinant factor XIII

Recombinant active Factor XIII (rFXIIIa) was expressed in *Pichia Pastoris* following published methods [56–58]. The activity was determined using Pefakit (Pentapharm, Norwalk, CT).

2.3. Preparation of fibrinogen and fibronectin from human plasma [8]

Three units of human plasma that had been stored at −80 °C were thawed at 4 °C. The plasma was centrifuged at 4000 rpm for 20 min. The cryoprecipitate was re-suspended in 45 mM sodium citrate, 100 mM 6-aminocaproic acid, pH 7.0 at 37 °C. The solution was then centrifuged for 25 min at 4000 rpm. The supernatant was treated with a solvent detergent to inactivate the virus by addition of 0.15% TnBP, 0.5% Triton X-100 and stirred at room temperature for 60 min. The supernatant was adjusted to 1 M ammonium sulfate. The sample was stirred at room temperature for 30 min and then centrifuged at 2000 rpm for 15 min at room temperature. The pellet was re-suspended in 20 mM sodium citrate, 100 mM NaCl. The sample was dialyzed overnight at room temperature against the same buffer. The dialyzed sample was centrifuged at 2000 rpm for 15 min at room temperature.

The supernatant was fractionated to isolate γγF1, γγ′F1 and pFN using DEAE Sepharose Fast Flow chromatography at room temperature [59]. The sample was applied to a DEAE column then washed with 10 column volumes of 20 mM sodium citrate, 100 mM NaCl, pH 7.4. The unabsorbed fraction was γγF1. Bound protein was eluted with a linear gradient of 0.1 M–1.0 M NaCl. The pooled eluate produced an approximately equimolar mixture of γγ′F1 and pFN that was dialyzed against 20 mM citrate buffer, 20 mM NaCl at pH 6.8. The dialyzed mixture was concentrated using a 10 kDa centrifugal ultrafiltration device at 4000 g for 30 min.

Pure pFN and γγ′F1 were produced by application of the DEAE eluate pool to gelatin-Sepharose. Briefly, a 10 mL γγ′F1:pFN ("γγ'F1:pFN" that we will name from here as "complex") was applied to a 3 mL analytical gelatin-Sepharose column. The column was washed with 10 vol of the dialysis buffer then eluted with the same buffer containing 6 M urea. pFN was eluted by urea while the γγ′F1 fell through the column.

2.4. 2D adhesion assay

Human foreskin fibroblasts were isolated and cultured in DMEM with 10% FBS. The use of primary human fibroblasts from anonymous donors was approved by the Institutional Review Board at the University of Nebraska Medical Center and by the Research and Development Committee at the Omaha VA Medical Center. Passage 4 to 6 cells were used. HUEVCs were purchased from Lonza and cultured in EGM2 medium. Passage 3 and 4 cells were used for the experiments. 100 μl fibrin matrix was made in one well of the 96-well plate. 1×10^4 cells were placed in each well with 200 μl medium. Three hours after plating, medium, and unattached cells were removed. Cells were washed with 200 μl PBS once. 100 μl fresh medium with 10 μl Alamar blue reagent was added and incubated for 3 h. 100 μl medium was collected for measuring the fluorescence that was calibrated to a standard curve to calculate the numbers of attached cells within each well. After the quantification, cells were fixed with 4% PFA and stained with DAPI. The nuclei were recorded with a fluorescence microscope.

2.5. 3D cell culture within the fibrin matrix

100 μl fibrin matrix with 2×10^4 cells were made in individual wells of a 96-well format plate. 200 μl medium was added to each well. At varied time points after plating, cell morphologies were recorded by phase-contrast microscopy. The medium was removed and 100 μl fresh medium with 10 μl Alamar blue reagent were added and incubated for 3 h. 100 μl medium was collected for measuring the fluorescence that was calibrated to a standard curve to calculate the numbers of cells in each matrix. The viability of cells within the gel was accessed with a Live/Dead cell assay kit (Invitrogen) according to the Manufacturer's instruction.

2.6. Fibrin formulation

To make the fibrin matrix for the above cell culture experiment, the following components were mixed to the final concentration of fibrinogen (γγF1, γγ′F1) at 2.5 mg/mL; thrombin at 1 U/mL; rFXIII at 15.4 U/mL; and pFN at 3.3 mg/mL. F1 and pFN were at a 1 to 1 M ratio. The mixtures were incubated at 37 ˚C for 15 min to form the fibrin matrix.

2.7. SEM and confocal microscopy

Fibrin matrices were made according to the formulation above. For SEM, samples were fixed with 2.5% glutaraldehyde in 100 mM phosphate buffer (PH 7.0) at room temperature for 1 h, then at 4 ˚C overnight. Samples were rinsed with phosphate buffer twice, 10 min each. Ethanol dehydration series were performed: 30%, 50%, 70%, 2 × 95%, 2 × 100%, 5 min for each procedure. Then samples were treated with hexamethyldisilazane (HMDS) as the following: 33% HMDS, 66% HMDS, 2 × 100% HMDS, 2 min for each procedure. Samples were left in 100% HMDS to air-dry at least overnight before sputter-coated with gold-palladium and imaged with the scanning electron microscope (Hitachi S4700 Field-Emission SEM, Hitachi, Tokyo, Japan) at 10 kV. For confocal microscopy, samples were fixed with 4% paraformaldehyde (PFA) at 4 ˚C overnight, washed with PBS for 3 times, and blocked with 5% goat serum for 1 h before incubating with primary antibodies at 4 ˚C overnight. After extensive washing, secondary antibodies were added and incubated for 2 h at room temperature. Samples were then washed with PBS before imaged with confocal microscopy (Nikon A1-R confocal system on a Nikon Eclipse 90i upright fluorescence microscopy).

2.8. Animal research

All animal protocols were approved by the Institutional Animal Care and Use Committee of the State University of Campinas (protocol number 4467–1/2017) and the University of Nebraska-Lincoln (protocol 1571). All experimental procedures were performed following the guidelines of the Institutional Animal Care and Use Committee of the University of Campinas and the University of Nebraska-Lincoln and. For the surgical procedure, mice were anesthetized using intraperitoneal of xylazine (10 mg/kg) and ketamine (100 mg/kg). Individual doses were calculated using *Labinsane App* (Labsincel, 2017). A deep anesthetic plane was verified by the loss of pedal and corneal reflexes. Two symmetrical 6-mm full-thickness excisional wounds were created on the back of each mouse as described previously [60]. Donut-like splints with an 8 mm diameter of the center hole and 15-mm diameter of the disc were created. The splint was carefully placed around the wound and secured to the skin with eight interrupted sutures. After surgery, animals were maintained in a warm bed for anesthetic recovery. We applied intraperitoneal injection of tramadol (25 mg/kg) at 0, 12, and 24 h after surgery as an analgesic treatment.

2.9. Mice fibrin sealant treatment

First, we cleaned the unwounded surrounding skin with a saline solution to remove any traces of biological residue. We sealed the wound with 50 μL fibrin. The fibrin sealant contained 2.5 mg/mL fibrinogen, 3.3 mg/mL fibronectin, 15.4U/mL rFXIIIa, 5 U/mL thrombin, 16 ng/mL VEGF, 5 mM $CaCl_2$ in the Ringer solution. Control animals received the same amount of $CaCl_2$ and VEGF in the Ringer solution. The wounds were covered with a sterile transparent Tegaderm dressing. On days 2, 4, 6, and 9, we cleaned and disinfected the surrounding skin as described above and reapplied 25 μL fibrin sealant.

2.10. Wound healing process documentation and analysis

Macroscopic evaluation of the healing process was evaluated by photographs taken at 0, 2, 4, 6, 9, and 11 days after wounding using a Nikon D610 (Nikon Systems, Inc., Tokyo, Japan) camera with an AF-S DX NIKKOR 18–55 mm f/3.5–5.6G VR objective. The same distance (wound to the objective lens), top white fluorescence illumination, and operator were used on each occasion. We calculate Wound Area as follows: Wound Area (%) = [(wound area of day 0 - wound area of day x)/wound area of day 0] × 100. In each group, we use 16 to 20 photographs per day of analysis. The percentage of wounds with complete closure was calculated by the number of mice that achieve 100% of reepithelization over the total of mice. Wound re-epithelization was examined by ImageJ Software (1.49v).

2.11. Histology

The skin samples containing wounded and unwounded areas were carefully harvested using an 8 mm biopsy punch. The samples were fixed in cold 4% (wt/vol) formaldehyde in PBS at 4 ˚C overnight. Formaldehyde was discarded, and the tissues were washed 3 times using PBS 1x. We divided the circular sample in the middle of the circle to standardize the diameter of the sectioned samples. Then, the samples were treated with increasing concentration of alcohol (70%, 80%, 95%, and 100%) followed by xylol and paraffin and finally fixed in paraffin blocks. We sectioned at 5.0 μm and set 4–6 slices on microscope slides pretreated with poly-L-lysine. Following this procedure, we stained the skin sections with hematoxylin and eosin (Sigma). We incubated the slices with hematoxylin for 30 s, rinsed them in distilled water, incubated them for 30 s with eosin, washed them over in distilled water, and dehydrated them. For Picrosirius red staining (Picro Sirius Red Stain Kit, Sigma), we soaked the section for 30 min in distilled water. Then we incubated the section with Picro-Sirius red solution for 60 min. Slides were washed with acetic acid solution, and then they were washed with absolute alcohol. For Masson's Trichrome Staining, we incubated slides in preheated Bouin's Fluid for 60 min and cool for 10 min. We rinsed it in distilled water, and then we incubated in

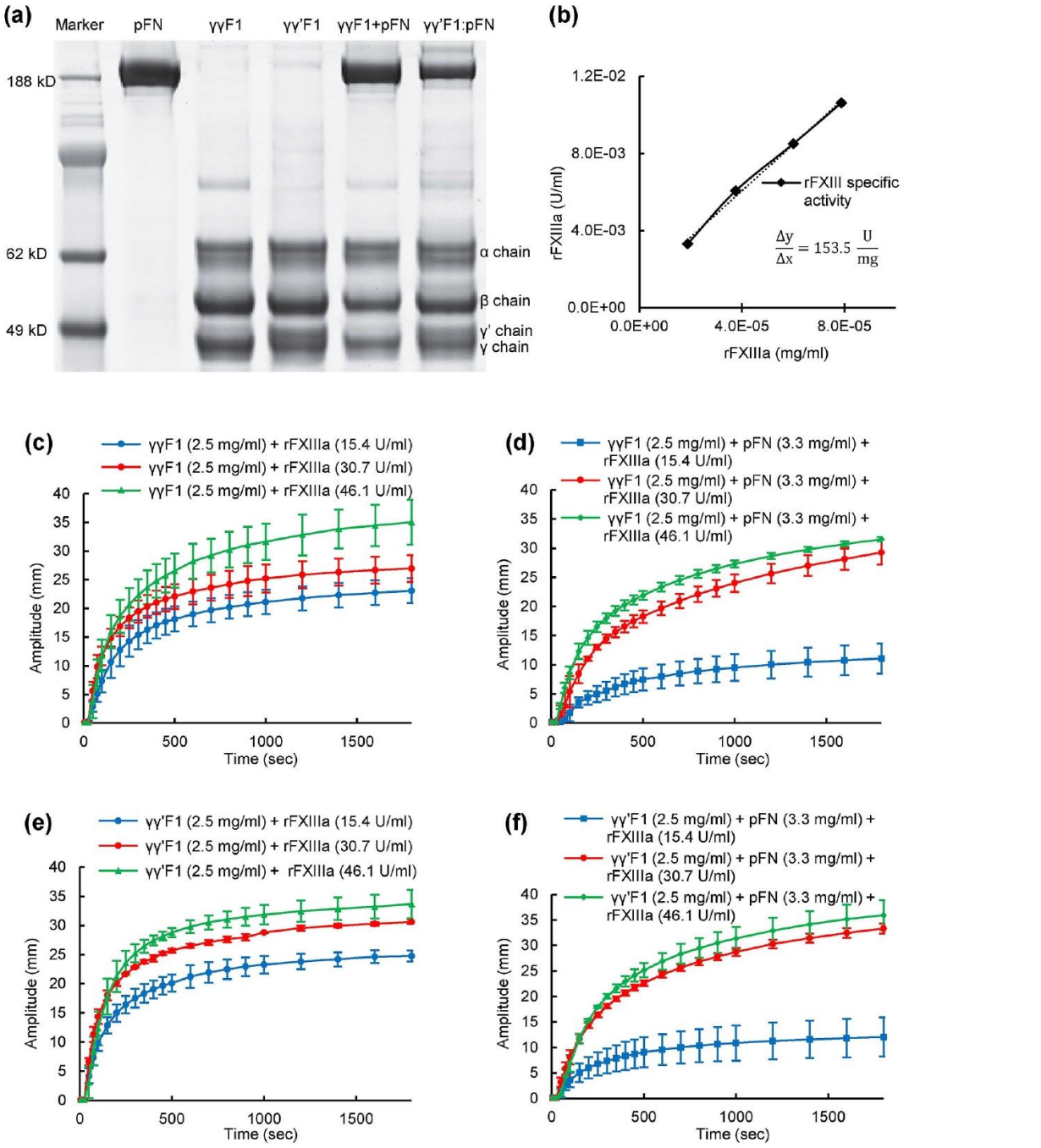

Fig. 1. a) Reducing SDS-PAGE gel. b) rFXIIIa activity (153.5 ± 19 U/mg) was measured using the 5-(biotinamido) pentylamine incorporation assay. The effect of rFXIIIa on the viscoelastic and clotting kinetics of γγF1 (c), γγF1 + pFN mixture (d), γγ′F1 (e), and γγ′F1:pFN complex (f) were evaluated via TEG assay.

Weigert's Iron Hematoxylin for 5 min, Biebrich Scarlet Acid Fuchsin solution for 15 min, differentiate in the phosphomolybdic acid solution for 15 min, Aniline Blue solution for 10 min and acetic acid solution for 5 min. Finally, we mounted the slices on Entellan®, digitally captured the images under bright field microscopy (Leica DM4500B), and processed with Leica Application Suite 3v for *Full view reconstruction*.

2.12. Collagen quantification

To analyze the birefringence patterns, we used microscopy (Nikon® Corp., Kanagawa, Japan) with two CPL polarized filters. We captured the images with a 10x or 40x objective and assessed them for collagen Type III (bright green color) and collagen Type I (red color), with a total magnification of 100X and 400X. The birefringence for Type I collagen was dense, strongly birefringent red fibers, whereas Type III collagen showed thin, green, and softly birefringents [61]. We used Image Pro Plus (version 4) to measure the stained collagen fibers as the percentage of total pixels in each wound pictures.

2.13. Full view reconstruction

To increase the precision of evaluation, we reconstructed the whole skin section using unwounded and wounded images. We used a Nikon Microscopy to take 10-15 adjacent microphotographs (with 30% of

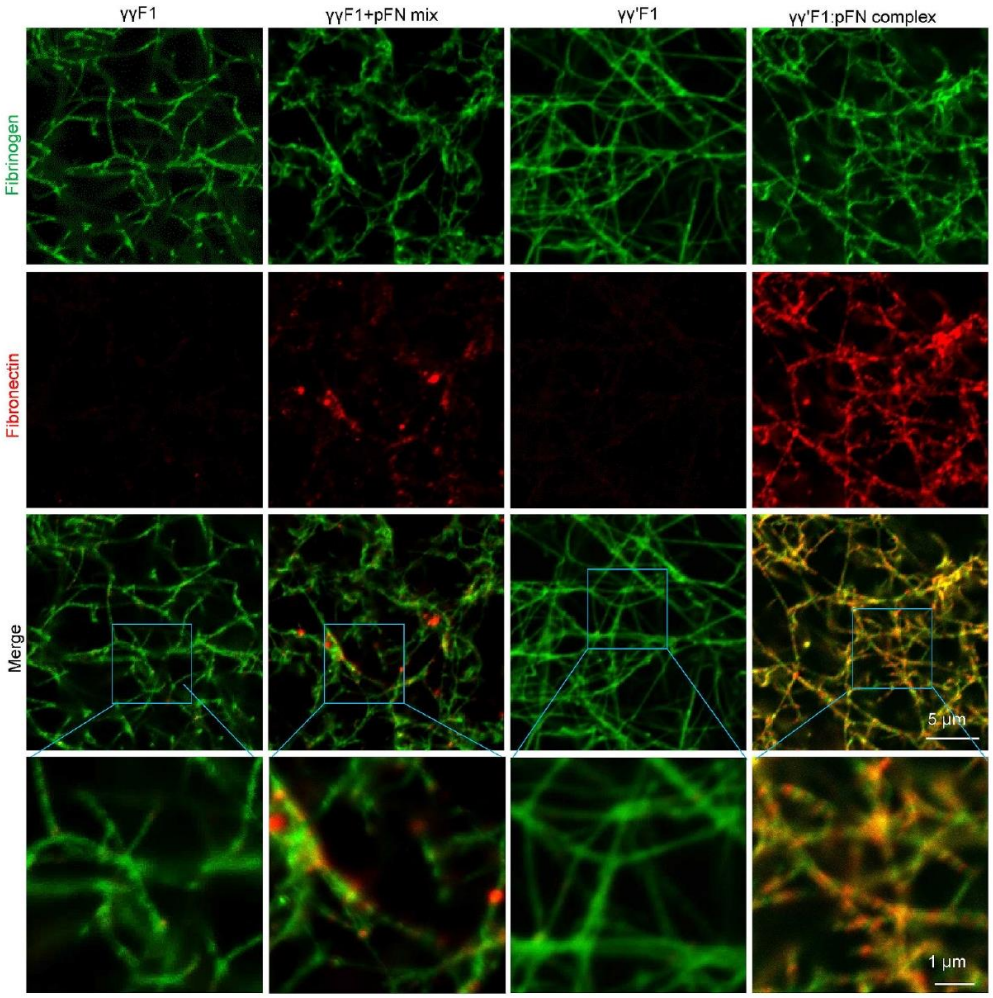

Fig. 2. Confocal microscopy fibrin matrices made from γγF1, γγ′F1, 1:1 mixture of γγF1 and pFN, or γγ′F1:pFN complex.

common areas, 5x objective) and then reconstructed each skin section. We applied the *Photomerge tool* with the *perspective* layout in Adobe Photoshop (19.1v).

2.14. Transcript expression determination by real-time polymerase chain reaction (PCR

We used sample aliquots with 5.0 ng RNA for reverse transcription, applying random hexamer primers and Superscript Moloney-MLV reverse transcriptase. PCR reactions were performed in real-time using the TaqMan™ system (Applied Biosystems). The GAPDH gene (TaqMan™—Applied Biosystems) was employed as the endogenous control for the reaction to which the expression levels of the gene of interest in different samples were normalized. After calculating the efficiencies of amplification, a scatter plot was constructed to define the series of concentrations for which the system was competent. Primers for the target genes were purchased from Applied Biosystems and IDT DNA Technology against the TGF-1β (Mm.PT.58.43.479940), TNF-α (Mm00443258_ m1), IL-6 (Mm00446190_m1), VEGF-α (Mm. PT.58.14200306), FGF-1 (Mm.PT.56a.41158563), IGF-1 (Mm.PT.58.5811533), IL-1β n (Mm00434228_m1), MCP-1 (Mm99999056_m1), IL-10 (Mm01288386_m1), SDF-1 (Mm00445553_m1), ITGA (NM_010577.3), Plaur (ENSG00000011422), MMP9 (ENSG00000100985), Procr (ENSG00000101000) FLRT2 (ENSG00000185070), F4/80 (Mm00802529_m1), Cd11b (Mm00434455_m1), iNos (Mm.PT.5843705194), Cd163 (Mm00474091_m1), Arg1 (Mm.PT.58.8651372) and GAPDH (4352339E). We Used the StepOnePlus Real-Time PCR System™ (Thermo Fisher Scientific). For transcript quantification, the PCR in real-time were carried out in duplicate in reactions containing 3 μl of TaqMan Universal PCR Master Mix 2X, 0.25 μl of primers and probe solution, 0.25 μl of water and 4.0 μl of cDNA. The negative control used 4.0 μl of water in place of cDNA. The cycling conditions were as follows: 45 cycles of 95 °C for 2 min, 95 °C for 5 s, and 60 °C for 30 s. The relative gene expression values were obtained by analyzing the results in the StepOne™ 2.2.2v (Applied Biosystems).

2.15. Statistical analysis

The data are presented as the mean ± S.D. We used an unpaired *t*-test to compare two groups and one-way ANOVA to compare more than two groups. $P < 0.05$ was considered statistically significant. We used GraphPad Prism 6 for Windows 6.01v to perform statistical analysis.

3. Results

3.1. Highly active factor XIII was critical to forming a stable fibrin matrix at low sealant concentration

Recently, we developed a scalable process to separate γγF1 and γγ′F1 from human plasma at production scale [8]. We observed that γγ′F1 and pFN isolated as a noncovalent complex at about 1:1 M ratio [8]. This complex could be dissociated by passing through a gelatin affinity column where the pFN was absorbed, and γγ′F1 passed through the affinity column. We also found that the dissociated γγ′F1 and pFN

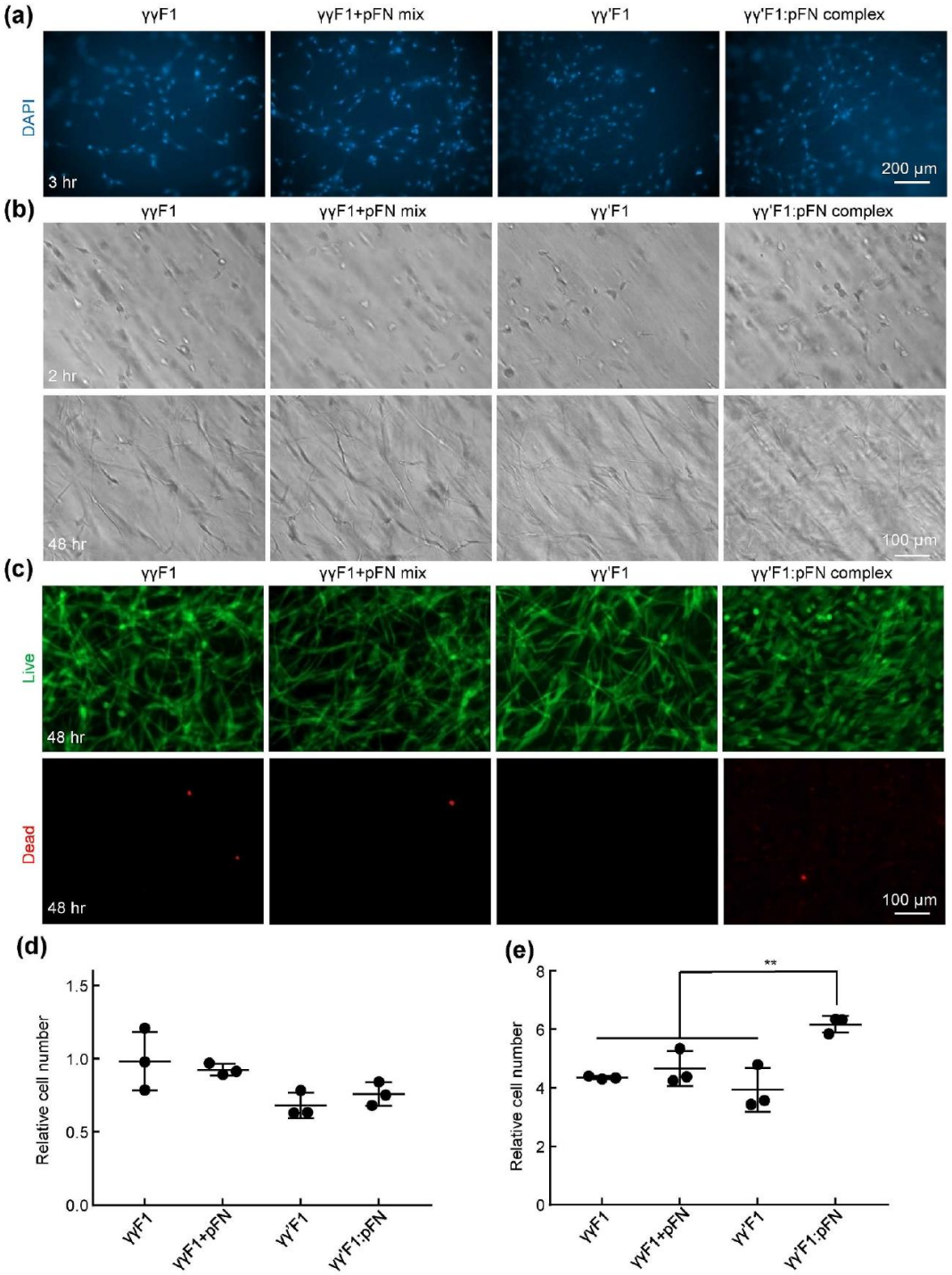

Fig. 3. Culturing primary human fibroblasts on top of (a, d) and within 3D fibrin matrices (b, c, e). a) The nuclei of cells attached to fibrin matrices at 3 h. b) Fibroblasts in 3D fibrin matrices at 2 h and 48 h. c) Live and dead cells at 48 h. d) Cells attached to the fibrin matrices were quantified with alamar blue assay. e) Cells in 100 μl fibrin matrices at 48 h were quantified with alamar blue assay. Cell numbers are related to the initial seeded cells. **: $p < 0.01$.

could quickly re-associate at room temperature [62]. The high purity of the compositions used in this paper consisting of pFN, γγF1, γγ′F1, γγ′F1:pFN and a 1:1 mixture of γγF1 and pFN (γγF + pFN) were confirmed with reduced SDS-PAGE (Fig. 1a).

The normal concentration of fibrinogen in blood plasma is 2–4 mg/mL [63]. The natural fibrin clot is strengthened by platelets. In literature, the fibrin matrix is typically prepared at high protein concentration, such as > 25 mg/mL F1, to provide sufficient stability and strength [56]. However, our previous research found human cells typically did not grow well in fibrin matrix > 9 mg/mL due to the dense fiber structures [56]. Thus, we recommended using < 9 mg/mL fibrin for 3D *in vitro* cell culture, cell delivery, and wound healing application [56]. However, at such low concentration, it required FXIII-catalyzed covalent crosslinking to form a stable fibrin matrix [56]. To achieve this, we expressed a recombinant FXIII [56] with a specific cross-linking activity of 154 U/mg, which was about 6-fold higher than plasma-derived FXIII (Fig. 1b).

We then tested if stable fibrin matrix could be formed with low F1 concentration using this recombinant FXIIIa, and how the pFN influenced the gelation kinetics and resultant matrix mechanical properties.

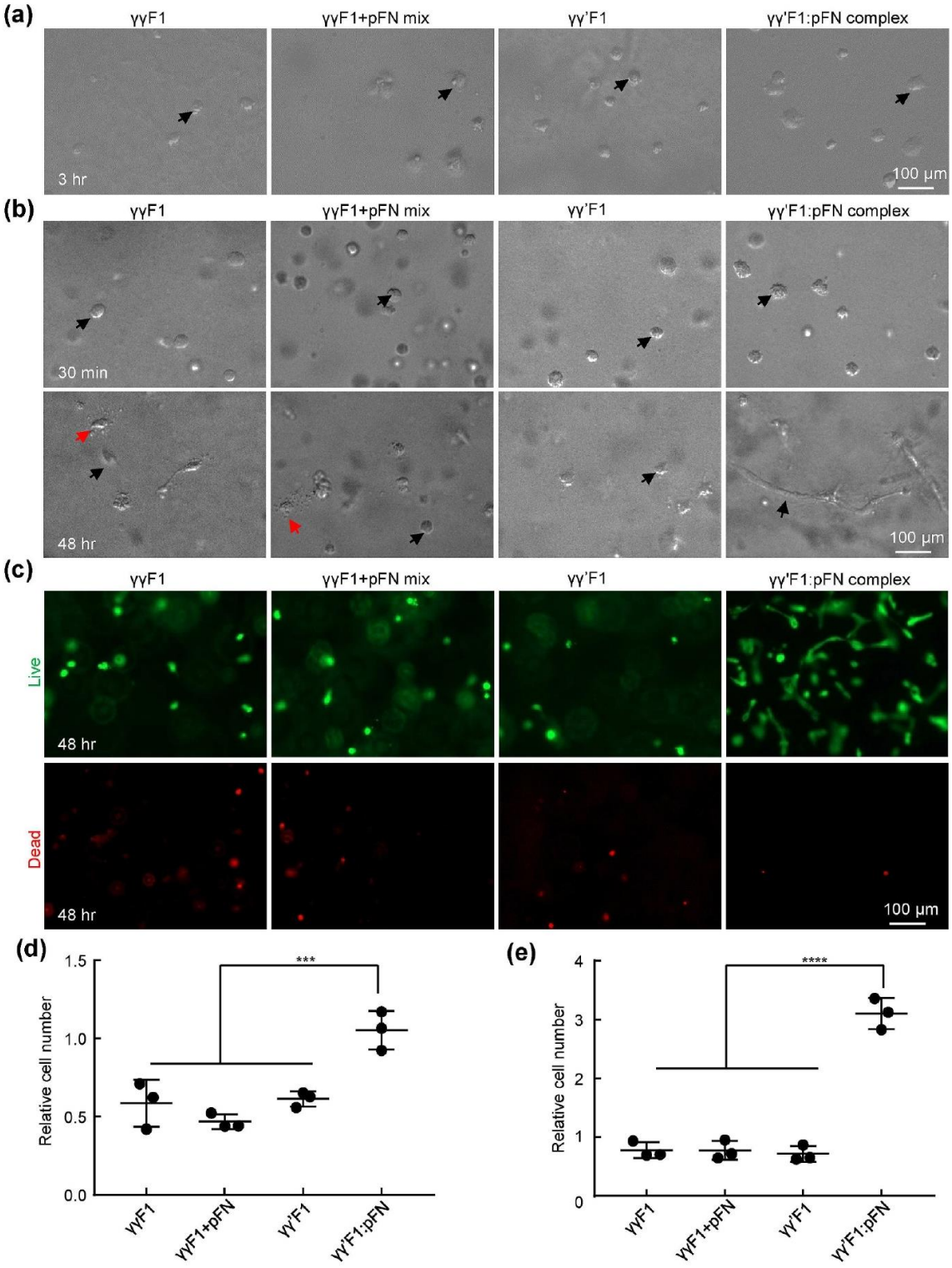

Fig. 4. Culturing primary human umbilical vein endothelial cells (HUVECs) on top of (a, d) and within 3D fibrin matrices (b, c, e). a) HUVECs attached to fibrin matrices at 3 h. b) HUVECs in 3D fibrin matrices at 30 min and 48 h. Red and black arrows point to apoptotic and live cells respectively. c) Live and dead cells at 48 h. d) Cells attached to the fibrin matrices were quantified with alamar blue assay. e) Cells in 100 μl fibrin matrices at 48 h were quantified with alamar blue assay. Cell numbers are related to the initial seeded cells. ***: $p < 0.001$ and ****: $p < 0.0001$.

We used a commercially available, biotherapeutic grade recombinant thrombin and our rFXIIIa at different concentrations to make fibrin matrices with γγF1 alone, γγ′F1 alone, γγ′F1:pFN complex, or a 1:1 mixture of γγF1 and pFN. All sealants were formulated at an F1 concentration of 2.5 mg/mL with 3.3 mg/mL pFN for both γγ′F1:pFN and analogous γγF1 + pFN mixtures. All groups formed stable matrices with higher concentrations of rFXIIIa observed to accelerate gelation and improve the mechanical properties of the fibrin (Fig. 1c–f). Thus, this highly active rFXIIIa allowed us to use a low concentration fibrin matrix for our following *in vitro* cell culture and *in vivo* studies.

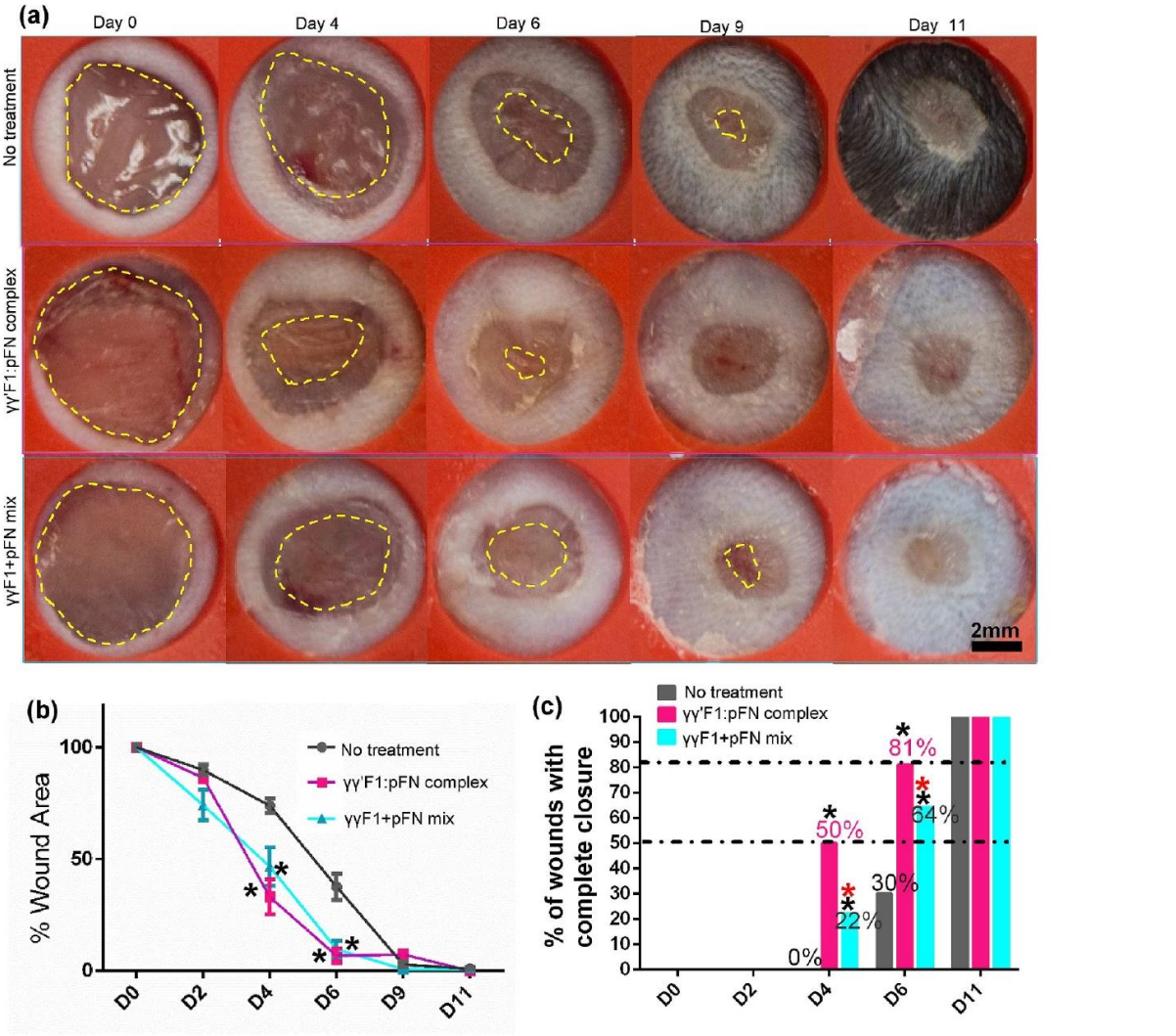

Fig. 5. (a) Macroscopic wound morphology on different days. Yellow dash line highlights the leading edge of the new epithelium. (b) The percentage of wound area, and (c) the percentage of mice achieved 100% re-epithelization on different days. 10 mice with 20 wounds were used. *: $p < 0.05$; *:compared to no treatment group; *: compared to complex.

3.2. 3D fibronectin presentation on the γγ′F1:pFN matrix

We used immunostaining and confocal microscopy to study the distribution of pFN and F1 in the fibrin matrices (Fig. 2). We found that all formulations produced similar fibrin fiber networks. Most fibers were between 100 and 400 nm in diameter while having a similar degree of branching. Large depots of pFN sporadically occurred within the fibrin matrix made from the γγF1 + pFN mixture. The fibrin made from the γγ′F1:pFN complex presented pFN throughout the matrix as nanoclusters superimposed on the continuous γγ′F1 fiber network.

3.3. The 3D fibronectin presentation enhanced the adhesion, migration, proliferation, and function of healing cells

As previously documented, healing cells interact with the fibrin provisional matrix through binding fibronectins with their integrin receptors [32–35]. We hypothesized that the 3D fibronectin nanoclusters could potentiate the cell-matrix interaction. We first tested the interactions of fibroblasts with these 4 different fibrin matrices. The adhesion of fibroblasts to fibrin made with γγF1, γγ′F1, 1:1 γγF1 + pFN mixture, and γγ′F1:pFN complex were examined through culturing them on top of the matrix. Cells were allowed to attach to the matrix for 3 h, a time that is sufficient for cellular adhesion. The nuclei of the attached fibroblasts were stained by DAPI (Fig. 3a). Adhered cells were also quantified with Alamar blue assay (Fig. 3d). The results showed that fibroblasts had similar adhesion to these matrices.

For efficient wound healing, the provisional matrix also needs to support the survival, proliferation, and morphogenesis of both fibroblasts and endothelial cells (ECs) in addition to good adhesion. Since cells *in vivo* are in the 3D matrix, we also used 3D culture to study these phenomena in the 4 matrices. Fibroblasts were cultured within the fibrin matrix. After 48 h, fibroblasts exhibited extended morphology, indicating good adhesion in all matrices (Fig. 3b). Fibroblasts survived well in all matrices, as shown by the live/dead cell staining (Fig. 3c). However, the numbers of cells in the γγ′F1:pFN complex matrix was significantly higher (~1.5 fold) than in other matrices (Fig. 3e). These results showed the γγ′F1:pFN matrix or the 3D pFN presentation promoted the proliferation of fibroblasts.

The interactions of HUVECs with these 4 matrices were also investigated. HUVECs adhered to the surfaces of all fibrin matrices after 3 h. The numbers of HUVECs adhered to the γγ′F1:pFN matrix was 2 fold of these to the γγF1, γγ′F1, and 1:1 γγF1 + pFN mixture matrix, indicating HUVECs had stronger adhesion to γγ′F1:pFN complex matrix (Fig. 4a and 4d). After 48 h of culturing in 3D fibrin matrices, HUVECs in γγF1, γγ′F1, and γγF1 + pFN matrix showed spherical morphology, indicating poor adhesion to the matrices. Some cells showed blebs, a

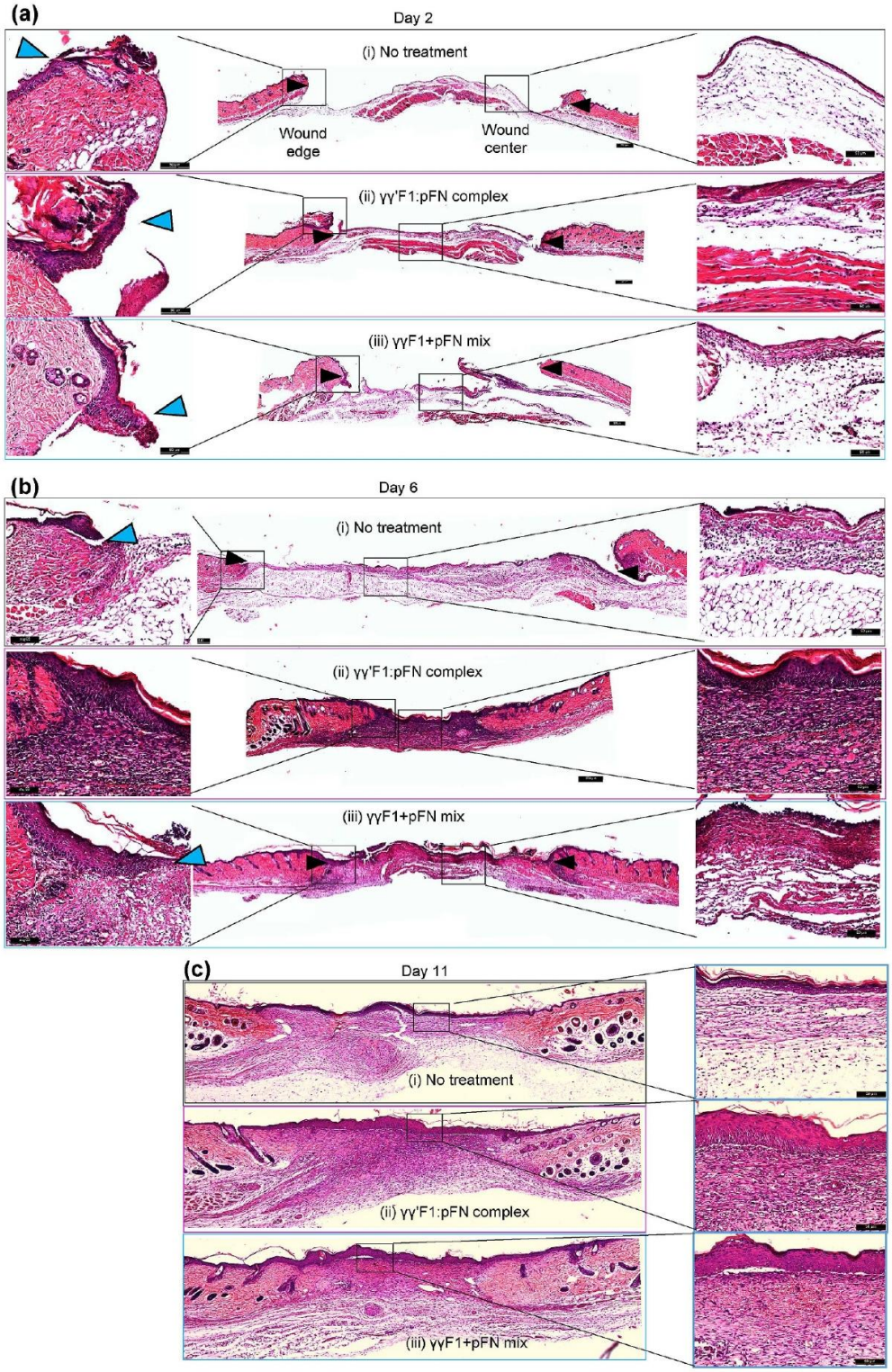

Fig. 6. H&E staining of days 2, 6 and 11 wounds. Reprehensive images from 5 animals or 10 wounds.

sign of apoptosis (Fig. 4b). The existence of apoptosis was confirmed by live/dead cell staining (Fig. 4c). HUVECs in γγ′F1:pFN complex matrix showed no apoptosis. Also, they showed a high level of morphological sprouting. Quantification found 400% more cells in the γγ′F1:pFN matrix than other formulations (Fig. 4e). These results showed the γγ′F1:pFN complex matrix or the 3D pFN presentation significantly promoted the adhesion, survival, proliferation, and morphogenesis of HUVECs.

3.4. The 3D fibronectin presentation accelerated skin wound healing in healthy mice

Based on the *in vitro* cell culture data, we hypothesized that the novel matrix could enhance the granulation tissue formation and wound closure *in vivo*. We tested this hypothesis in a full-thickness model in healthy mice. Wounds were treated with γγ′F1:pFN complex, or γγF1 and pFN mixture. The macroscopic evaluation showed the

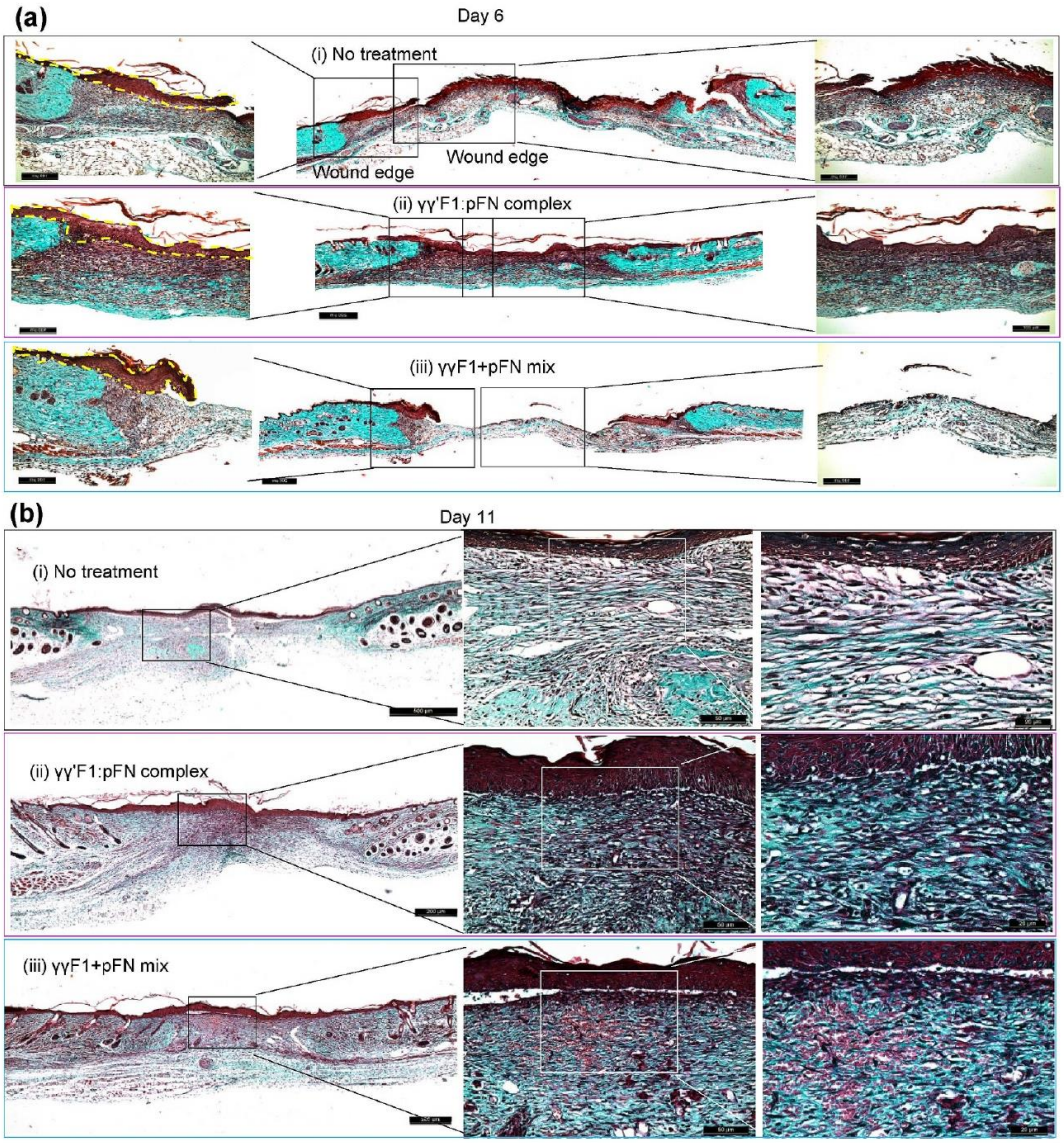

Fig. 7. Masson's trichrome staining was done to evaluate the total collagen deposition. Collagen (blue) on the wound bed was much less than the surrounding normal skin. Reprehensive images from 5 animals or 10 wounds.

γγ′F1:pFN complex significantly speeded up wound closure (Fig. 5a). Indeed, 50% and 81% of wounds treated with the γγ′F1:pFN complex achieved full re-epithelization on days 4 and 6, respectively. On the other hand, 22% and 64% of wounds treated with the mixture achieved full re-epithelization on days 4 and 6, respectively, and 0% and 30% of the control wounds (without treatment) achieved full re-epithelization on day 4 and 6 respectively (Fig. 5c). The microscopic evaluation confirmed these observations. The migration of epidermal cells was significantly increased in the γγ′F1:pFN complex treated group just (i.e., the leading edge) 2 days post-treatment (Fig. 6a) and showed a complete epithelization over the wound bed on day 6 (Fig. 6b). Histology also showed dense granulation tissue at the wound center only in the γγ′F1:pFN complex treated group (Fig. 6b). These data supported that the novel fibrin sealant/matrix or the 3D pFN presentation promoted epidermal cell migration, resulting in faster re-epithelization *in vivo*.

We also evaluated the extracellular matrix formation via histocolorimetric analysis of collagen content (Fig. 7). Total collagen deposition was identified by Masson's trichrome staining on days 6 and 11 post-wound, period when the highest production of collagen is reached [64]. Animals treated with γγ′F1:pFN complex or γγF1 + pFN mixture treatments showed no differences in total collagen deposition. However, the quality of collagen was different. Staining showed dense and aligned reticular collagen fibers in the γγ′F1:pFN complex group on day 6, suggesting high-quality granulation tissue (Fig. 7a). The other treatment groups had a distinctly more sparse and randomly oriented collagen layer showing less mature granulation tissue.

We evaluated the collagen subtype progression through Picrosirius Red Staining, which stains collagen III in green and collagen I in red (Fig. 8). In physiological wound healing, granulation tissue mainly consists of collagen III in the proliferative phase that gradually changes to mesh-like collagen I in the remodeling phase. Our data of control wounds agreed with this (Fig. 8). However, wounds treated with the γγ′F1:pFN complex on day 6 showed higher collagen I content. Even more, γγ′F1:pFN complex on day 6 was similar to day 11 of control group wounds (Fig. 8a–c). On day 11, the γγ′F1:pFN complex group had the mesh-like collagen organization (Fig. 8b). These data showed the γγ′F1:pFN complex shifted the granulation formation, collagen remodeling about 5 days earlier, and improved the quality of the new tissue.

We assessed the expression of 20 signature genes associated with the transitioning between sequences of inflammation, cell migration, and proliferation [65] that could corroborate macroscopic changes in

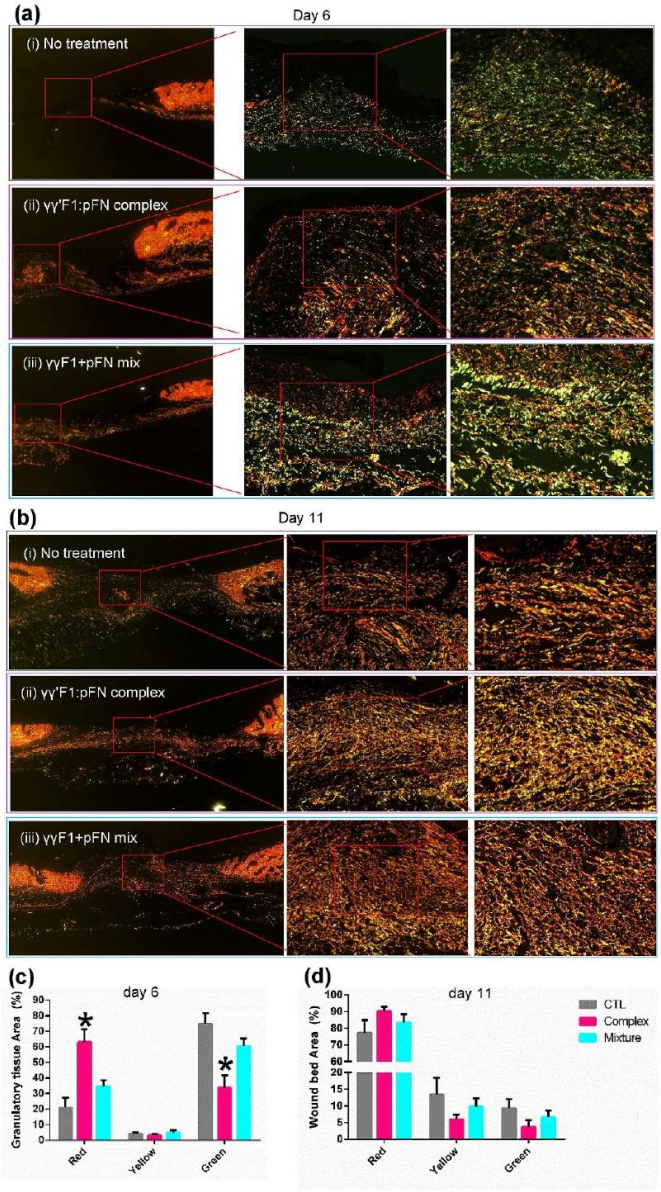

Fig. 8. Picrosirius red staining on collagen I (red) and III (green) on day 6 (a, c) and 11 (b, d). Reprehensive images from 5 animals or 10 wounds. Standard error is presented in (c, d). *:$p < 0.05$. CTL: control without treatment. Complex: γγ′F1:pFN complex. Mixture: 1:1 mixture of γγF1 and pFN.

dermal tissue structure. Several statistically significant changes in gene expression related to the sequence of these processes were observed among the broad panel of assays presented here (Fig. 9a). For signals associated primarily with an active inflammatory phase, we observed by day 2 the γγ′F1:pFN fibrin treatment group had decreased expression of inflammatory cytokines IL-β1 and IL-10 relative to the other treatment groups(Fig. 9a). Furthermore, by day 6 both relative levels of IL-β1 and IL-6 had receded to very low relative levels as had the macrophage marker F4/80 and monocyte chemoattractant MCP-1. These already diminished signal profiles related to the inflammatory phase indicates that the inflammatory phase was resolved very early in the healing process.

The transition from inflammation to signaling needed for keratinocyte migration also occurred early. We found that PROCR, a gene highly expressed by migrating keratinocytes [66], was increased by the complex and Mixture treatments on day 6 (Fig. 9a). Moreover, the complex group showed an early expression of PROCR on day 2. The Fibronectin Leucine Rich Transmembrane Protein 2 (FLRT2), a cell-cell adhesion marker for keratinocytes, is highly expressed in the leading edge during wound healing [65]. FLRT2 is not expressed in healthy skin epidermis but is expressed during the granulation tissue formation. Our result showed that the FLRT2 expression was decreased on days 6 and 11 in the γγ′F1:pFN complex group, supporting that the cell migration was completed before day 6 in the complex group (Fig. 9b). Keratinocytes bind to the fibrin matrix using alpha 5 integrins (ITGA5), in order to migrate. We found ITGA5 expression increased on day 2 and significantly decreased on days 6 and 11 for the complex group, supporting that cell migration was completed before day 6 (Fig. 9b). These data agree with the acceleration of tissue structure observed, such as the complete re-epithelization and granulation tissue structure found on day 6 for the γγ′F1:pFN treatment group.

Growth factor signaling is critical for granulation formation. We found the γγ′F1:pFN treatment decreased expression of TGF-β1, FGF1, SDF1, VEFG-α and IGF1 genes on day 11, supporting that cell proliferation, granulation tissue formation, and re-epithelization were completed before day 11 in the γγ′F1:pFN complex group (Fig. 9a). Even more, IGF1 early declined on day 6, showing the end of the proliferative phase. Taking all together, animals treated with the γγ′F1:pFN complex showed a non-inflammatory, non-proliferative, and non-migrative profile on day 11, suggesting an early resolution of the wound healing process. In short, our data showed the γγ′F1:pFN complex or the 3D pFN nanoclusters significantly accelerated skin wound healing in healthy mice.

4. Discussion

The topical application of the fibrin matrix represents a promising approach to enhance the healing of skin wounds. The natural provisional matrix contains a small number of fibronectins [1,67–69]. Previous reports have shown that raising the fibronectin content in the matrix promotes wound healing. For instance, human fetus [70–72] and invertebrate animals newts [73] heal wounds much faster because their provision matrices contain much more fibronectins that allow cells to migrate and proliferate faster. The topical application of pure soluble fibronectins enhances normal and diabetic wound healing in animals [70,74–78]. These soluble fibronectins aggregate or attach to surrounding tissue, but do not form a 3D matrix in the wound bed. A recent study shows that if processed into a 3D nanofiber scaffold, fibronectins can heal normal skin wound much faster [70]. However, processing fibronectin nanofibers at a large scale is extremely challenging, limiting their clinical applications.

Both receptor occupancy and clustering are required for integrin signaling [79–81]. Most recent research shows that one way to boost integrin signaling is to present fibronectins as nanoclusters that can cluster the integrin receptors. For example, when cells are cultured on a uniformly fibronectin-coated substrate, high fibronectin density is required to trigger the integrin signaling. On the other hand, if fibronectins are patterned into nanoclusters, they trigger a much higher integrin clustering, signaling, and cell function [81–87]. However, nano-patterning fibronectin has only be achieved on a 2D substrate to date. How to pattern fibronectins as nanoclusters in a 3D matrix, especially on the fibrin nanofibers, and how the 3D nanoscale presentation influences the cell-matrix interaction and cell signaling are still unknown.

In our previous paper [8], we reported a bioprocess to separate γγF1 and γγ′F1 from plasma, and we found that γγ′F1 and pFN formed a tight complex. The γγ′F1 and pFN occur at nearly a 1:1 M ratio in normal human plasma [9,10,88,89], thus the γγ′F1:pFN complex we isolated may already exist in human plasma (Fig. 1). The γγ′F1:pFN complex formed a matrix with fibronectin nanoclusters on the fibrin nanofibers in the presence of highly active thrombin and rFXIIIa (Fig. 2). We showed that the fiber diameters and branch points are markedly similar for all of the fibrins studied. Thus, the fibronectin nanoclusters likely

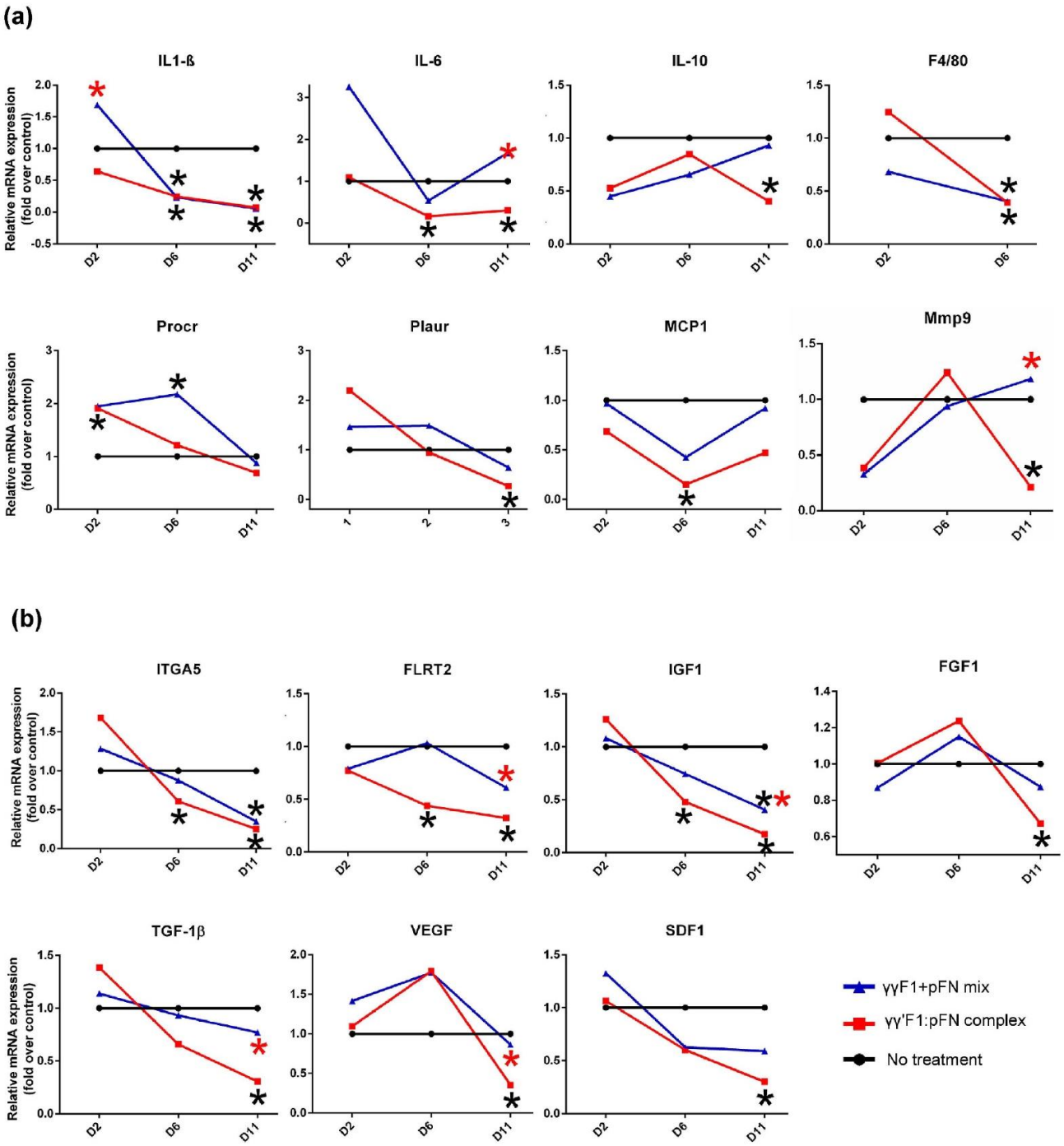

Fig. 9. The relative expression of genes related to inflammation (a), and cell migration and proliferation (b). RNA level was normalized to the untreated group. *:p < 0.05, *:compared to no treatment group; *: compared to complex.

arose from interactions of pFN with the γ′ tails that are uniquely displayed by the γγ′F1 fibrils. Future research should make clear the dynamics of forming these nanoclusters, as well as how the sealant composition affects the matrix structure and properties. This report successfully reproduced all our previous findings (Figs. 1 and 2), showing the robustness of the separation process, the γγ′F1:pFN complex, and the novel nanostructures.

We found that the γγ′F1:pFN matrix potentiated the adhesion of key cells that participate in the wound healing process, including fibroblasts (Fig. 3) and endothelial cells (Fig. 4) *in vitro*. This enhanced interaction led to boosted cell survival, proliferation, migration, and morphogenesis in 3D culture. This was particularly clear for endothelial cells. Because of the similarities in core fiber matrix structure among all fibrins studied here, the enhanced interaction of ECs with γγ′F1:pFN fibrin was likely due to the pFN nanoclusters. As said, angiogenesis is the rate-limiting step of granulation tissue formation, and granulation tissue formation is the rate-limiting step of wound healing. Thus the capability to stimulate endothelial cells has a significant impact on wound healing. The plasma-derived fibrin has a 10:1 ratio of F1 to pFN [7]. This fibrin has been previously shown to support the colonization of fibroblasts [90], but not EC. FGF-2 and or VEGF supplementation has been reported as the primary catalyst of EC colonization in plasma-derived fibrin [91–93]. In contrast, we observed an accelerated EC colonization in the γγ′F1:pFN fibrin without using these growth factors. Future research should systematically make clear the

dynamics of cell-matrix interaction and integrin clustering, and how the interaction alters the global gene expression and cell phenotypes. It is also very valuable to systematically study how the sealant composition and matrix structure influence the matrix interaction with the major cell types of the wound healing process.

Our *in vivo* studies agreed well with the *in vitro* cell culture results. The novel nanostructure significantly accelerated the re-epithelization (Figs. 5 and 6), granulation tissue formation, and modeling (Figs. 7 and 8). The whole wound healing process was speeded up about 5 days. Additionally, the quality of the granulation tissue was significantly improved. This conclusion was supported by the macroscopic morphology (Fig. 5) and microscopic structure analysis (Figs. 6–8) as well as molecule profiles (Fig. 9). Here we have shown that animals treated with γγ′F1:pFN complex accelerated cell migration. The previous report showed that cells at the leading edge in direct contact with the fibrin matrix do not proliferate actively but migrate to the center of the wound [65,94]. Animal treated with the γγ′F1:pFN complex modulated two key membrane proteins that guide cell migration and cell adhesion. It will be valuable to systematically study the cellular profiles at different time points along the healing process in the future.

As said, large acute skin wounds after surgery, trauma, and burn heal slowly (e.g., take > 1 month) and result in scarred skin that has an abnormal appearance, structure, and function. We believe our novel matrix has a high potential to promote the healing of these wounds. Since all materials used in our matrix are human proteins, their safety is expected. Thus our matrix can be quickly translated to bedside once the efficacy and underlying mechanisms are made clear. Since our matrix is fibrin-based, it can be used for both hemostasis and enhancing wound healing. In addition to the acute wounds, our matrix may be used to treat the chronic wound as well. Skin wounds in the aged population, people with diabetes, obesity, and vascular diseases present serious difficulties to heal [95,96]. Current treatments have limited success [95–98]. It will be very valuable to study treating chronic wounds with our novel sealant in the future.

In conclusion, we confirmed that the 10% γγ′F1 in plasma could be separated from the 90% γγF1 using our previously reported method [8], as well as γγ′F1 formed a complex with pFN. We also confirmed that the γγ′F1:pFN complex formed a fibronectin-nanocluster-on-fibrin-nanofiber structure. We found that the 3D nano-scale presentation of the FN could significantly potentiate the cell-matrix interaction *in vitro* and accelerate the granulation formation, re-epithelization in a mice skin wound.

CRediT authorship contribution statement

Carlos Poblete Jara: Investigation, Methodology, Data curation, Formal analysis, Writing - original draft. **Ou Wang:** Investigation, Methodology, Data curation, Formal analysis, Writing - original draft. **Thais Paulino do Prado:** Investigation. **Ayman Ismail:** Investigation. **Frank Marco Fabian:** Investigation. **Han Li:** Investigation. **Licio A. Velloso:** Conceptualization, Writing - review & editing. **Mark A. Carlson:** Resources. **William Burgess:** Investigation. **Yuguo Lei:** Funding acquisition, Conceptualization, Supervision, Writing - original draft, Writing - review & editing, Project administration. **William H. Velander:** Funding acquisition, Conceptualization, Supervision, Writing - original draft, Writing - review & editing, Project administration. **Eliana P. Araújo:** Funding acquisition, Conceptualization, Supervision, Writing - original draft, Writing - review & editing, Project administration.

Declaration of competing interest

All authors declared no competing interests.

Acknowledgements

This research was supported by the University of Nebraska Research Initiative 2018–2019 (YL and WV); the University of Nebraska-Lincoln start-up (YL); the Nebraska DHHS Stem Cell Grant 2019 (YL and WV); the U.S. Army GRANT10824516 (WV); and the Department of Defense, USA, W81XWH-BAA-11-1 (WV). This study was financed in part by the Coordenação de Aperfeiçoamento de Pessoal de Nível Superior – Brasil (CAPES) – Finance Code 88882.434714/2019–01 (EPA and LAV). Confocal microscopy imaging was done in the Morrison Microscopy Core Research Facility at the University of Nebraska, Lincoln.

References

[1] R.a. Clark, Fibrin and wound healing, Ann. N. Y. Acad. Sci. 936 (2001) 355–367.
[2] Y. Wang, et al., Plasma fibronectin supports hemostasis and regulates thrombosis, J. Clin. Invest. 124 (2014) 4281–4293.
[3] P.A. McKee, P. Mattock, R.L. Hill, Subunit structure of human fibrinogen, soluble fibrin, and cross-linked insoluble fibrin, Proc. Natl. Acad. Sci. U. S. A 66 (1970) 738–744.
[4] G. Spraggon, S.J. Everse, R.F. Doollttle, Crystal structures of fragment D from human fibrinogen and its crosslinked counterpart from fibrin, Nature 389 (1997) 455–462.
[5] J.W. Weisel, C.V. Stauffacher, C.C. E Bullitt, A model for fibrinogen: domains and sequence, Science 80 (1985) 1388–1391.
[6] L.M. Maurer, W. Ma, D.F. Mosher, Dynamic structure of plasma fibronectin, Crit. Rev. Biochem. Mol. Biol. 51 (2016) 213–227.
[7] S.U. De Willige, K.F. Standeven, H. Philippou, R.A.S. Ariëns, The pleiotropic role of the fibrinogen γ′ chain in hemostasis, Blood 114 (2009) 3994–4001.
[8] A.E.A. Ismail, et al., The isolation of a plasma-derived γγ' fibrinogen: fibronectin mixture that forms a novel polymeric matrix, Process Biochem. 75 (2018) 257–265.
[9] D.F. Mosher, Physiology of fibronectin, Annu. Rev. Med. 35 (1984) 561–575.
[10] R.O. Hynes, K.M. Yamada, Fibronectins: multifunctional modular glycoproteins, J. Cell Biol. 95 (1982) 369–377.
[11] R.A.S. Ariëns, T.S. Lai, J.W. Weisel, C.S. Greenberg, P.J. Grant, Role of factor XIII in fibrin clot formation and effects of genetic polymorphisms, Blood 100 (2002) 743–754.
[12] R. Chen, R.F. Doolittle, Identification of the polypeptide chains involved in the cross-linking of fibrin, Proc. Natl. Acad. Sci. U. S. A 63 (1969) 420–427.
[13] M.W. Mosesson, Fibrin polymerization and its regulatory role in hemostasis, J. Lab. Clin. Med. 116 (1990) 8–17.
[14] D.F. Mosher, R.B. Johnson, Specificity OF fibronectin-fibrin cross-linking, Ann. N. Y. Acad. Sci. 408 (1983) 583–594.
[15] S.A. Corbett, C.L. Wilson, J.E. Schwarzbauer, Changes in cell spreading and cytoskeletal organization are induced by adhesion to a fibronectin-fibrin matrix, Blood 88 (1996) 158–166.
[16] D.F. Mosher, Cross-linking of cold-insoluble globulin by fibrin-stabilizing factor, J. Biol. Chem. 250 (1975) 6614–6621.
[17] T. Takagi, R.F. Doolittle, Amino acid sequence studies on factor XIII and the peptide released during its activation by thrombin, Biochemistry 13 (1974) 750–756.
[18] E. Makogonenko, G. Tsurupa, K. Ingham, L. Medved, Interaction of fibrin(ogen) with fibronectin: further characterization and localization of the fibronectin-binding site, Biochemistry 41 (2002) 7907–7913.
[19] K.R. Siebenlist, et al., Studies on the basis for the properties of fibrin produced from fibrinogen-containing γ′ chains, Blood 106 (2005) 2730–2736.
[20] P. Martin, R. Nunan, Cellular and molecular mechanisms of repair in acute and chronic wound healing, Br. J. Dermatol. 173 (2015) 370–378.
[21] T.A. Wilgus, S. Roy, J.C. McDaniel, Neutrophils and wound repair: positive actions and negative reactions, Adv. Wound Care 2 (2013) 379–388.
[22] P. Krzyszczyk, R. Schloss, A. Palmer, F. Berthiaume, The role of macrophages in acute and chronic wound healing and interventions to promote pro-wound healing phenotypes, Front. Physiol. 9 (2018) 1–22.
[23] I. Goren, et al., A transgenic mouse model of inducible macrophage depletion: effects of diphtheria toxin-driven lysozyme m-specific cell lineage ablation on wound inflammatory, angiogenic, and contractive processes, Am. J. Pathol. 175 (2009) 132–147.
[24] R. Mirza, L.A. DiPietro, T.J. Koh, Selective and specific macrophage ablation is detrimental to wound healing in mice, Am. J. Pathol. 175 (2009) 2454–2462.
[25] V.A. Fadok, et al., Macrophages that have ingested apoptotic cells in vitro inhibit proinflammatory cytokine production through autocrine/paracrine mechanisms, J. Clin. Invest. 101 (1998) 890–898.
[26] S. Khanna, et al., Macrophage dysfunction impairs resolution of inflammation in the wounds of diabetic mice, PloS One 5 (2010).
[27] K. Wicks, T. Torbica, K.A. Mace, Myeloid cell dysfunction and the pathogenesis of the diabetic chronic wound, Semin. Immunol. 26 (2014) 341–353.
[28] Okizaki Shin-ichiro, et al., Suppressed recruitment of alternatively activated macrophages reduces TGF-β1 and impairs wound healing in streptozotocin-induced diabetic mice, Biomed. Pharmacother. 70 (2015) 317–325.
[29] P. Bannon, et al., Diabetes induces stable intrinsic changes to myeloid cells that contribute to chronic inflammation during wound healing in mice, Dis. Model. Mech. 6 (2013) 1434–1447.
[30] R.E. Mirza, et al., Macrophage PPARγ and impaired wound healing in type 2 diabetes, J. Pathol. 236 (2015) 433–444.
[31] A.J. Singer, R.A.F. Clark, Cutaneous wound healing, N. Engl. J. Med. 341 (1999) 738–746.
[32] D. Greiling, R.a. Clark, Fibronectin provides a conduit for fibroblast transmigration from collagenous stroma into fibrin clot provisional matrix, J. Cell Sci. 110 (1997)

861–870.
[33] R. a F. Clark, et al., Fibronectin and fibrin provide a provisional matrix for epidermal cell migration during wound reepithelialization, J. Invest. Dermatol. 79 (1982) 264–269.
[34] M.G. Tonnesen, X. Feng, R. a F. Clark, Angiogenesis in wound healing, J. Invest. Dermatol. Symp. Proc. 5 (2000) 40–46.
[35] E.a. Lenselink, Role of fibronectin in normal wound healing, Int. Wound J. 12 (2015) 313–316.
[36] P. Knox, S. Crooks, C.S. Rimmer, Role of fibronectin in the migration of fibroblasts into plasma clots, J. Cell Biol. 102 (1986) 2318–2323.
[37] K.M. Sawicka, M. Seeliger, T. Musaev, L.K. Macri, a.F.R. Clark, Fibronectin interaction and enhancement of growth factors: importance for wound healing, Adv. Wound Care 4 (2015) 469–478.
[38] J. Zhu, R. a F. Clark, Fibronectin at select sites binds multiple growth factors and enhances their activity: expansion of the collaborative ECM-GF paradigm, J. Invest. Dermatol. 134 (2014) 895–901.
[39] N. Balanis, C.R. Carlin, Mutual cross-talk between fibronectin integrins and the EGF receptor Molecular basis and biological significance, Cell. Logist. 2 (2012) 46–51.
[40] M. Fujita, et al., Cross-talk between integrin α6β4 and insulin-like growth factor-1 receptor (IGF1R) through direct α6β4 binding to IGF1 and subsequent α6β4-IGF1-IGF1R ternary complex formation in anchorage-independent conditions, J. Biol. Chem. 287 (2012) 12491–12500.
[41] M.B. Grant, S. Caballero, D.M. Bush, P.E. Spoerri, Fibronectin fragments modulate human retinal capillary cell proliferation and migration, Diabetes 47 (1998) 1335–1340.
[42] D.J. Sieg, et al., FAK integrates growth-factor and integrin signals to promote cell migration, Nat. Cell Biol. 2 (2000) 249–256.
[43] J. Veevers-lowe, S.G. Ball, A. Shuttleworth, C.M. Kielty, Mesenchymal stem cell migration is regulated by fibronectin through a 5 b 1-integrin-mediated activation of PDGFR- b and potentiation of growth factor signals, J. Cell Sci. 124 (2011) 1288–1300.
[44] G.S. Schultz, A. Wysocki, Interactions between extracellular matrix and growth factors in wound healing, Wound Repair Regen. Interact. 17 (2009) 153–162.
[45] S. Rahman, et al., Novel hepatocyte growth factor (HGF) binding domains on fibronectin and vitronectin coordinate a distinct and amplified Met-integrin induced signalling pathway in endothelial cells, BMC Cell Biol. 6 (2005) 8.
[46] F. Lin, et al., Fibronectin growth factor-binding domains are required for fibroblast survival, J. Invest. Dermatol. 131 (2011) 84–98.
[47] S.K. Kuwada, X. Li, Epithelial cell proliferation through epidermal growth factor receptor activation, Mol. Biol. Cell 11 (2000) 2485–2496.
[48] J. Kim, A.R. Asthagiri, Matrix stiffening sensitizes epithelial cells to EGF and enables the loss of contact inhibition of proliferation, J. Cell Sci. (2011) 1280–1287.
[49] W.D. Spotnitz, Fibrin sealant: past, present, and future: a brief review, World J. Surg. 34 (2010) 632–634.
[50] W.D. Spotnitz, Fibrin sealant: the only approved hemostat, sealant, and adhesive-a laboratory and clinical perspective, ISRN Surg 2014 (2014) 203943.
[51] D. Amrani, J. Diorio, Y. Delmotte, Wound healing: role of commercial fibrin sealants, Ann. N. Y. Acad. Sci. 936 (2001) 566–579.
[52] A. Gugerell, et al., Thrombin as important factor for cutaneous wound healing: comparison of fibrin biomatrices in vitro and in a rat excisional wound healing model, Wound Repair Regen. 22 (2014) 740–748.
[53] J.B. Eby, et al., The effect of fibrin sealant on the healing of laser-resurfaced skin, Aesthetic Surg. J. 21 (2001) 509–517.
[54] H.S. Yoon, Y.C. Na, K.H. Choi, W.H. Huh, J.M. Kim, Wound healing effect of regenerated oxidized cellulose versus fibrin sealant patch: an in vivo study, Arch. Craniofacial Surg. 20 (2019) 289–296.
[55] J.E. Mogford, B. Tawil, S. Jia, T.A. Mustoe, Fibrin sealant combined with fibroblasts and platelet-derived growth factor enhance wound healing in excisional wounds, Wound Repair Regen. 17 (2009) 405–410.
[56] O. Wang, et al., A totally recombinant fi brin matrix for mesenchymal stem cell culture and delivery, J. Biomed. Mater. Res. 6 (2018) 3135–3142.
[57] D.S. Park, J.H. Kim, S.W. Lee, J.M. Jeong, Secretory expression of the alpha-subunit of human coagulation factor XIII in the yeast Pichia pastoris, Biotechnol. Lett. 24 (2002) 97–101.
[58] M.A. Carlson, et al., A totally recombinant human fibrin sealant, J. Surg. Res. 187 (2014) 334–342.
[59] K.R. Siebenlist, D.A. Meh, M.W. Mosesson, Plasma factor XIII binds specifically to fibrinogen molecules containing $γ$' chains, Biochemistry 35 (1996) 10448–10453.
[60] X. Wang, J. Ge, E.E. Tredget, Y. Wu, The mouse excisional wound splinting model, including applications for stem cell transplantation, Nat. Protoc. 8 (2013) 302–309.
[61] L.C.U. Junqueira, W. Cossermelli, R. Brentani, Differential staining of collagens type I, II and III by Sirius red and polarization microscopy, Arch. Histol. Jpn. 41 (1978) 267–274.
[62] F.M. Fabian, A.E.A. Ismail, O. Wang, Y. Lei, W.H. Velander, Reversible associations between human plasma fibronectin and fibrinogen γγ' heterodimer observed by high pressure size exclusion chromatography and dynamic light scattering, Anal. Biochem. 598 (2020) 113701.
[63] C.M. Ogston, D. Ogston, Plasma fibrinogen and plasminogen levels in health and in ischaemic heart disease, J. Clin. Pathol. 19 (1966) 352–356.
[64] M. Sinha, et al., Direct conversion of injury-site myeloid cells to fibroblast-like cells of granulation tissue, Nat. Commun. 9 (2018) 1–19.
[65] M. Aragona, S. Dekoninck, S. Rulands, S. Lenglez, G. Mascré, B.D. Simons, C. Blanpain, Defining stem cell dynamics and migration during wound healing in mouse skin epidermis, Nat. Commun. 8 (2017) 14684.
[66] K. McKelvey, C.J. Jackson, M. Xue, Activated protein C: a regulator of human skin epidermal keratinocyte function, World J. Biol. Chem. 5 (2014) 169–179.
[67] M. Okada, B. Blombäck, M.D. Chang, B. Horowitz, Fibronectin and fibrin gel structure, J. Biol. Chem. 260 (1985) 1811–1820.
[68] S.A. Corbett, L. Lee, C.L. Wilson, J.E. Schwarzbauer, Covalent cross-linking of fibronectin to fibrin is required for maximal cell adhesion to a fibronectin-fibrin matrix, J. Biol. Chem. 272 (1997) 24999–25005.
[69] A. Ramanathan, N. Karuri, Fibronectin alters the rate of formation and structure of the fibrin matrix, Biochem. Biophys. Res. Commun. 443 (2014) 395–399.
[70] C.O. Chantre, et al., Production-scale fibronectin nano fibers promote wound closure and tissue repair in a dermal mouse model, Biomaterials 166 (2018) 96–108.
[71] B.M.T. Longaker, et al., Studies in fetal wound Healing : III . Early deposition of fibronectin, J. Pediatr. Surg. 24 (1989) 799–805.
[72] A.L. Moore, et al., Scarless wound healing : transitioning from fetal research to regenerative healing, Wiley Interdiscip Rev Dev Biol 7 (2018) 2.
[73] S. Calve, S.J. Odelberg, H.G. Simon, A transitional extracellular matrix instructs cell behavior during muscle regeneration, Dev. Biol. 344 (2010) 259–271.
[74] Z. Qiu, D. Ph, A. Kwon, Y. Kamiyama, Effects of plasma fibronectin on the healing of full-thickness skin wounds in streptozotocin-induced diabetic rats, J. Surg. Res. 138 (2007) 64–70.
[75] S. Hamed, et al., Fibronectin potentiates topical erythropoietin-induced wound repair in diabetic mice, J. Invest. Dermatol. 131 (2011) 1365–1374.
[76] J.P. McCulley, B. Horowitz, Z.M. Husseini, M. Horowitz, Topical fibronectin therapy of persistent corneal epithelial defects, Trans. Am. Ophthalmol. Soc. 91 (1993) 367–386.
[77] A.H. Kwon, Z. Qiu, Y. Hiraon, Topical application of plasma fibronectin in full-thickness skin wound healing in rats, Exp. Biol. Med. 232 (2007) 935–941.
[78] M.B. Johnson, et al., Topical fibronectin improves wound healing of irradiated skin, Sci. Rep. 7 (2017) 3876.
[79] D. Chester, A.C. Brown, The role of biophysical properties of provisional matrix proteins in wound repair, Matrix Biol. 60–61 (2017) 124–140.
[80] S. Miyamoto, et al., Integrin function: molecular hierarchies of cytoskeletal and signaling molecules, J. Cell Biol. 131 (1995) 791–805.
[81] J.H. Slater, W. Frey, Nanopatterning of fibronectin and the influence of integrin clustering on endothelial cell spreading and proliferation, J. Biomed. Mater. Res. 87 (2008) 176–195.
[82] G. Maheshwari, G. Brown, D.A. Lauffenburger, A. Wells, L.G. Griffith, Cell adhesion and motility depend on nanoscale RGD clustering, J. Cell Sci. 1686 (2000) 1677–1686.
[83] M. Arnold, E.A. Cavalcanti-adam, R. Glass, W. Eck, Activation of integrin function by nanopatterned adhesive interfaces, ChemPhysChem 5 (2004) 383–388.
[84] G. Le Saux, et al., Spacing of integrin ligands influences signal transduction in endothelial cells, Biophys. J. 101 (2011) 764–773.
[85] T.A. Petrie, et al., Multivalent integrin-specific ligands enhance tissue healing and biomaterial integration, Sci. Transl. Med. 2 (2010) 45.
[86] J.E. Gautrot, Cell sensing of the physical properties of the microenvironment at multiple scales: cells sense their mechanical microenvironment at the nanoscale level, Mechanobiol. Exploit. Med. Benefit chapter 19 (2017) 297–329.
[87] S. Di Cio, J.E. Gautrot, Cell sensing of physical properties at the nanoscale: mechanisms and control of cell adhesion and phenotype, Acta Biomater. 30 (2016) 26–48.
[88] D.W. Chung, E.W. Davie, Gamma and gamma' chains of human fibrinogen are produced by alternative mRNA processing, Biochemistry 23 (1984) 4232–4236.
[89] R.A.S. Ariens, Role of factor XIII in fibrin clot formation and effects of genetic polymorphisms, Blood 100 (2002) 743–754.
[90] M.A. Carlson, A.K. Prall, J.J. Gums, A. Lesiak, V.K. Shostrom, Biologic variability of human foreskin fibroblasts in 2D and 3D culture: implications for a wound healing model, BMC Res. Notes 2 (2009) 229.
[91] D.A. Cheresh, Human endothelial cells synthesize and express an Arg-Gly-Asp-directed adhesion receptor involved in attachment to fibrinogen and von Willebrand factor, Proc. Natl. Acad. Sci. U. S. A 84 (1987) 6471–6475.
[92] A. Sahni, C.W. Francis, W. Dc, Vascular endothelial growth factor binds to fibrinogen and fibrin and stimulates endothelial cell proliferation Vascular endothelial growth factor binds to fibrinogen and fibrin and stimulates endothelial cell proliferation, Blood 96 (2014) 3772–3778.
[93] A. Sahni, L.A. Sporn, C.W. Francis, Potentiation of endothelial cell proliferation by fibrin(ogen)-bound fibroblast growth factor-2, J. Biol. Chem. 274 (1999) 14936–14941.
[94] S. Park, et al., Tissue-scale coordination of cellular behaviour promotes epidermal wound repair in live mice, Nat. Cell Biol. 19 (2017) 155–163.
[95] G. Han, R. Ceilley, Chronic wound healing: a review of current management and treatments, Adv. Ther. 34 (2017) 599–610.
[96] Oo, N. I. J. S.-. Skin Substitutes for Treating Chronic Wounds, Technol. Assess. Program, Agency Healthc. Res. Qualtiy, 2019, https://www.ahrq.gov/sites/default/files/wysiwyg/r.
[97] W.J. Jeffcoate, L. Vileikyte, E.J. Boyko, D.G. Armstrong, A.J.M. Boulton, Current challenges and opportunities in the prevention and management of diabetic foot ulcers, Diabetes Care 41 (2018) 645–652.
[98] D.G. Armstrong, A.J.M. Boulton, S.A. Bus, Diabetic foot ulcers and their recurrence, N. Engl. J. Med. 376 (2017) 2367–2375.

ARTICLE IN PRESS

Bioprinting xxx (xxxx) xxx

Contents lists available at ScienceDirect

Bioprinting

journal homepage: www.elsevier.com/locate/bprint

Demonstration of re-epithelialization in a bioprinted human skin equivalent wound model

Carlos Poblete Jara [a,b,c], Carolina Motter Catarino [d], Yuguo Lei [d,e], Lício Augusto Velloso [b,c], Pankaj Karande [f], William H. Velander [d], Eliana Pereira de Araujo [a,b,c,*]

[a] Faculty of Nursing, University of Campinas, Brazil
[b] Laboratory of Cell Signaling, University of Campinas, Brazil
[c] Obesity and Comorbidities Research Center, University of Campinas, Brazil
[d] Department of Chemical and Biomolecular Engineering, University of Nebraska, Lincoln, NE, 68588-0643, United States
[e] Biomedical Engineering Program, University of Nebraska, Lincoln, NE, 68588-0643, United States
[f] Department Chemical and Biological Engineer, Rensselaer Polytechnic Institute, NY, United States

ARTICLE INFO

Keywords:
Wound healing
Human skin equivalent
Re-epithelialization
3D bioprinting

ABSTRACT

Wound healing is life-dependent feature for animal survival. After a skin insult, keratinocytes, fibroblasts, and immune cells are recruited to restore the protective skin function. Immediately after injury, soluble fibrinogen is cleaved by thrombin and polymerize to insoluble fibrin clot. Immune cells infiltrate into the fibrin clot to activate the inflammatory response. Surrounding keratinocytes in contact with the fibrin clot migrate to the wounded area meanwhile distant keratinocyte proliferate. However, *in vitro* wound models have important limitations related to wound fibrinogen polymerization and immune cell recruitment. This study expands previous *in vitro* 3D skin equivalent co-culture platforms to include the installation of a physiologically relevant fibrin provisional matrix.
Method: Here, we developed a fibrin provisional matrix installed into a wound facsimile of a bioprinted human skin equivalent (HSE). A mixture of plasma-derived fibrinogen-containing factor XIII, fibronectin, thrombin, and macrophages (an FPM "bioink") was extruded into the wound site. The surrounding *in vitro* tissue culture became a source of keratinocytes to achieve wound closure by a re-epithelialization process signaled by the FPM.
Results: An *in vitro* analog of wound closure and re-epithelialization by keratinocytes occurred over the FPM after a normal migration initiation at 3 days.
Conclusion: This co-culture model was shown to temporally synchronize a re-epithelization process for initiation of keratinocyte migration from a surrounding tissue and the migration process over the top of an FPM. A future study of the analogous subepithelial healing pathway is envisioned using the same *in vitro* bioprinted tissue study platform for co-culture of keratinocytes, melanocytes, fibroblasts, endothelial cells, and macrophages using more specialized FPMs.

1. Introduction

Cutaneous healing begins with a hemostatic response that integrates several physiologic processes: the cessation of blood loss, immediate wound stabilization by sealing tissue from the environment, the initiation of the inflammatory cell response [1], and the simultaneous installation of the fibrin provisional matrix (FPM) to initiate the recruitment and proliferation of healing cells. Thus, the FPM mediates the initiation of re-epithelialization and the construction of a well vascularized, provisional subepithelial tissue. The FPM is penultimately generated by the activation of thrombin from the coagulation cascade and by the thrombin-activation of coagulation factor XIII (FXIIIa).

The re-establishment of the epidermis is a fibrin-receptor-mediated process that guides keratinocyte migration from the interfollicular epidermis that surrounds the FPM sealed wound surface. While keratinocytes migrate along the FPM to the wound center, they are continually re-supplied by proliferating keratinocytes in order to complete the wound closure process [2,3]. Provisional subdermal tissue repair is simultaneously initiated to re-epithelialization by the infiltration of the FPM by fibroblasts, endothelial cells and macrophages [4,5].

In vitro wound healing models are advancing to 3D culture formats: these models strive to emulate cell interactions with clustered integrins

* Corresponding author. Faculty of Nursing, University of Campinas, UNICAMP, Tessalia Vieira de Camargo St, 126, 13083-887, Campinas, SP, Brazil.
E-mail addresses: pjaracarlos@gmail.com (C. Poblete Jara), earaujo@unicamp.br, pa.eliana@gmail.com (E. Pereira de Araujo).

https://doi.org/10.1016/j.bprint.2020.e00102
Received 1 July 2020; Received in revised form 18 September 2020; Accepted 21 September 2020

Please cite this article as: C. Poblete Jara et al., Demonstration of re-epithelialization in a bioprinted human skin equivalent wound model, Bioprinting, https://doi.org/10.1016/j.bprint.2020.e00102

positioned all around the cell membrane surface. However, engineering of the FPM-cell interface with a complement of different cell types does not re-capitulate the natural tissue healing process. This study expands the *in vitro* 3D skin equivalent co-culture platform to include the installation of a physiologically relevant FPM. This includes using the physiological ratio of macrophages to wound-site fibrin clot volume [6], the physiological concentration of fibrinogen used to form fibrin [7], and the spatial positioning of the re-epithelialization behavior of keratinocytes over FPM at the skin insult [3]. We include a physiological concentration of human fibrinogen and plasma Fibronectin (pFN) [7] and macrophages during the formation of fibrin. The resultant FPM simulates what typically exists during the animal initiation of granulation tissue construction beginning at about 24 h after injury [6]. This FPM fills the subepithelial wound space and within a surrounding store of keratinocytes derived from dermal tissue after a wound insult [3]. Our study presents the re-epithelialization and corresponding wound closure phenomena stimulated within a bio-printed tissue co-culture platform. A temporal comparison is made between dermal wound healing in the 3D bio-printed platform and a murine dermal wound model. This platform also serves as a basis for future granulation tissue formation studies.

2. Materials and methods

2.1. Experimental animals

Eight-week-old male C57BL/6J isogenic mice (n = 6) were obtained from the Breeding Animal Center of University of Campinas. Animals were maintained under pathogen-free conditions in individual cages on a 12:12 h dark:light cycle at 21–23 °C. Mice received chow and water *ad libitum*. Mice were anesthetized with intraperitoneal injections (according to body weight) using ketamine hydrochloride 80 mg/kg and xylazine chlorhydrate 8 mg/kg. Under general anesthesia, we created two full-thickness excisional wounds (6.0 mm diameter each) on the back of each animal, according to the mouse excisional wound splinted model protocol [8]. Animal experiments were approved by The Animal Ethical Committee at the University of Campinas, Brazil (certificate of approval no. 4467-1).

2.2. Animal photo documentation

Photo documentation of the wound healing process was obtained using a D610 Nikon digital camera (Nikon Systems, Inc., Tokyo, Japan). To ensure a similar distance from the camera to wound site, we used a stand and the same person took the photos.

2.3. Fibrin provisional matrix (FPM)–macrophage and FPM– human endothelial cells (HUVEC) bioink mixture formulations

We created two master solutions to produce a fibrin sealant delivering pFN and macrophages to the mechanical insult of the tissue culture. Mixture 1 contained whole population Fibrinogen (2.5 mg/ml) from normal human plasma, pFN (0.25 mg/ml) and 200 macrophages/μL or 500 HUVEC/μL in phosphate buffered saline (1 × PBS) suspension. Polymerization and protein crosslinking were catalyzed by Mixture 2, which contained thrombin (5 U/ml), calcium (5 mM), and FXIII (50 μg/ml). The same amount of PBS 1 × without cells was used as the control. To convert fibrinogen to fibrin, we used F2 (activated thrombin). All values are the final concentration in the fibrin polymer matrix.

2.4. FPM droplet studies for bio-ink formulation

FPM–macrophage mixture droplets (30 μL and 50 μL) were applied to autoclaved glass slides with 8-well silicone cell culture chamber wells (Ibidi) by first combining Mixture 1 and Mixture 2, with 200 macrophages/μL or 500 HUVEC/μL (Fig. 1a). After 15 min at 37 °C in a 7% CO_2 incubator, the polymerized/cross-linked FPM, 400 μL Iscove's Modified Dulbecco's Medium (IMDM) 20% Fetal Bovine Serum (FBS) medium was added to each well and cultured at 37 °C in a 7% CO_2 incubator for 7 days. The macroscopic FPM stability was evaluated using photographs taken 0 and 7 days after confection using a 1 × Olympus SZX16 microscope and cellSens Standards Software 1.11 (Olympus Corporation) with KL1500 LCD (Schott) 3200K top illumination.

2.5. Primary cell culture preparations

Primary keratinocytes and fibroblasts were harvested and isolated from human skin, as previously described [9], and under institutional review board approved #AAAB2666 protocol. About 2–4 passages of primary keratinocytes were made in culture in 37 °C in a 7% CO_2 incubator with KBM-Gold supplemented with KGM-Gold Single Quots (Lonza) medium to 80% confluence in 100 mm Petri dishes. Primary fibroblasts (passages 2–6) were achieved in culture in 37 °C in a 5% CO_2 incubator with DMEM High Glucose (Gibco™) with 10% FBS to 80% confluence in 100 mm Petri dishes. HUVEC cells were cultured to <8 passages in EBM-2 (Lonza) supplemented with EGM-2 Single Quots (Lonza). Bone marrow human macrophages (KG-1 ATCC® CCL246™, passages 2–5) were cultured in cell suspension flasks using IMDM medium (Gibco™ GlutaMAX™, HEPES) with 20% FBS. Macrophage suspensions were cultured at 37 °C in a 5% CO_2 incubator. We maintained macrophages at a concentration of less than 1 × 10^6 viable cells/mL, replacing the culture medium twice a week by centrifugation at 130×*g* for 7 min.

2.6. Preparation of printed human skin equivalent

Human skin equivalent (HSE) was prepared according to previous protocols [9]. In brief, Collagen I (2.5 mg/ml final solution), reconstitution buffer 10 × (Table 1), 1:1 HAM:F12 10×, and primary fibroblast (1.5 × 10^5 final solution) were mixed, gently homogenized, and then manipulated over a cooled metal rack at 4 °C. The solution was manipulated over a cooler cartridge head to 4–8 °C, and then applied to a printer bed at 4 °C with 2200 μL of the mixture into a 3 mL-printer cartridge. This collagen–fibroblast solution was extruded (Table 2) into each of the 6 wells of a 24 mm transwell (200 s of extrusion; pressure, 50 kpa; Nozzle type, 30G; no top piston). Next, more 1100 μL (130 s of extrusion; pressure, 50 kpa; Nozzle type, 30G; no top piston) were mixed in the previous transwell totaling 3000 μL per transwell (Fig. 2a). Then, 6-well plates were incubated in a 5% CO_2 incubator for 30 min at 37 °C to assure gel formation. Next, 0.5 ml of DMEM was applied to the top of each individual culturing skin equivalent, with 2 ml between the transwell and plate, while incubating for 1 h at 37 °C in the 5% CO_2.

After all DMEM medium was removed, 450 μL of 1:1 KGM gold/Creation medium containing 1 × 10^6 primary keratinocyte was extruded into the center of each transwell (55 s of extrusion time at 10 kPa pressure using Nozzle type 30G with no top piston). An additional 2 ml of 1:1 KGM gold/Creation medium was added underneath the transwell. Keratinocyte culturing on the top of each skin equivalent layer was maintained for 24 h to achieve cell adhesion at 37 °C in 7.5% CO_2. After 24 h, the keratinocyte media was discarded and each skin equivalent was detached from the transwell walls using a sterile surgical spatula and transferred to the air–liquid interphase, and placed in a deep 6-well plate using sterile forceps. Twelve milliliters of Creation Medium (Table 3) was added below each transwell, while avoiding bubble formation where these air–liquid interphase incubation samples were maintained at 37 °C in 5% CO_2. The Culture medium schedule (Table 3) was maintained for 10 days.

A surplus stock of 10% solutions for treating all cell layers is used for bubble formation management. The sterility of the print chamber was maintained by UV light within a HEPA-filtered chamber. The initial extrusion of collagen–fibroblast solutions used a Z0 position 1 mm above the transwell membrane, and with secondary extrusions set Z0 position 1 mm application above the previous dermal solution layer. Keratinocyte

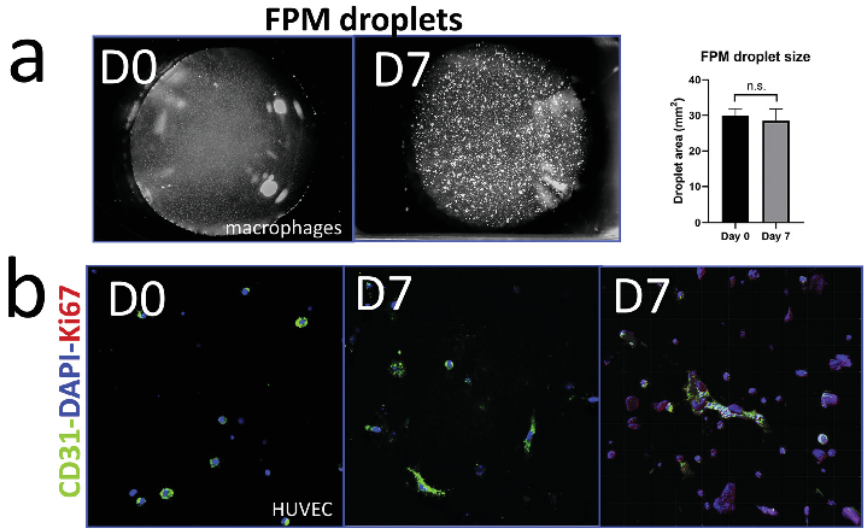

Fig. 1. Droplet experiment using the fibrin clot bioink. Day 0 and day 7 after the droplet experiment (a). CD31, DAPI, and Ki67 labeling using HUVECs in the fibrin clot on days 0 and 7 (b).

solution extrusion used a Z0 position of 1 mm, applied above the polymerized collagen–fibroblast gel layer.

2.7. Wound creation of the HSE

Full-thickness injuries were made at the middle of each HSE sample on day 11 using a sterile 4 mm or 7 mm dermal biopsy punch [10]. Each HSE was placed in a dry Petri dish after treatment with 10 ml of 1:1 Trypsin inhibitor and HEPES for 1 min to remove traces of culture medium. The injury motion consisted of a single, quick perpendicular stroke accompanied by one rotatory movement to free the punch from the HSE (Figs. 2a and 3a). The cleared wound HSE cavity was immediately filled with FPM–macrophage "bioink."

2.8. 8- printing fibrin clots in a wounded HSE

Macrophages were washed by centrifugation and suspended in 1 × PBS without calcium to eliminate medium traces. The fibrin clot–macrophage bioink containing Mix 1 (2.5 mg/ml F1, 0.25 mg/ml FN, 200 macrophages/μL, and 25 μM aprotinin) was pipetted into a bioprinter cartridge. Forty microliters of fibrin clot bioink was extruded (6 s of extrusion; 10 kpa; 30G needle; 20 mm/s; no top piston; 400 μL of Mixture 1 inside the cartridge) into the center of each wound. Ten microliters of Mixture 2 were manually applied on the top of each fibrin clot bioink (Fig. 2a and b). The cartridge head and printer bed were maintained at room temperature. We added aprotinin because, in a pilot experiment, the fibrin clot bioink was enzymatically digested during the first 24 h after wounding the skin (data no shown). All values are final concentration in the fibrin clot bioink. To extrude the fibrin clot bioink, we set the Z0 position to 1 mm above the transwell membrane, in the center of the injured HSE. This extrusion system could be easily replaced by a less restrictive method, such as the use of pipettes.

Table 1
Reconstitution buffer.

Ingredient	Concentration	Amount
NaOH	0.05 M	0.1 g
$NaHCO_3$	2.2%	1.1 g
HEPES	200 mM	2.38 g
Water (milli-Q)	–	q.s.p. 50 ml

2.9. HSE wound healing photo documentation

The healing process was evaluated through photographs taken 0, 2, 6, 8, and 10 days after wounding using a 1 × Olympus SZX16 microscope and cellSens Standard Software 1.11 (Olympus Corporation) with KL1500 LCD (Schott) 3200K top illumination. The wounded areas and re-epithelialized areas were analyzed with ImageJ Software (1.49v).

2.10. HSE culture medium refreshment for managing the transition between the inflammatory phase and proliferative phase cell culture environment

Newly prepared HSEs were maintained for 10 days before injury using "Creation medium." On day 10 of the pre-wounding phase, the HSE media was refreshed with "Pre-Wound Media" to clear traces of hydrocortisone and toxic choleric. The newly wounded HSE was then maintained for an additional 10 days using a sequence of media designed to mimic the natural transition from the inflammatory phase to the proliferative phase. The composition of the media regimen is detailed in Table 3. After injury, the HSE were refreshed with inflammatory phase media. On day 2 after wounding, 20 μg/ml (final medium concentration) of aprotinin [11] was added to manage FPM degradation. On day 3 post-injury, 50% of the inflammatory phase media (6 ml) was removed and replaced with an equal volume (6 ml) of proliferative phase medium to begin the transition to the proliferative phase. This gradual dilution by

Table 2
GCodes for bioprinting experiments.

Dermis	Dermis	Epidermis	Fibrin-clot
G0 X0 Y0	G0 X0 Y0	G0 X0 Y0	G0 X0 Y0
G0 Z15	G0 Z15	G0 Z15	G0 Z15
T1	T1	T1	T1
G1 Z0 F600	G1 Z0 F600	G1 Z1 F600	G1 Z1 F600
M400	M400	M400	M400
M750 T1	M750 T1	M750 T1	M750 T1
G4 S200.000	G4 S130.000	G4 S55.000	G4 S6.000
G1 Z10 F90	G1 Z10 F90	G1 Z10 F90	G1 Z10 F90
M400	M400	M400	M400
M751 T1	M751 T1	M751 T1	M751 T1
G0 Z15	G0 Z15	G0 Z15	G0 Z15
G1 X0 Y0	G1 X0 Y0	G1 X0 Y0	G1 X0 Y0

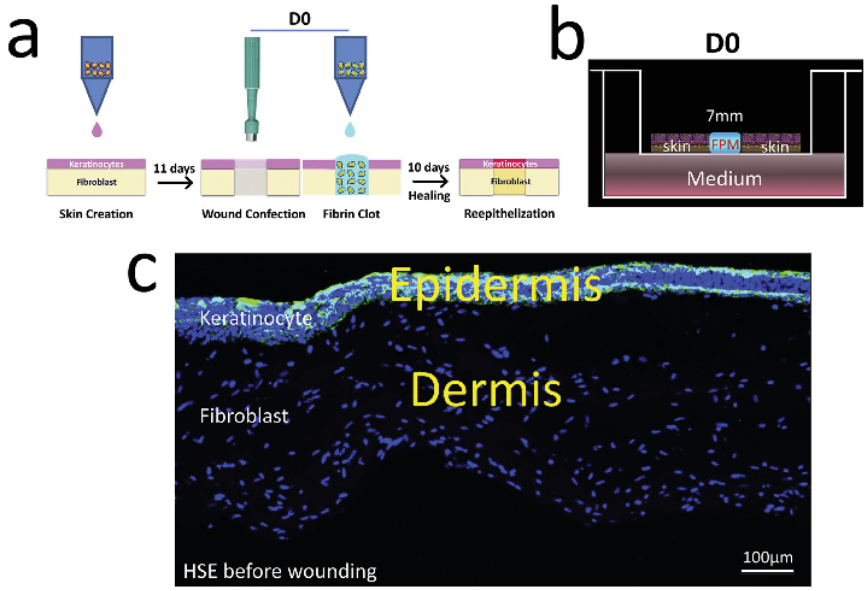

Fig. 2. Bioprinted human skin equivalent. Schematic representation of wound creation, wound confection, fibrin clot extrusion, and re-epithelization (a). Human skin equivalent in the air–liquid interphase (b). Cytokeratin-DAPI labeling in a skin equivalent after 10 days of air–liquid interphase (c).

proliferative phase medium occurred on day 6 and 9, with harvest occurring on day 10.

2.11. Immunofluorescence viability analysis of FPM–macrophage droplet bioink

To assess viability after 7 days in culture, IMDM medium was discarded from droplets of FPM–macrophage. These droplets were then fixed using 4% PFA for 15 min (7.5 pH; corrected with NaOH). PFA was discarded and fibrin clots were washed 3 × 15 min with PBS 1 × . Fibrin clots were blocked for 1 h with PBS 1 × , 0.05% Tween 20, and 5% BSA. Antibodies were prepared with PBS 1 × , 0.05% Tween 20, and 1% BSA solution. Anti-CD31 (1:50, ab28364) and Ki-67 (1:100, BD 610968) were maintained at 4 °C overnight. Secondary antibodies, Alexa 488 (1:200, ab150077) and Alexa 647 (1:200, ab150115), were maintained at 4C° overnight. Vectashield with DAPI was used for mounting and counter nuclear staining.

2.12. Immunofluorescence analysis of HSE and mice

After 10 days post wounding, the proliferative medium was discarded from the HSE, and these samples were fixed by 4% PFA (7.5 pH; corrected with NaOH), with incubation at 4 °C overnight. The PFA was discarded from the samples, followed by three 15-min washes with PBS 1 × . Samples were then embedded in Optimal Cutting Temperature (OCT) inside of a quadrangular prism foil form and quickly frozen using 100% ethanol in dry ice. Tissue sections (50 µM) were obtained using Microm HM505E Cryostat and placed in a glass slide. To remove OCT, tissue sections were washed for 30 min in distillated water, and peripheral marking was made using a hydrophobic marker. These tissue sections were blocked for 3 h with PBS 1 × , 0.05% Tween 20, and 5% BSA. *Anti*-K14 (1:200, ab7800) antibodies in PBS 1 × , 0.05% Tween 20, and 1% BSA solution were incubated with samples at 4 °C overnight and then warmed for 30 min at room temperature. Secondary antibody Anti-Mouse Alexa Fluor 488 (1:1000 Invitrogen A1101) was incubated with samples at room temperature for 4 h. VECTASHIELD with DAPI was then applied for counter nuclear staining, with images obtained by confocal microscopy (Zeiss LSM 510 Meta Spectral Confocal) at a penetration thickness of 20 µM. Mice wound-site immune cells were evaluated by Cd11b immunostaining. After 1-day post wounding, animal wounds samples were fixed by 4% PFA (7.5 pH) overnight. Section samples (20 µm) were incubated overnight with Cd11b primary antibody (sc28664,

Table 3
Culture medium schedule.

				Medium	
Reagent	Unit	Creation	Pre	Inflammatory	Proliferative
Medium treatment	days	10	1	2	8
Inflammatory:proliferative	ratio	–	–	–	1:1, 1:3, 1:7
DMEM	%	67.5	71	74.5	67.5
HAM/F12 1 ×	%	22.5	24	25	22.5
FBS	%	10	5	1	10
Aprotinin	µm	–	–	–	30
Toxin coleric	pM	100	–	–	50
Insulin	µg/mL	5	5	10	10
Apo-Transferin	µg/mL	5	5	5	5
Hydrocortisone	µg/mL	400	–	–	200
EGF	µg/mL	1	1	1	1

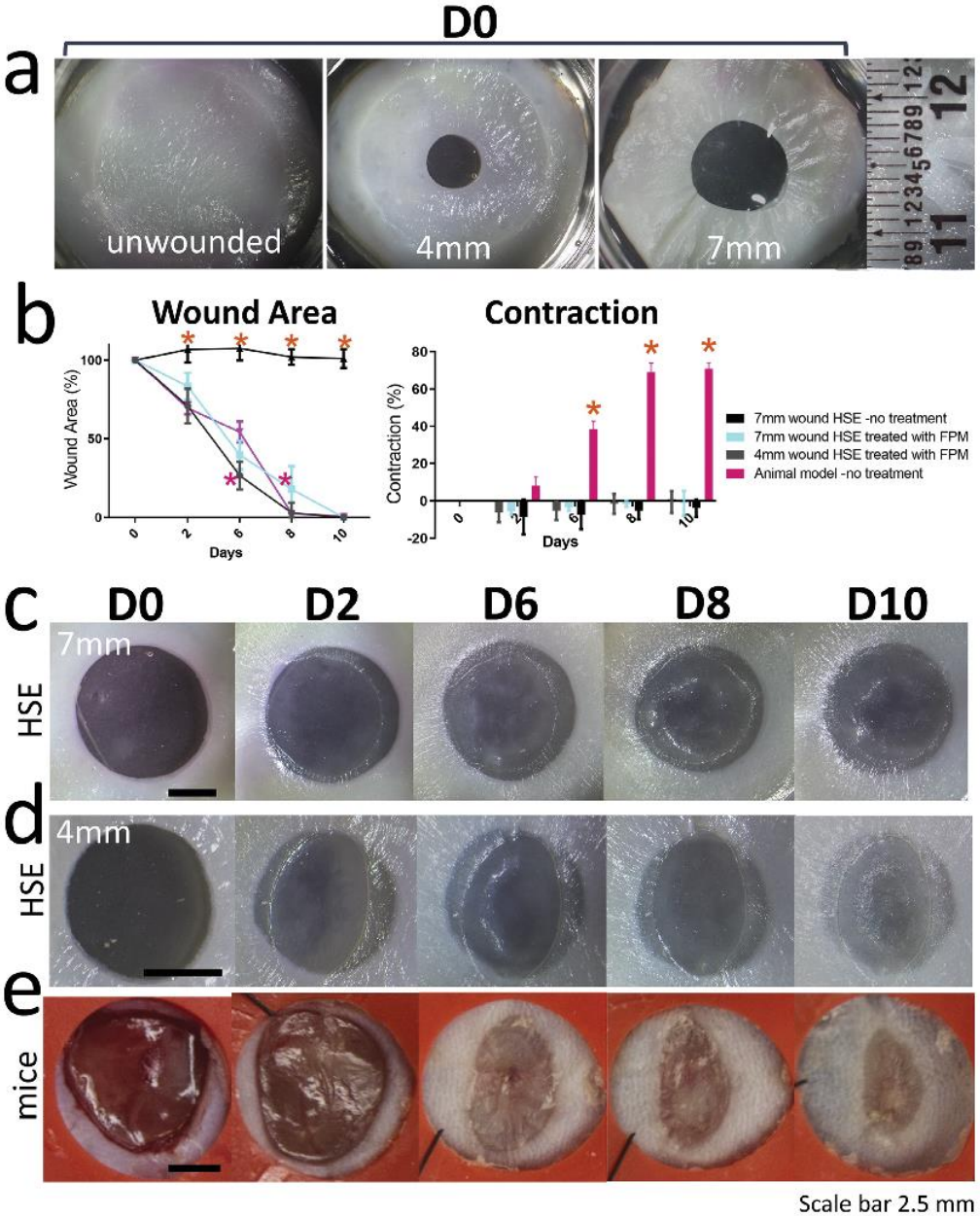

Fig. 3. Comparison of the wound healing process with human bioprinted skin and skin from an animal model. Human skin equivalents (n:6) versus animal healing (n:6) and wound contraction rate comparison graphs (b). Human skin equivalent 11 days post-creation (D0), unwounded, using a 4 mm or 7 mm biopsy punch (a). *In vitro* wound healing process (c–d) compared to the mice healing process (e) using 7 mm (c), 4 mm (d), and 6 mm (e) biopsy punches. The images are representative of three distinct experiments.

1:200). Section samples (20 μm) were incubated with secondary antibody Alexa 488 (A11008). VECTASHIELD with DAPI was used as mounting medium and nuclear counterstaining. Images were obtained using a confocal microscope (Leica TCS SP5 II).

2.13. Hematoxilin/eosin (HE) staining for histological imaging

After 10 days post wounding, HSE samples were fixed as above. Tissue sections were stained as follows using HE: 30-min soak in distillated water followed by a 2-min soak in hematoxylin (Sigma-Aldrich) and rinsing with tap water for 5 min. Tissue sections were stained with Eosin (Sigma-Aldrich) soak for 10 min, then the following ethanol drying sequence of 5 min soaks: 50% ethanol, 70% ethanol, 90% ethanol, 95% ethanol, 100% ethanol, fresh 100% ethanol, fresh 100% ethanol, Xylol I, and fresh Xylol II for the last 5 min. Slide assemblies were made with DPX mounting solution and a coverslip.

2.14. Full view tissue image reconstruction

To improve the accuracy of the analysis, we reconstructed the whole skin section (unwounded and injured sample). We used a Nikon digital camera (Nikon Systems, Inc., Tokyo, Japan) to take 10–20 adjacent

microphotographs (with 10–20% of common areas; 10 × objective) used to reconstruct every skin section. We used the Photomerge tool with the perspective layout in Adobe Photoshop (19.1v).

2.15. Wound area and wound contraction evaluation

We calculated wound area and contraction as previously described [12,13]. Wound Area (%) = [(wound area of day 0 – inner wound area of day x)/wound area of day 0] × 100. Wound contraction (%) = [(wound area of day 0 - outer visible wound border area of day x)/wound area of day 0] × 100.

3. Results

3.1. Fibrin stability and cell viability of the FPM–cell mixtures

Bioinks made containing Macrophages or HUVECs were observed for 7 days. The macroscopic matrix stability of the FPM–macrophage and FPM–HUVEC bioinks were stable for >7 days as judged by the lack of macroscopic matrix degradation (Fig. 1a–b). The Macrophages or HUVECs cultured within this FPM droplets were observed to proliferate for the entire 7-day culture period (Fig. 1b).

3.2. Re-epithelization over an injured HSE sealed with the FPM–macrophage bioink tissue sealant

The entire 21-day HSE and HSE wound healing sequence is schematically shown in Fig. 2a. HSEs maintained for 1 day while submerged and for 10 days in the air–liquid interphase were harvested and histologically visualized. The keratinocyte layer was observed on top of the fibroblast–collagen layer (Fig. 2c). A typical unwounded HSE is shown in Fig. 3a (left). Also, two different wound sizes were made using a 4 mm (Fig. 3a, center) and a 7 mm (Fig. 3a, right) biopsy punch. The wounds were sealed with just FPM (Supplementary material) and FPM–macrophage bioink after injury. After 8 days post wounding, the 4 mm injured HSE showed complete reepithelization (Fig. 3b, d). After 10 days post wounding, the 7 mm injured area showed complete reepithelization (Fig. 3b and c). This contrasted the wounded HSE without the FPM–macrophage bioink treatment, which showed an inhibited wound closure (Fig. 3b). Both 4 mm and 7 mm wounds (Fig. 3c and d) were observed to mimic the macroscopic animal wound closure (Fig. 3b–e). Next, we evaluated if our HSE wound model follows the mice wound contraction process [14]. In this way, 4 mm and 7 mm wounds showed different wound contraction starting from 6 day after wounding (Fig. 3b, right).

During mammalian skin wound healing, keratinocytes proliferate and

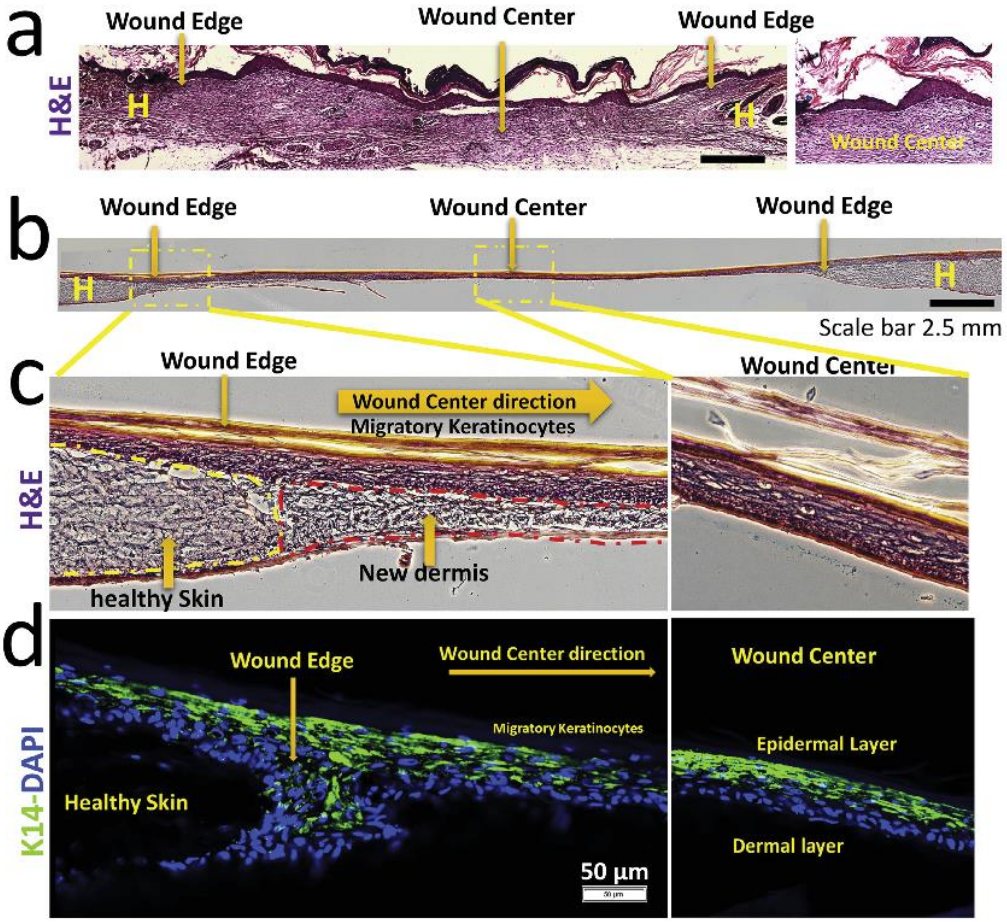

Fig. 4. Microscopic evaluation of the wound healing process. Representative images of wound sections on day 10 post-injury with hematoxylin–eosin staining. A full-view reconstruction approach was used for section analysis (a–b). Animal wound sections (a) and skin equivalent wound sections (b). 10 Days after fibrin matrix extrusion, keratinocytes migrated from the healthy skin to the new dermis, reaching the wound center (c–d). Cytokeratin staining for keratinocytes (green) and DAPI-labeling nuclei (blue). Immunofluorescent sections showed keratinocyte migration from the healthy skin (d, left) to the new dermis (d, right). The yellow "H" in the figure indicates healthy skin. (For interpretation of the references to colour in this figure legend, the reader is referred to the Web version of this article.)

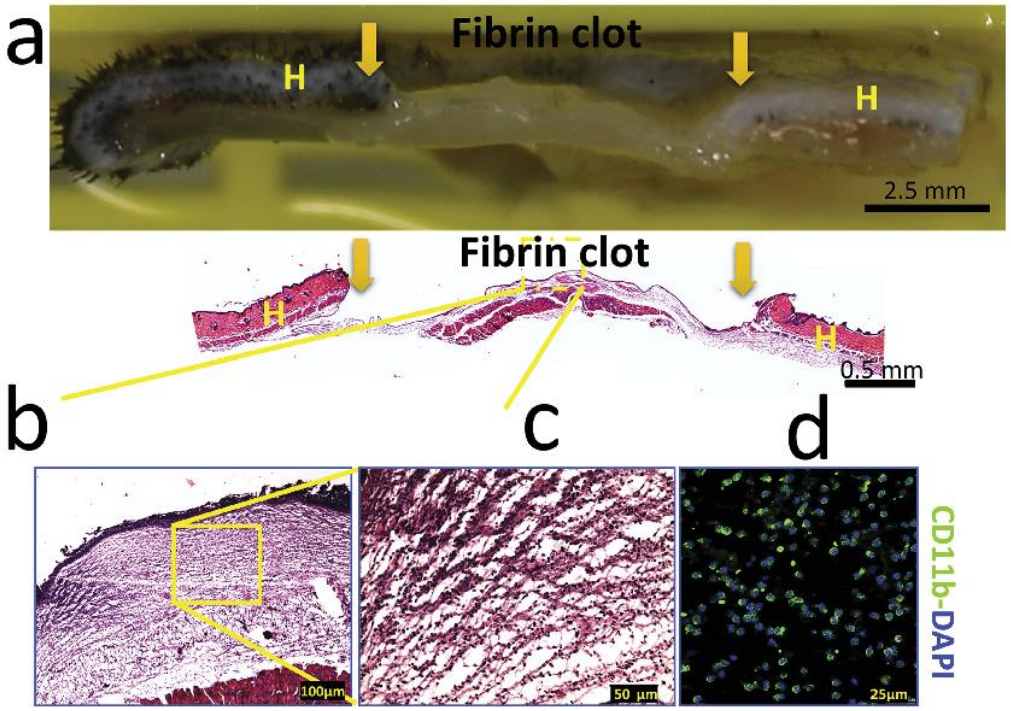

Fig. 5. Macroscopic and microscopic evaluation of the fibrin clot structure. Representative macrophotograph of the animal fibrin clot on the top (a) and histological full view reconstruction on bottom (b). Yellow arrows indicate wound edges, and the yellow "H" indicates healthy skin. Representative fibrin clot sections on day 1 post-injury using hematoxylin–eosin staining and immunofluorescence showing immune cell infiltration into the fibrin clot (b–d). (For interpretation of the references to colour in this figure legend, the reader is referred to the Web version of this article.)

migrate from the interfollicular epidermis to the wound center [2,3]. Our results suggest that keratinocytes migrated from the wound edge to the wound center using the fibrin clot–macrophage bioink as a platform (Fig. 4c and d). In the same way as the animal model (Fig. 4a), wounded HSE model (Fig. 4b) regenerated a new layer in the wound center. The re-epithelization in the wounded HSE model is dependent on the initial wound size and the presence of hemostatic fibrin clot bioink (Fig. 3b).

3.3. *Bioprinted HSE mimics epidermal differentiation of the animal healing process after injury*

Microscopic evaluation of the HSE suggested that keratinocytes within the wound center could differentiate. After 10 days post wounding, a new stratum corneum appear to be formed (Fig. 4c, right) in the wound center of the HSE. A similar differentiation process was observed in the wound center of the animal model (Fig. 4a, right).

4. Discussion

Our study demonstrates *in vitro* a 3-D wound healing model incorporating a bioprinted human skin equivalent, a mechanical injury of that skin facsimile, and an FPM–macrophage installed that seals the wound. Importantly, the FPM utilizes the intimate contact of fibrin, pFN, and macrophages to sustain macrophage viability that normally includes the catalysis of M1 to M2 *trans*-differentiation. This FPM-viable-macrophage mixture was stable for 7 days and installed as a "bioink" using an extrusion system. Once installed the FPM–macrophage mixture served to guide keratinocytes for emulating the wound closure portion of the mammalian skin repair process. For example, on day 1 after mouse dermal injury, the fibrin clot structure presented a high infiltration of immune cells (Fig. 5b–d) as previously shown [6]. The FPM-macrophage sealed HSE wound seeks to establish a structural platform for normal keratinocyte migration. This contrasts previous *in vitro* wound healing models that lack a FPM [15–18], fibroblast incorporation into a dermal layer [19], and a corresponding epidermal layer [20]. Other scaffolds employed in past models were made from non-fibrin nanofibers [21], collagen– glycosaminoglycan, commercially available collagen matrices, or collagen–elastin materials [22].

Normal FPM integrin engagement [1,23] uses Ita5, α5β1, or other fibronectin alpha class receptors belonging to the (RGD)-binding class integrins. These integrins bind to extracellular matrix proteins, such as fibronectin and fibrinogen [24], and are expressed in keratinocytes and fibroblasts. The α5 integrin class is expressed by keratinocytes only after a skin injury and at the wound edge on day 1 post wounding and then steadily progresses to decreased levels during migration [2]. Previous *in vitro* cell cultures have used supraphysiological concentrations of fibrinogen (F1) without fibrin suspension of macrophages [10]. Our FPM formulation used a physiologic 10:1 ratio of purified F1 and pFN with a suspension of macrophages to promote keratinocyte wound surface migration. Future formulations will use pFN nanostructures incorporated into the fibrin network.

As a 3D co-culture model, we purposely altered the culture media environment to emulate the progression from an inflammatory to a proliferative healing phase environment. Table 3 shows the transition of this culture media achieved by sequential media dilution over day 3 to day 10 of HSE healing. For example, we decreased the insulin and FBS concentrations during the wound inflammatory phase and increased the concentration during the proliferative phase. The gradual dilution of the initial inflammatory media by proliferative media every 2.5 days was designed to empirically taper the cytokines and microRNA levels, as well as temporally changed the growth factor signaling described in the wound healing process [2,4–6,25,26]. The need for an inflammatory phase and a transitional dilution series of media typical of inflammation to one typical of proliferation has been documented. In the normal

wound healing process, keratinocytes migrate to the wound center at the end of the inflammatory phase [2,3]. Furthermore, *in vitro* models typically show keratinocyte migration immediately to the mimetic wound center after injury [10]. Importantly, the re-epithelialization phenomena over the HSE, in this case, displayed stratification and differentiation where prior *in vitro* models did not show stratum corneum formation [10].

A healthy wound healing pathway requires macrophages engagement with the FPM [4,5]. Initially M1 phenotype macrophages promote an inflammatory response at the wound site. The inflammatory phase that is needed for the process of debridement is normally resolved by M1 apoptosis and with a *trans*-differentiation component of M1 to M2 macrophages [4,5]. Thereafter fibroblast colonization results in the secretion of collagen based provisional scaffolding to stage angiogenesis by endothelial cells (ECs). In previous reports, we isolated specific fractions of pF1/pFN mixture [27,28]. Also, we demonstrated that specific fractions of pF1/pFN polymeric matrix accelerated wound healing process in healthy mice [13]. Here, we analyzed the first level compatibility of FPM-EC bioink formulation where EC viability was observed. Based on the feasibility demonstrated here for FPM-macrophage bioink installation into the HSE wound site, our future work will explore the engineering of a vascularized granulation by EC and fibroblasts co-culture using FPM that are more specialized for EC colonization. Importantly, the current model formulation produced no fibrotic scar tissue structures where future studies will strive to develop capillary structures within a sub-epithelial granulation. In summary, the 3D bioprinted dermal wound healing model incorporating FPM-macrophage bioink provides an *in vitro* co-culture study platform for staging re-epithelialization by keratinocytes. These future studies of an analogous subepithelial healing pathway is envisioned using co-culture of keratinocytes, fibroblasts, endothelial cells, and macrophages.

We visualize several benefits of using bioprinting approach for construct our human skin equivalent wound model. For example, as a candidate platform for pharmacological tests and dermatological research, future versions may improve throughput and scalability in the production of equal wounded skin samples. Indeed, the generation of a precise and reproducible *in vitro* wound model is essential to guarantee comparable results between different test runs [17]. Beside the generation of a bioprinted wound healing model in a HSE itself is challenging, but also to establish a highly standardized wound sealant application by hand is awkward. In the same way, a previous report showed the benefits of using a bioprinting sealant approach in the injured site. The Albanna and colleagues described a mobile skin bioprinting system that provides on-site management of wounded skin. The authors showed a wound model sealed with different layers of dermal fibroblasts and epidermal keratinocytes in a hydrogel bioink which accelerated re-epithelialization [29]. The proof-of-concept here showed using a bioprinting approach facilitated the precise delivery of our macrophage bioink directly into an injured area, replicating the instantaneous natural installation of the fibrin clot structures.

5. Conclusion

The FPM here is analogous to a tissue sealant composed of a physiologic mixture of macrophage/fibrinogen/fibronectin that is applied to a mechanically wounded, bioprinted dermal tissue culture. This treatment is shown to temporally synchronize a normal re-epithelization process by keratinocyte migration from the surrounding tissue and over the top of the FPM. Both the keratinocyte migration and wound closure phenomena were demonstrated by the FPM-macrophage tissue sealant mixture.

Author disclosure and ghostwriting

No competing financial interests exist. No ghostwriters were used to write this article.

Financial support

Coordination of Improvement of Higher-Level Personnel of Brazil (CAPES).

CRediT authorship contribution statement

Carlos Poblete Jara: Conceptualization, Formal analysis, Methodology, Investigation, Writing - original draft. **Carolina Motter Catarino:** Methodology. **Yuguo Lei:** Validation, Data curation, Writing - review & editing. **Lício Augusto Velloso:** Formal analysis, Writing - review & editing, Supervision. **Pankaj Karande:** Validation, Formal analysis, Resources, Funding acquisition. **William H. Velander:** Validation, Data curation, Writing - original draft, Writing - review & editing. **Eliana Pereira de Araujo:** Conceptualization, Methodology, Formal analysis, Resources, Writing - original draft, Writing - review & editing, Supervision.

Declaration of competing interest

The authors declare that they have no known competing financial interests or personal relationships that could have appeared to influence the work reported in this paper.

Acknowledgments and funding sources

The review and wound healing research in the authors' laboratory were supported by Coordination for the Improvement of Higher Education Personnel (88882.434714/2019-01 and 88881.190035/2018-01). This study was financed in part by the Coordenação de Aperfeiçoamento de Pessoal de Nível Superior, Brasil (CAPES), Finance Code 001 and CNPQ 203415/2014-0.

Appendix A. Supplementary data

Supplementary data to this article can be found online at https://doi.org/10.1016/j.bprint.2020.e00102.

References

[1] G.C. Gurtner, S. Werner, Y. Barrandon, M.T. Longaker, Wound repair and regeneration, Nature 453 (2008) 314–321, https://doi.org/10.1038/nature07039.
[2] M. Aragona, S. Dekoninck, S. Rulands, S. Lenglez, G. Mascré, B.D. Simons, C. Blanpain, Defining stem cell dynamics and migration during wound healing in mouse skin epidermis, Nat. Commun. 8 (2017), 14684, https://doi.org/10.1038/ncomms14684.
[3] S. Park, D.G. Gonzalez, B. Guirao, J.D. Boucher, K. Cockburn, E.D. Marsh, K.R. Mesa, S. Brown, P. Rompolas, A.M. Haberman, Y. Bellaïche, V. Greco, Tissue-scale coordination of cellular behaviour promotes epidermal wound repair in live mice, Nat. Cell Biol. 19 (2017) 155–163, https://doi.org/10.1038/ncb3472.
[4] C.F. Guerrero-Juarez, P.H. Dedhia, S. Jin, R. Ruiz-Vega, D. Ma, Y. Liu, K. Yamaga, O. Shestova, D.L. Gay, Z. Yang, K. Kessenbrock, Q. Nie, W.S. Pear, G. Cotsarelis, M.V. Plikus, Single-cell analysis reveals fibroblast heterogeneity and myeloid-derived adipocyte progenitors in murine skin wounds, Nat. Commun. 10 (2019) 650, https://doi.org/10.1038/s41467-018-08247-x.
[5] M. Sinha, C.K. Sen, K. Singh, A. Das, S. Ghatak, B. Rhea, B. Blackstone, H.M. Powell, S. Khanna, S. Roy, Direct conversion of injury-site myeloid cells to fibroblast-like cells of granulation tissue, Nat. Commun. 9 (2018) 936, https://doi.org/10.1038/s41467-018-03208-w.
[6] T. Muliaditan, J. Caron, M. Okesola, J.W. Opzoomer, P. Kosti, M. Georgouli, P. Gordon, S. Lall, D.M. Kuzeva, L. Pedro, J.D. Shields, C.E. Gillett, S.S. Diebold, V. Sanz-Moreno, T. Ng, E. Hoste, J.N. Arnold, Macrophages are exploited from an innate wound healing response to facilitate cancer metastasis, Nat. Commun. 9 (2018) 2951, https://doi.org/10.1038/s41467-018-05346-7.
[7] D.J. Geer, S.T. Andreadis, Fibrin-mediated delivery of KGF in 2D and 3D models of wound regeneration, in: Proc. Second Jt. 24th Annu. Conf. Annu. Fall Meet. Biomed. Eng. Soc. Eng. Med. Biol., vol. 1, 2002, pp. 481–483, https://doi.org/10.1109/IEMBS.2002.1136906.
[8] X. Wang, J. Ge, E.E. Tredget, Y. Wu, The mouse excisional wound splinting model, including applications for stem cell transplantation, Nat. Protoc. 8 (2013) 302–309, https://doi.org/10.1038/nprot.2013.002.
[9] C.M. Catarino, T. do Nascimento Pedrosa, P.C. Pennacchi, S.R. de Assis, F. Gimenes, M.E.L. Consolaro, S.B. de Moraes Barros, S.S. Maria-Engler, Skin corrosion test: a comparison between reconstructed human epidermis and full thickness skin

models, Eur. J. Pharm. Biopharm. Off. J. Arbeitsgemeinschaft Pharm. Verfahrenstechnik EV. 125 (2018) 51–57, https://doi.org/10.1016/j.ejpb.2018.01.002.

[10] K. Iyer, Z. Chen, T. Ganapa, B.M. Wu, B. Tawil, C.S. Linsley, Keratinocyte migration in a three-dimensional in vitro wound healing model Co-cultured with fibroblasts, Tissue Eng. Regen. Med. 15 (2018) 721–733, https://doi.org/10.1007/s13770-018-0145-7.

[11] Q. Ye, G. Zünd, P. Benedikt, S. Jockenhoevel, S.P. Hoerstrup, S. Sakyama, J.A. Hubbell, M. Turina, Fibrin gel as a three dimensional matrix in cardiovascular tissue engineering, Eur. J. Cardio-Thorac. Surg. Off. J. Eur. Assoc. Cardio-Thorac. Surg. 17 (2000) 587–591, https://doi.org/10.1016/s1010-7940(00)00373-0.

[12] A.M. Jorgensen, M. Varkey, A. Gorkun, C. Clouse, L. Xu, Z. Chou, S.V. Murphy, J. Molnar, S.J. Lee, J.J. Yoo, S. Soker, A. Atala, Bioprinted skin recapitulates normal collagen remodeling in full-thickness wounds, Tissue Eng. 26 (2019) 512–526, https://doi.org/10.1089/ten.tea.2019.0319.

[13] C.P. Jara, O. Wang, T. Paulino do Prado, A. Ismail, F.M. Fabian, H. Li, L.A. Velloso, M.A. Carlson, W. Burgess, Y. Lei, W.H. Velander, E.P. Araújo, Novel fibrin-fibronectin matrix accelerates mice skin wound healing, Bioact. Mater. 5 (2020) 949–962, https://doi.org/10.1016/j.bioactmat.2020.06.015.

[14] L. Chen, R. Mirza, Y. Kwon, L.A. DiPietro, T.J. Koh, The murine excisional wound model: contraction revisited, Wound Repair Regen, Off. Publ. Wound Heal. Soc. Eur. Tissue Repair Soc. 23 (2015) 874–877, https://doi.org/10.1111/wrr.12338.

[15] M. Breetveld, C.D. Richters, T. Rustemeyer, R.J. Scheper, S. Gibbs, Comparison of wound closure after burn and cold injury in human skin equivalents, J. Invest. Dermatol. 126 (2006) 1918–1921, https://doi.org/10.1038/sj.jid.5700330.

[16] Y. Marquardt, P.M. Amann, R. Heise, K. Czaja, T. Steiner, H.F. Merk, C. Skazik-Voogt, J.M. Baron, Characterization of a novel standardized human three-dimensional skin wound healing model using non-sequential fractional ultrapulsed CO2 laser treatments, Laser Surg. Med. 47 (2015) 257–265, https://doi.org/10.1002/lsm.22341.

[17] A. Rossi, A. Appelt-Menzel, S. Kurdyn, H. Walles, F. Groeber, Generation of a Three-Dimensional Full Thickness Skin Equivalent and Automated Wounding, 2015, https://doi.org/10.3791/52576.

[18] K. Safferling, T. Sütterlin, K. Westphal, C. Ernst, K. Breuhahn, M. James, D. Jäger, N. Halama, N. Grabe, Wound healing revised: a novel reepithelialization mechanism revealed by in vitro and in silico models, J. Cell Biol. 203 (2013) 691–709, https://doi.org/10.1083/jcb.201212020.

[19] I.M. Herman, A. Leung, Creation of human skin equivalents for the in vitro study of angiogenesis in wound healing, Methods Mol. Biol. Clifton NJ 467 (2009) 241–248, https://doi.org/10.1007/978-1-59745-241-0_14.

[20] B. Lombardi, C. Casale, G. Imparato, F. Urciuolo, P.A. Netti, Spatiotemporal evolution of the wound repairing process in a 3D human dermis equivalent, Adv. Healthc. Mater. 6 (2017), https://doi.org/10.1002/adhm.201601422.

[21] A. Schneider, J.A. Garlick, C. Egles, Self-assembling peptide nanofiber scaffolds accelerate wound healing, PloS One 3 (2008), https://doi.org/10.1371/journal.pone.0001410 e1410.

[22] J.W.J. van Kilsdonk, E.H. van den Bogaard, P.A.M. Jansen, C. Bos, M. Bergers, J. Schalkwijk, An in vitro wound healing model for evaluation of dermal substitutes, Wound Repair Regen. Off. Publ. Wound Heal. Soc. Eur. Tissue Repair Soc. 21 (2013) 890–896, https://doi.org/10.1111/wrr.12086.

[23] S. Dekoninck, C. Blanpain, Stem cell dynamics, migration and plasticity during wound healing, Nat. Cell Biol. 21 (2019) 18–24, https://doi.org/10.1038/s41556-018-0237-6.

[24] J. Schnittert, R. Bansal, G. Storm, J. Prakash, Integrins in wound healing, fibrosis and tumor stroma: high potential targets for therapeutics and drug delivery, Adv. Drug Deliv. Rev. 129 (2018) 37–53, https://doi.org/10.1016/j.addr.2018.01.020.

[25] A. Simões, L. Chen, Z. Chen, Y. Zhao, S. Gao, P.T. Marucha, Y. Dai, L.A. DiPietro, X. Zhou, Differential microRNA profile underlies the divergent healing responses in skin and oral mucosal wounds, Sci. Rep. 9 (2019) 7160, https://doi.org/10.1038/s41598-019-43682-w.

[26] S. Joost, T. Jacob, X. Sun, K. Annusver, G. La Manno, I. Sur, M. Kasper, Single-cell transcriptomics of traced epidermal and hair follicle stem cells reveals rapid adaptations during wound healing, Cell Rep. 25 (2018) 585–597, https://doi.org/10.1016/j.celrep.2018.09.059, e7.

[27] F.M. Fabian, A.E.A. Ismail, O. Wang, Y. Lei, W.H. Velander, Reversible associations between human plasma fibronectin and fibrinogen γγ' heterodimer observed by high pressure size exclusion chromatography and dynamic light scattering, Anal. Biochem. 598 (2020), 113701, https://doi.org/10.1016/j.ab.2020.113701.

[28] A.E.A. Ismail, F.M. Fabian, O. Wang, Y. Lei, M.A. Carlson, W.H. Burgess, W.H. Velander, The isolation of a plasma-derived γγ' fibrinogen: fibronectin mixture that forms a novel polymeric matrix, Process Biochem. 75 (2018) 257–265, https://doi.org/10.1016/j.procbio.2018.09.013.

[29] M. Albanna, K.W. Binder, S.V. Murphy, J. Kim, S.A. Qasem, W. Zhao, J. Tan, I.B. El-Amin, D.D. Dice, J. Marco, J. Green, T. Xu, A. Skardal, J.H. Holmes, J.D. Jackson, A. Atala, J.J. Yoo, In situ bioprinting of autologous skin cells accelerates wound healing of extensive excisional full-thickness wounds, Sci. Rep. 9 (2019) 1856, https://doi.org/10.1038/s41598-018-38366-w.

Glossary

FPM: fibrin provisional matrix
HSE: human skin equivalent
FXIII: coagulation factor XIII
3D: three-dimensional
pFN: plasma Fibronectin
F1: fibrinogen
pF1: plasma fibrinogen
F2: Thrombin
HUVEC: Primary Human Umbilical Vein Endothelial Cells
DMEM: Dulbecco's Modified Eagle Medium
KGM: Keratinocyte Growth Medium
FBS: Fetal bovine serum
IMDM: Iscove Modified Dulbecco Media
HEPA: High Efficiency Particulate Air
PFA: Paraformaldehyde
OCT: Optimal Cutting Temperature
DAPI: 4′,6-diamidino-2-phenylindole
RGD: tripeptide Arginine, Glycine, and Aspartate
M1: macrophage type 1
M2: macrophage type 2
ECs: endothelial cells
CAPES: Coordenação de Aperfeiçoamento de Pessoal de Nível Superior

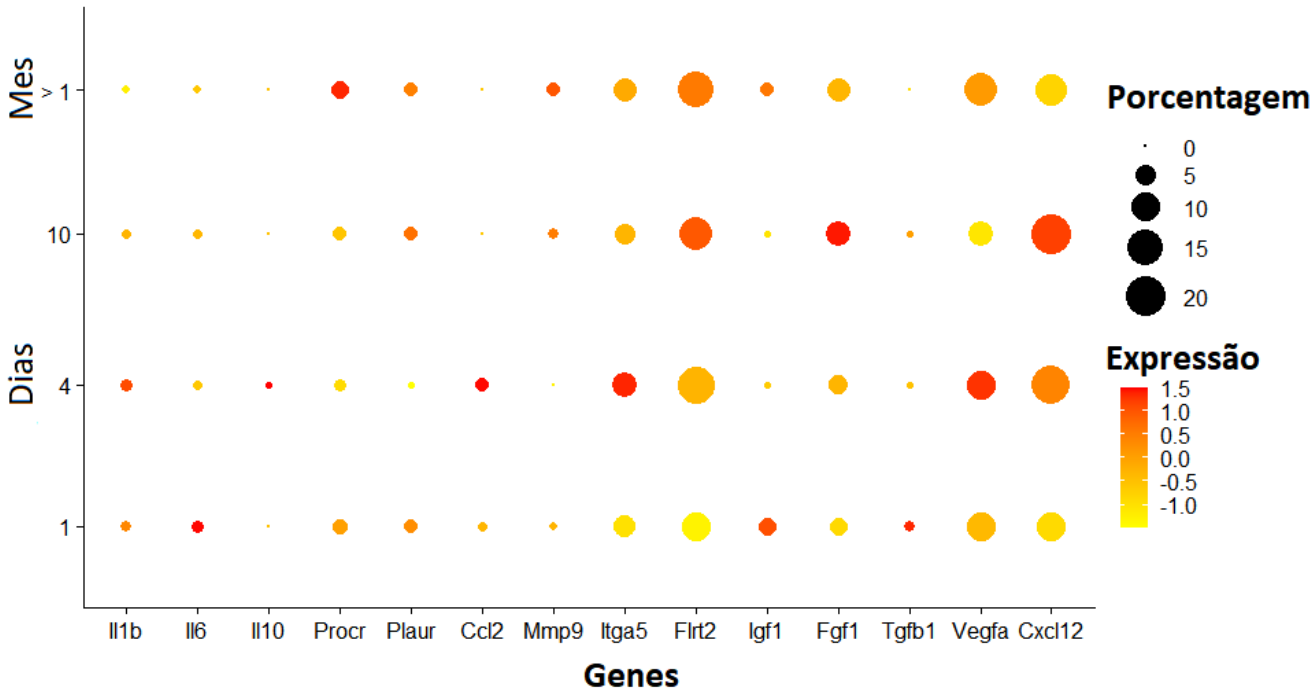

Figura 3: Gráfico de pontos (Dotplot) de feridas de pele de camundongos *wildtype.* Os genes foram escolhidos do PCR dos genes diferencialmente expressos dos animais tratados com o Complexo F1 gama prima e FN, e com a mistura F1:FN. Transcriptoma público (82) de ferida de pele de camundongo extraída nos dias 1, 4, 10 e 1 mês após lesão. A produção e a análise de dados foram realizadas usando o pacote Seurat R 3.1. Figura construída pelo autor.

Análise transcriptômica usando Sequenciamento de célula única (Single Cell RNA-sequencing) de células da camada epidérmica, mostrou que integrina α5 (Itga5) é altamente expressa no dia 4 após a lesão e diminui a sua expressão com o passar dos dias até a fase de remodelação (Figura 3). A Proteína Transmembrana 2 Rica em Leucina e Fibronectina (Flrt2) demostrou incrementar a sua expressão no dia 4 alcançando a sua máxima no dia 10 após lesão e diminui a sua expressão com

o passar dos dias até a fase de remodelação (Figura 3). O gene que codifica para o receptor da proteína C (Procr) é altamente expresso por células da camada epidérmica na fase de remodelação tardia (Figura 3). A Interleucina 6 é altamente expressa no primeiro dia após a lesão, mas diminui sua expressão na fase proliferativa e de remodelação (Figura 3). FGF1 mostrou baixa expressão na fase inflamatória e um aumento progressivo na fase proliferativa e de remodelação inicial (Figura 3). Vegf-α mostrou aumentar sua expressão nas células da camada epidérmica na fase de proliferação e criação de tecido de granulação (Figura 3). O gene Cxcl12, que codifica para o Fator 1 Derivado de Célula Estromal (SDF-1) inicia sua expressão no dia 4 após lesão, alcançando sua máxima expressão no dia 10, para logo diminuir até a fase de remodelação final (Figura 3). O gene Ccl2, que codifica para a Proteína quimioatraente de monócitos 1 (MCP-1) é expresso na fase inflamatória, mas sua expressão diminui na fase proliferativa e de remodelação (Figura 3).

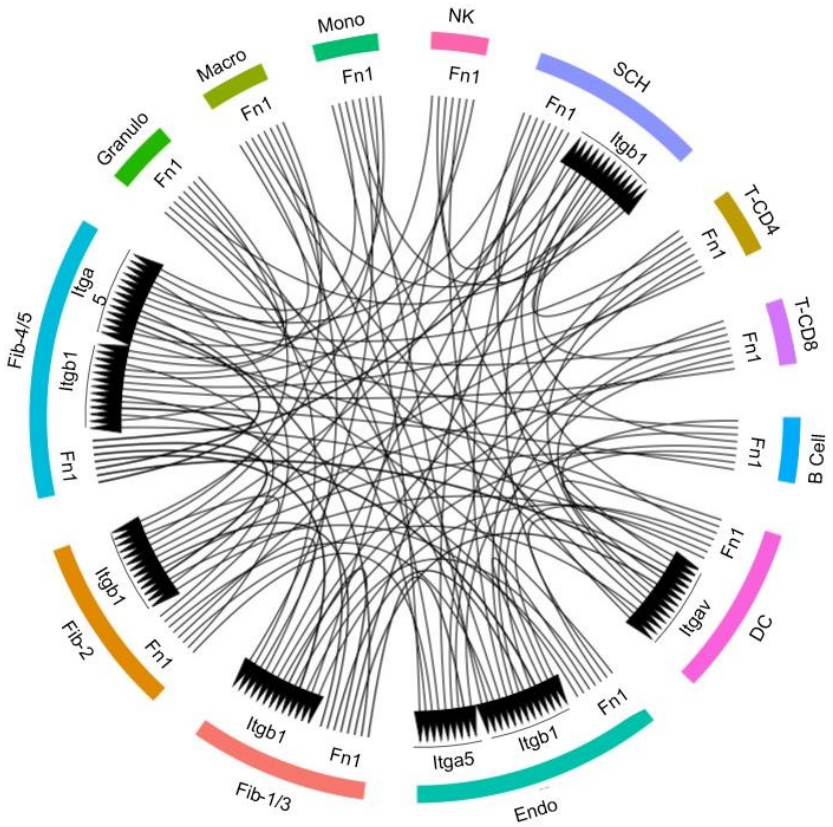

Figura 4: Interatômica de pares receptor-ligante de feridas de pele de camundongo de 12 dias após lesão. Ponta de flecha representa o tipo celular produtor do receptor para o determinado ligante. Início da flecha representa o tipo celular produtor do ligante. DC: células dendríticas, B cell: Linfócitos B, T-CD8: Linfócito T CD8+, T-CD4: Linfócito T CD4+, SCH: Células Shwann, NK: Natural killers, Mono: monócitos, Macro: macrófagos, Granulo: Granulócitos, Fig4/5: mix de fibroblastos 4 e 5, Fig2: fibroblastos 2. Fig1/3: mix de fibroblastos 1 e 3, Endo: células endoteliais. Interactoma público (83) de ferida de pele de camundongo extraída no dia 12 após lesão. A produção e a análise de dados foram realizadas usando iTalk e o Pacote Seurat R 3.1 e. Figura construída pelo autor.

Análise Interatômica usando Sequenciamento de célula única (Single Cell RNA-sequencing) de células da camada dérmica, mostrou que em feridas de pele de camundongo 12 dias após lesão todos os tipos celulares aqui mostrados codificam o gene de Fibronectina (FN1), embora, só as células endoteliais e o mix de fibroblastos 4 e 5 codificam o gene de receptor específico para a integrina alfa 5 (Itga5). Outra integrina capaz de se acoplar ao FN é a integrina beta 1 ou Itgb1(85-87). Análise interatômica mostrou que tanto células endoteliais, o mix de fibroblastos do 1 até o 5, como também as Células Shwann codificam o gene para a integrina beta 1, doze dias após lesão. Por outro lado, Células dendríticas da ferida interagem com a Fibronectina por meio da Integrina Subunidade Alfa V, ou Itgav 12 dias após lesão (Figura 4).

DISCUSSÃO GERAL

A evolução diversificou as defesas dos vertebrados selecionando células imunes adaptativas específicas para determinadas famílias de antígenos, como também expandiu um sistema de coagulação para defesa e reparo tecidual (88). Em um contexto de vida ou morte, uma resposta rápida na contenção da perda de sangue, é uma característica vital. Especificamente, os animais têm a capacidade de responder rapidamente frente a perda de sangue, criando um tampão fibroso, ocluindo um ferimento em segundos (88, 89). A afinação evolutiva levou os humanos para o desenvolvimento de receptores de superfície celular, como o fator tissular (88, 89), crucial para iniciar uma serie de ativações consecutivas ou “efeito cascata” para a formação do tampão de fibrina. Mas não só essa afinação evolutiva tem a potência de ativar a cascata da coagulação. Os humanos preservam algumas características dos seus ancestres invertebrados. Uma resposta imune inata coagulante é desencadeada por bactérias e lesões, similar como acontece com a hemolinfa dos insetos (88, 89). Hoje, nós entendemos esses dois braços evolutivos da cascata da coagulação que possuem os mamíferos, como Ativação Intrínseca e Extrínseca (88). Por outro lado, existem proteínas do sistema da coagulação conservadas entre animais. Um exemplo disso, são as transglutaminases que parecem contribuir para a coagulação em todos os invertebrados como também o seu homólogo, o fator XIII no humano (89).

A fibrina derivada do plasma tem uma proporção de 10:1 de F1 para FN (90). Em um coágulo sanguíneo, a fibrina e a fibronectina plasmática são reticuladas covalentemente pelo fator XIII ativado para formar multímeros de fibrina e FN (91). O fator XIII ativado pertence à família das transglutaminases e é necessário para

estabilizar o coágulo pela união de complexos de fibrina-fibrina por meio de ligações covalentes entre glutaminas e lisinas (89).

A coagulação do sangue é iniciada quando o fator tissular é exposto ao sangue após lesão. O fator VII, uma proteína circulante no sangue, liga-se ao fator tissular agora exposto e, após sua ativação (FVIIa), o complexo FVIIa / fator tissular ativa os fatores X e IX (92). E assim, como se fosse uma “bola de neve”, uma proteína ativa especificamente uma outra, um efeito cascata de serina proteases que culminam na ativação da trombina. Embora a trombina possua um receptor específico de membrana celular, quando ativada, esta cliva o monômero fibrinogênio em monômeros fibrinas os quais se acoplam um com os outros iniciando a formação da matriz de fibrina ou coágulo. Mas esse processo vital não poderia depender da fabricação de fibrinogênio sob demanda. Por exemplo, se uma pessoa decidisse reparar uma parede quebrada da sua casa, e fazer um tijolo desde o zero ou fabricar seu próprio concreto, demoraria mais tempo do que obter o tijolo pronto para seu uso. O mesmo princípio de construção acelerada ou “pronto para usar” acontece no tamponamento de feridas. Em indivíduos saudáveis, o fibrinogênio circula no sangue em altas concentrações de 2-5g/L (93, 94). O Fibrinogênio é a terceira proteína de maior concentração no sangue, depois das albuminas e globulinas (95, 96). Especificamente, no coagulo, o fibrinogênio ganha mais protagonismo ainda, sendo a proteína com maior concentração, seja sua fita alfa, beta ou gama (7). Então, parece aceitável a apreciação que, o aumento do fibrinogênio e da trombina no leito da ferida, poderia, pelo menos, melhorar a hemostasia. De fato, a aplicação tópica da matriz de fibrina é uma realidade na prática clínica no contexto de selante cirúrgico (97-100).

Fisiologicamente, o tampão de fibrina contém uma pequena fração de fibronectinas (101-103). Para os nossos estudos *in vivo*, nós incrementamos 10 vezes a mais a concentração de fibronectina, comparado com a fibrina, no entanto para o nosso modelo de feridas *in vitro* usamos a razão fisiológica de 10:1 de fibrina: fibronectina. Publicações anteriores que estudaram a aplicação tópica de fibronectinas puras em feridas, mostraram que estas aceleram a cicatrização de feridas diabéticas e não diabéticas em animais (104-108). Essas fibronectinas solúveis agregam-se ao tecido circundante no leito da ferida, mas elas não formam uma matriz 3D *per se*. Um estudo recente mostrou que as fibronectinas podem acelerar o processo de cicatrização em feridas cutâneas, se processada em *nano fibras* (104). No entanto, o processamento de *nano fibras* de fibronectina em grande escala parece ser extremamente desafiador.

O nosso parceiro da Universidade de Nebraska-Estados Unidos, durante o processo para separar as fibras γγF1 e γγ′F1 do plasma humano, identificou que uma porção das γγ′F1 formava um complexo compacto com a FN (38). No plasma humano, o γγ′F1 e o FN estão presente em uma proporção de 1: 1 M (15, 109-111). No presente trabalho, para o estudo *in vivo* nós usamos um complexo de γγ′F1: pFN e uma mistura de γγF1 e pFN de alta pureza para as nossas matrizes, as quais foram confirmadas por meio de SDS-PAGE. Por outro lado, a pureza da pdF1 e pdFN utilizada na matriz *in vitro*, foi confirmada sob pedido nosso pelo Serviços Analíticos da Sigma-Aldrich (Anexo 2).

Aqui nós apresentamos três novas formulações da matriz de fibrina-fibronectina feitas a partir de diferentes proporções entre fibrina e fibronectina (Figura 2). Estas combinações entre fibrina e fibronectina mostraram tanto acelerar o

processo de cicatrização em camundongo quanto simular uma matriz transitória da fase hemostática da ferida na pele humana equivalente 3D.

O complexo de γγ′F1: pFN aqui usado, na presença de trombina e FXIIIa formou uma matriz 3D com *nano aglomerados* de fibronectina nas fibras de fibrina. Nesse sentido, sugerimos que os *nanoclusters* de fibronectina da matriz γγ′F1:FN aqui estudada, podem interagir com as caudas *γ′* que são exclusivamente exibidas pelas fibrinas γγ′F1. Estudos anteriores mostraram que a presença de FN em *nano domínios* promove fortemente a disseminação celular (112). Além disso, *nano padrões* de FN influenciam a proliferação e a disseminação em HUVECs (113).

Para elucidar o efeito das matrizes de fibrina e fibrinogênio na migração, proliferação e resposta imune do processo de cicatrização, confeccionamos e testamos um perfil de genes regulados positivamente durante as fases de cicatrização e comparamos com sequenciamento de RNA de células únicas. Seguindo os principais genes modulados no processo de cicatrização de feridas (19), e usando a técnica de pós-analise de sequenciamento de células únicas da camada epidérmica, identificamos que o gene do Receptor da Proteína C (Procr), que é altamente expresso por queratinócitos no contexto migratório (114), fisiologicamente aumenta a sua expressão na fase de remodelação. Feridas de animais tratados com o Complexo e a Mistura aumentam a expressão de Procr no dia 6 pós-ferimento. Além disso, o grupo tratado com o Complexo mostrou uma expressão do gene Procr aumentada já no dia 2 após o ferimento. A Proteína Transmembrana 2 Rica em Leucina e Fibronectina (Flrt2) modula a adesão célula-célula e a migração celular. De fato, a proteína Flrt2 não está presente na epiderme da pele sem feridas, mas sim no tecido de granulação da pele lesionada (19). Usando a técnica de pós-análise de sequenciamento de células únicas da camada

epidérmica, identificamos que a Flrt2 é altamente expressa 10 dias após o ferimento, na fase de remodelação. Nos animais tratados com o Complexo, a expressão de Flrt2 diminuiu nos dias 6 e 11, sugerindo que a migração celular neste grupo ocorreu nos dias anteriores. Estes dados são consistentes com a observação macroscópica e análise histológica no qual o dia 6 mostrou reepitelização completa no grupo do Complexo. Para apoiar ainda mais esta hipótese de que o Complexo e a Mistura poderiam modular a migração no contexto de feridas, avaliamos a principal integrina que se liga ao fibrinogênio, e que também orienta a migração dos queratinócitos na matriz de fibrina, a integrina alfa 5 (Itga5). A análise de sequenciamento de células únicas mostrou que a Itga5 é altamente expressa no dia 4 após lesão. Uma diminuição significativa da expressão de Itga5 nos dias 6 e 11 foi achada nas feridas de animais tratados com Complexo e Mistura, o que sugere que a migração celular em ambos os grupos ocorreu nos dias anteriores. Se a observação de que o Complexo e a Mistura aceleram o processo de cicatrização, diferenças na resolução inflamatória deveriam ser mostradas também. Nesse sentido, animais tratados com o Complexo e a Mistura diminuíram a expressão de IL-1β e IL-6. Além disso, os animais tratados com Complexo e Mistura diminuíram a expressão de F4 / 80, apoiando que a resolução inflamatória ocorreu nos dias anteriores em comparação com o grupo controle. Seguindo a hipótese de que tanto o Complexo como a Mistura poderiam acelerar o processo de cicatrização, então, diferenças na expressão gênica dos fatores de crescimento poderiam ser achadas. Os animais tratados com o Complexo e a Mistura diminuíram a expressão dos genes TGF-β1, FGF1, SDF1, VEFG-α e IGF1 no dia 11 pós-ferimento, apoiando o conceito de que a proliferação celular ocorreu nos dias anteriores. Ainda mais, o IGF1 mostrou uma diminuição precoce no dia 6, sugerindo o fim da fase proliferativa.

Estudos descritivos sobre a dinâmica das células-tronco e a migração durante a cicatrização de feridas na epiderme da pele de camundongo, demostraram que as células epidérmicas da borda das feridas, em contato direto com a matriz de fibrina, não proliferam, mas migram aceleradamente para o centro da ferida (19, 115). Nesse sentido, sugerimos que queratinócitos ao redor da ferida, em contato com as nossas matrizes de fibrina-fibronectina migraram rapidamente em resposta aos *nano aglomerados* de FN no modelo animal, como também, sugerimos que a presença do FN tenha estimulado a migração dos queratinócitos no modelo de ferida *in vitro*.

Estudos prévios *in vitro,* tem demostrado a capacidade de imitar determinadas características do processo de cicatrização animal. Estes estudos mostraram tentativas de imitar determinadas características do processo de cicatrização animal com importantes limitações, como por exemplo, modelo *in vitro* sem uso de fibroblastos na camada dérmica (67), sem camada epidérmica (68), a imitação de uma primeira fase do processo com o uso de peptídeos sintéticos (69), ou matrizes de colágeno- glicosaminoglicano (70). Embora, em todos estes modelos não houve reprodução da fase hemostática inicial nem uso de fibrinogênio ou fibronectina (63-66).

Nossas perspectivas sobre um possível uso na prática clínica, são que baseados no uso de fibrinogênio gama prima e fibronectina de origem humana, a nossa matriz possa ser transladada a prática clínica mais rápido, e após validada com ensaios clínicos, consiga ser usada tanto para hemostasia quanto para melhorar a cicatrização de feridas. As nossas perspectivas sobre o uso do modelo de feridas em pele humana reconstituída, é que seja um modelo no qual próximos

estudos consigam progressivamente recapitular toda e cada uma das fases do processo de cicatrização da pele humana.

Apesar das doses anestésicas recomendadas serem conhecidas mundialmente, as doses finais injetadas podem ser diferentes das calculadas. As principais causas dos erros na administração de medicamentos em humanos estão relacionadas às falhas no preparo e à falta de padronização na administração destes (116). A segurança do animal experimental também deve garantir o cálculo e administração adequados dos anestésicos. Dessa forma, o aplicativo Labinsane busca garantir a segurança dos camundongos. A plataforma do Instituto de Tecnologia de Massachusetts (MIT) *App Inventor* (appinventor.mit.edu) permite que os pesquisadores criem facilmente aplicativos para telefones inteligentes. Nesse sentido, um estudo prévio validou o uso de um aplicativo móvel para cálculo anestésico inalatório (117). Esperamos que *Labinsane*, um aplicativo móvel baseado na plataforma App inventor do MIT, ajude reduzir significativamente a mortalidade relacionada à anestesia intraperitoneal.

Em 1959 Russell e Burch (118) propuseram que todos os esforços deveriam ser feitos para minimizar o uso e o sofrimento de animais experimentais em pesquisas biológicas e de saúde (3R). Hoje, após 60 anos, ainda estamos lutando para atingir os altos padrões idealizados por eles. As nossas perspectivas sobre o uso do nosso modelo de feridas em pele humana equivalente como o uso de Labinsane para o cálculo individual de anestésico, convergem na possibilidade de ajudar na diminuição do uso de animais experimentais nas pesquisas.

CONCLUSÃO

Concluímos que o 10% de γγ′F1 no plasma separado do total de γγF1, bem como γγ′F1 formam um complexo com pFN. Também confirmamos que o complexo γγ′F1: pFN formou uma estrutura de fibronectina em nano aglomerados na fibrina. Sugerimos que a apresentação em nano escala 3D do FN pode potencializar significativamente a interação célula-matriz e acelerar a formação de tecido de granulação, como potencializar a reepitelização em feridas na pele de camundongos e em modelo de feridas em pele humana equivalente em 3D. A matriz de fibrina-fibronectina, representa uma abordagem eficiente tanto para melhorar a cicatrização de feridas na pele de camundongos quanto como matriz transitória em modelos de pele humana equivalente em 3D.

REFERÊNCIAS

1. Romana-Souza B, Nascimento AP, Monte-Alto-Costa A. Propranolol improves cutaneous wound healing in streptozotocin-induced diabetic rats. European Journal of Pharmacology. 2009;611(1–3):77-84.
2. Li J, Chen J, Kirsner R. Pathophysiology of acute wound healing. Clinics in Dermatology. 2007;25(1):9-18.
3. Singer AJ, Clark RAF. Cutaneous Wound Healing. New England Journal of Medicine. 1999;341(10):738-46.
4. Li Y, Jalili RB, Ghahary A. Accelerating skin wound healing by M-CSF through generating SSEA-1 and -3 stem cells in the injured sites. Scientific Reports. 2016;6:28979.
5. Schilling JA. Wound healing. Surg Clin North Am. 1976;56(4):859-74.
6. Gurtner GC, Werner S, Barrandon Y, Longaker MT. Wound repair and regeneration. Nature. 2008;453(7193):314-21.
7. Stachowicz A, Siudut J, Suski M, Olszanecki R, Korbut R, Undas A, et al. Optimization of quantitative proteomic analysis of clots generated from plasma of patients with venous thromboembolism. Clinical proteomics. 2017;14:38-.
8. Mosesson MW, Siebenlist KR, Meh DA. The structure and biological features of fibrinogen and fibrin. Ann N Y Acad Sci. 2001;936:11-30.
9. Herrick S, Blanc-Brude O, Gray A, Laurent G. Fibrinogen. Int J Biochem Cell Biol. 1999;31(7):741-6.
10. Hoppenbrouwers T, Tuk B, Fijneman EM, de Maat MP, van Neck JW. Fibrin improves skin wound perfusion in a diabetic rat model. Thromb Res. 2017;151:36-40.
11. Szpaderska AM, Egozi EI, Gamelli RL, DiPietro LA. The effect of thrombocytopenia on dermal wound healing. J Invest Dermatol. 2003;120(6):1130-7.
12. Broekman MJ, Handin RI, Cohen P. Distribution of fibrinogen, and platelet factors 4 and XIII in subcellular fractions of human platelets. Br J Haematol. 1975;31(1):51-5.
13. Kaplan DR, Chao FC, Stiles CD, Antoniades HN, Scher CD. Platelet alpha granules contain a growth factor for fibroblasts. Blood. 1979;53(6):1043-52.
14. Bar L, Malka O, Naboichenko E, Nur I. The binding of fibrin sealant to collagen is influenced by the method of purification and the cross-linked fibrinogen-fibronectin (heteronectin) content of the 'fibrinogen' component. Blood Coagul Fibrinolysis. 2005;16(2):111-7.
15. Chung DW, Davie EW. gamma and gamma' chains of human fibrinogen are produced by alternative mRNA processing. Biochemistry. 1984;23(18):4232-6.
16. Corbett SA, Wilson CL, Schwarzbauer JE. Changes in cell spreading and cytoskeletal organization are induced by adhesion to a fibronectin-fibrin matrix. Blood. 1996;88(1):158-66.
17. Kurkinen M, Vaheri A, Roberts PJ, Stenman S. Sequential appearance of fibronectin and collagen in experimental granulation tissue. Lab Invest. 1980;43(1):47-51.
18. Muliaditan T, Caron J, Okesola M, Opzoomer JW, Kosti P, Georgouli M, et al. Macrophages are exploited from an innate wound healing response to facilitate cancer metastasis. Nature Communications. 2018;9(1):2951.

19. Aragona M, Dekoninck S, Rulands S, Lenglez S, Mascré G, Simons BD, et al. Defining stem cell dynamics and migration during wound healing in mouse skin epidermis. Nature Communications. 2017;8:14684.
20. Sinha M, Sen CK, Singh K, Das A, Ghatak S, Rhea B, et al. Direct conversion of injury-site myeloid cells to fibroblast-like cells of granulation tissue. Nature Communications. 2018;9(1):936.
21. Balbino CA, Pereira LM, Curi R. Mecanismos envolvidos na cicatrização: uma revisão. Braz J Pharm Sci. 2005;41(1):27-51.
22. Clark RAF, Lanigan JM, DellaPelle P, Manseau E, Dvorak HF, Colvin RB. Fibronectin and Fibrin Provide a Provisional Matrix for Epidermal Cell Migration During Wound Reepithelialization. Journal of Investigative Dermatology.79(5):264-9.
23. Mosesson MW, Homandberg GA, Amrani DL. Human platelet fibrinogen gamma chain structure. Blood. 1984;63(5):990-5.
24. Mosesson MW. Update on antithrombin I (fibrin). Thromb Haemost. 2007;98(1):105-8.
25. Calcaterra J, Van Cott KE, Butler SP, Gil GC, Germano M, van Veen HA, et al. Recombinant human fibrinogen that produces thick fibrin fibers with increased wound adhesion and clot density. Biomacromolecules. 2013;14(1):169-78.
26. Olsen AL, Sackey BK, Marcinkiewicz C, Boettiger D, Wells RG. Fibronectin Extra Domain-A Promotes Hepatic Stellate Cell Motility but Not Differentiation Into Myofibroblasts. Gastroenterology. 2012;142(4):928-37.e3.
27. Seidl M, Hormann H. Affinity chromatography on immobilized fibrin monomer, IV. Two fibrin-binding peptides of a chymotryptic digest of human plasma fibronectin. Hoppe Seylers Z Physiol Chem. 1983;364(1):83-92.
28. Sekiguchi K, Hakomori S. Domain structure of human plasma fibronectin. Differences and similarities between human and hamster fibronectins. J Biol Chem. 1983;258(6):3967-73.
29. Lauer P, Metzner HJ, Zettlmeissl G, Li M, Smith AG, Lathe R, et al. Targeted inactivation of the mouse locus encoding coagulation factor XIII-A: hemostatic abnormalities in mutant mice and characterization of the coagulation deficit. Thromb Haemost. 2002;88(6):967-74.
30. Grinnell F, Feld MK. Distribution of fibronectin on peripheral blood cells in freshly clotted blood. Thromb Res. 1981;24(5-6):397-404.
31. Grinnell F, Billingham RE, Burgess L. Distribution of fibronectin during wound healing in vivo. J Invest Dermatol. 1981;76(3):181-9.
32. Bata-Csorgo Z, Cooper KD, Ting KM, Voorhees JJ, Hammerberg C. Fibronectin and alpha5 integrin regulate keratinocyte cell cycling. A mechanism for increased fibronectin potentiation of T cell lymphokine-driven keratinocyte hyperproliferation in psoriasis. Journal of Clinical Investigation. 1998;101(7):1509-18.
33. Lemanska-Perek A, Krzyzanowska-Golab D, Pupek M, Klimeczek P, Witkiewicz W, Katnik-Prastowska I. Analysis of Soluble Molecular Fibronectin-Fibrin Complexes and EDA-Fibronectin Concentration in Plasma of Patients with Atherosclerosis. Inflammation. 2016;39(3):1059-68.
34. Geoghegan JA, Monk IR, O'Gara JP, Foster TJ. Subdomains N2N3 of fibronectin binding protein A mediate Staphylococcus aureus biofilm formation and adherence to fibrinogen using distinct mechanisms. J Bacteriol. 2013;195(11):2675-83.
35. Choy HA, Kelley MM, Croda J, Matsunaga J, Babbitt JT, Ko AI, et al. The multifunctional LigB adhesin binds homeostatic proteins with potential roles in

cutaneous infection by pathogenic Leptospira interrogans. PLoS One. 2011;6(2):e16879.
36. Guzman Prieto AM, Urbanus RT, Zhang X, Bierschenk D, Koekman CA, van Luit-Asbroek M, et al. The N-terminal domain of the thermo-regulated surface protein PrpA of Enterococcus faecium binds to fibrinogen, fibronectin and platelets. Sci Rep. 2015;5:18255.
37. Stemberk V, Jones RP, Moroz O, Atkin KE, Edwards AM, Turkenburg JP, et al. Evidence for steric regulation of fibrinogen binding to Staphylococcus aureus fibronectin-binding protein A (FnBPA). J Biol Chem. 2014;289(18):12842-51.
38. Ismail AEA, Fabian FM, Wang O, Lei Y, Carlson MA, Burgess WH, et al. The isolation of a plasma-derived γγ' fibrinogen: Fibronectin mixture that forms a novel polymeric matrix. Process Biochemistry. 2018;75:257-65.
39. James GA, Swogger E, Wolcott R, Pulcini E, Secor P, Sestrich J, et al. Biofilms in chronic wounds. Wound Repair Regen. 16. United States2008. p. 37-44.
40. Labropoulos N, Wang ED, Lanier ST, Khan SU. Factors associated with poor healing and recurrence of venous ulceration. Plast Reconstr Surg. 2012;129(1):179-86.
41. Han Cho N, Whiting D, Guariguata L, Aschner P, Forouhi N, Hambleton I, et al. Atlas de la Diabetes de la Federación Internacional de la Diabetes. Federación Internacional de Diabetes; 2013. Report No.: 2-930229-80-2 Contract No.: 2-930229-80-2.
42. McLennan S, Min D, Yue D. Matrix Metalloproteinases and Their Roles in Poor Wound Healing in Diabetes. Wound Practice & Research: Journal of the Australian Wound Management Association. 2008;16(3):116-21.
43. Azevedo FF. Effect of topical insulin on cutaneous wound healing in diabetic rats. Campinas: Universidade Estadual de Campinas; 2013.
44. Lobmann R, Ambrosch A, Schultz G, Waldmann K, Schiweck S, Lehnert H. Expression of matrix-metalloproteinases and their inhibitors in the wounds of diabetic and non-diabetic patients. Diabetologia. 2002;45(7):1011-6.
45. Wysocki AB, Staiano-Coico L, Grinnell F. Wound fluid from chronic leg ulcers contains elevated levels of metalloproteinases MMP-2 and MMP-9. J Invest Dermatol. 1993;101(1):64-8.
46. Trengove NJ, Stacey MC, MacAuley S, Bennett N, Gibson J, Burslem F, et al. Analysis of the acute and chronic wound environments: the role of proteases and their inhibitors. Wound Repair Regen. 1999;7(6):442-52.
47. Yager DR, Zhang LY, Liang HX, Diegelmann RF, Cohen IK. Wound fluids from human pressure ulcers contain elevated matrix metalloproteinase levels and activity compared to surgical wound fluids. J Invest Dermatol. 1996;107(5):743-8.
48. Wysocki AB, Grinnell F. Fibronectin profiles in normal and chronic wound fluid. Lab Invest. 1990;63(6):825-31.
49. Grinnell F, Ho CH, Wysocki A. Degradation of fibronectin and vitronectin in chronic wound fluid: analysis by cell blotting, immunoblotting, and cell adhesion assays. J Invest Dermatol. 1992;98(4):410-6.
50. Grinnell F, Zhu M. Identification of neutrophil elastase as the proteinase in burn wound fluid responsible for degradation of fibronectin. J Invest Dermatol. 1994;103(2):155-61.
51. Cheung EY, Weijers EM, Tuk B, Scheffer R, Leebeek FW, van Neck JW, et al. Specific effects of fibrinogen and the γA and γ'-chain fibrinogen variants on angiogenesis and wound healing. Tissue Eng Part A. 2015;21(1-2):106-14.

52. Lima MH, Caricilli AM, de Abreu LL, Araujo EP, Pelegrinelli FF, Thirone AC, et al. Topical insulin accelerates wound healing in diabetes by enhancing the AKT and ERK pathways: a double-blind placebo-controlled clinical trial. PLoS One. 2012;7(5):e36974.
53. Mercurius KO, Morla AO. Cell adhesion and signaling on the fibronectin 1(st) type III repeat; requisite roles for cell surface proteoglycans and integrins. BMC Cell Biology. 2001;2:18-.
54. Xin X, Chen S, Khan ZA, Chakrabarti S. Akt activation and augmented fibronectin production in hyperhexosemia. Am J Physiol Endocrinol Metab. 2007;293(4):E1036-44.
55. Somanath PR, Kandel ES, Hay N, Byzova TV. Akt1 Signaling Regulates Integrin Activation, Matrix Recognition, and Fibronectin Assembly. The Journal of biological chemistry. 2007;282(31):22964-76.
56. Weil CS, Scala RA. Study of intra- and interlaboratory variability in the results of rabbit eye and skin irritation tests. Toxicol Appl Pharmacol. 1971;19(2):276-360.
57. De Jong WH, Hoffmann S, Lee M, Kandárová H, Pellevoisin C, Haishima Y, et al. Round robin study to evaluate the reconstructed human epidermis (RhE) model as an in vitro skin irritation test for detection of irritant activity in medical device extracts. Toxicol In Vitro. 2018;50:439-49.
58. do Nascimento Pedrosa T, Catarino CM, Pennacchi PC, de Moraes Barros SB, Maria-Engler SS. Skin Equivalent Models: Protocols for In Vitro Reconstruction for Dermal Toxicity Evaluation. Methods Mol Biol. 2021;2240:31-41.
59. Camarena DEM, Matsuyama L, Maria-Engler SS, Catalani LH. Development of Epidermal Equivalent from Electrospun Synthetic Polymers for In Vitro Irritation/Corrosion Testing. Nanomaterials (Basel). 2020;10(12).
60. Catarino CM, do Nascimento Pedrosa T, Pennacchi PC, de Assis SR, Gimenes F, Consolaro MEL, et al. Skin corrosion test: a comparison between reconstructed human epidermis and full thickness skin models. Eur J Pharm Biopharm. 2018;125:51-7.
61. Main KA, Mikelis CM, Doçi CL. In Vitro Wound Healing Assays to Investigate Epidermal Migration. Methods Mol Biol. 2020;2109:147-54.
62. Liang CC, Park AY, Guan JL. In vitro scratch assay: a convenient and inexpensive method for analysis of cell migration in vitro. Nat Protoc. 2007;2(2):329-33.
63. Breetveld M, Richters CD, Rustemeyer T, Scheper RJ, Gibbs S. Comparison of wound closure after burn and cold injury in human skin equivalents. J Invest Dermatol. 126. United States2006. p. 1918-21.
64. Marquardt Y, Amann PM, Heise R, Czaja K, Steiner T, Merk HF, et al. Characterization of a novel standardized human three-dimensional skin wound healing model using non-sequential fractional ultrapulsed CO2 laser treatments. Lasers Surg Med. 2015;47(3):257-65.
65. Rossi A, Appelt-Menzel A, Kurdyn S, Walles H, Groeber F. Generation of a three-dimensional full thickness skin equivalent and automated wounding. J Vis Exp. 2015(96).
66. Safferling K, Sütterlin T, Westphal K, Ernst C, Breuhahn K, James M, et al. Wound healing revised: A novel reepithelialization mechanism revealed by in vitro and in silico models. The Journal of Cell Biology. 2013;203(4):691.
67. Herman IM, Leung A. Creation of human skin equivalents for the in vitro study of angiogenesis in wound healing. Methods Mol Biol. 2009;467:241-8.

68. Lombardi B, Casale C, Imparato G, Urciuolo F, Netti PA. Spatiotemporal Evolution of the Wound Repairing Process in a 3D Human Dermis Equivalent. Adv Healthc Mater. 2017;6(13).
69. Schneider A, Garlick JA, Egles C. Self-assembling peptide nanofiber scaffolds accelerate wound healing. PLoS One. 2008;3(1):e1410.
70. van Kilsdonk JW, van den Bogaard EH, Jansen PA, Bos C, Bergers M, Schalkwijk J. An in vitro wound healing model for evaluation of dermal substitutes. Wound Repair Regen. 2013;21(6):890-6.
71. Wasiak J, Cleland H, Campbell F. Dressings for superficial and partial thickness burns. Cochrane Database Syst Rev. 2008(4):Cd002106.
72. Venzin CM JV, Berdichevsky A, Karol AA, Seliktar D, von Rechenberg B, Nuss KMR. Biocompatibility of Pegylated Fibrinogen and Its Effect on Healing of Full-Thickness Skin Defects: A Preliminary Study in Rats. In: Department of Small Animal Surgery VF, University of Zurich, Switzerland, editor. Journal of Biotechnology & Biomaterials2016.
73. Skovsø S. Modeling type 2 diabetes in rats using high fat diet and streptozotocin. Journal of Diabetes Investigation. 2014;5(4):349-58.
74. Dunn L, Prosser HCG, Tan JTM, Vanags LZ, Ng MKC, Bursill CA. Murine Model of Wound Healing. 2013(75):e50265.
75. Wang X, Ge J, Tredget EE, Wu Y. The mouse excisional wound splinting model, including applications for stem cell transplantation. Nat Protoc. 2013;8(2):302-9.
76. Jara CP, Carraro RS, Zanesco A, Andrade B, Moreira K, Nogueira G, et al. A smartphone app for individual anesthetic calculation decreased anesthesia-related mortality in mice. bioRxiv. 2020:2020.09.09.289728.
77. Hish GA, Jr., Diaz JA, Hawley AE, Myers DD, Jr., Lester PA. Effects of analgesic use on inflammation and hematology in a murine model of venous thrombosis. J Am Assoc Lab Anim Sci. 2014;53(5):485-93.
78. Spotnitz WD. Fibrin Sealant: The Only Approved Hemostat, Sealant, and Adhesive-a Laboratory and Clinical Perspective. ISRN surgery. 2014;2014:203943.
79. Carlson MA, Smith LM, Cordes CM, Chao J, Eudy JD. Attachment-regulated signaling networks in the fibroblast-populated 3D collagen matrix. Scientific reports. 2013;3:1880.
80. Park D-S, Kim J-H, Lee SW, Jeong J-M. Secretory expression of the α-subunit of human coagulation factor XIII in the yeast Pichia pastoris. Biotechnology Letters. 2002;24(2):97-101.
81. Yakovlev S, Medved L. Interaction of Fibrin(ogen) with the Endothelial Cell Receptor VE-Cadherin: Localization of the Fibrin-Binding Site within the Third Extracellular VE-Cadherin Domain(). Biochemistry. 2009;48(23):5171-9.
82. Joost S, Jacob T, Sun X, Annusver K, La Manno G, Sur I, et al. Single-Cell Transcriptomics of Traced Epidermal and Hair Follicle Stem Cells Reveals Rapid Adaptations during Wound Healing. Cell Rep. 2018;25(3):585-97.e7.
83. Guerrero-Juarez CF, Dedhia PH, Jin S, Ruiz-Vega R, Ma D, Liu Y, et al. Single-cell analysis reveals fibroblast heterogeneity and myeloid-derived adipocyte progenitors in murine skin wounds. Nat Commun. 2019;10(1):650.
84. Wang Y, Wang R, Zhang S, Song S, Jiang C, Han G, et al. iTALK: an R Package to Characterize and Illustrate Intercellular Communication. bioRxiv. 2019:507871.

85. Park HJ, Park JE, Lee H, Kim SJ, Yun JI, Kim M, et al. Integrins functioning in uterine endometrial stromal and epithelial cells in estrus. Reproduction. 2017;153(3):351-60.
86. Yang C, Wang C, Zhou J, Liang Q, He F, Li F, et al. Fibronectin 1 activates WNT/β-catenin signaling to induce osteogenic differentiation via integrin β1 interaction. Lab Invest. 2020;100(12):1494-502.
87. Schnittert J, Bansal R, Storm G, Prakash J. Integrins in wound healing, fibrosis and tumor stroma: High potential targets for therapeutics and drug delivery. Adv Drug Deliv Rev. 2018;129:37-53.
88. Ruf W, Ruggeri ZM. Neutrophils release brakes of coagulation. Nature Medicine. 2010;16(8):851-2.
89. Loof TG, Schmidt O, Herwald H, Theopold U. Coagulation systems of invertebrates and vertebrates and their roles in innate immunity: the same side of two coins? J Innate Immun. 2011;3(1):34-40.
90. Uitte de Willige S, Standeven KF, Philippou H, Ariëns RA. The pleiotropic role of the fibrinogen gamma' chain in hemostasis. Blood. 2009;114(19):3994-4001.
91. Corbett SA, Lee L, Wilson CL, Schwarzbauer JE. Covalent Cross-linking of Fibronectin to Fibrin Is Required for Maximal Cell Adhesion to a Fibronectin-Fibrin Matrix *. Journal of Biological Chemistry. 1997;272(40):24999-5005.
92. Fortenberry YM, Hlavacek AC, Church FC. Protein C inhibitor inhibits factor VIIa when bound to tissue factor. J Thromb Haemost. 2011;9(4):861-3.
93. Plasma fibrinogen. Annals of Clinical Biochemistry. 2004;41(6):430-40.
94. Kattula S, Byrnes JR, Wolberg AS. Fibrinogen and Fibrin in Hemostasis and Thrombosis. Arteriosclerosis, thrombosis, and vascular biology. 2017;37(3):e13-e21.
95. Kramer G, Woolerton Y, van Straalen JP, Vissers JPC, Dekker N, Langridge JI, et al. Accuracy and Reproducibility in Quantification of Plasma Protein Concentrations by Mass Spectrometry without the Use of Isotopic Standards. PloS one. 2015;10(10):e0140097-e.
96. Anderson NL, Anderson NG. The Human Plasma Proteome: History, Character, and Diagnostic Prospects*. Molecular & Cellular Proteomics. 2002;1(11):845-67.
97. Danker Iii W, DeAnglis A, Ferko N, Garcia D, Hogan A. Comparison of fibrin sealants in peripheral vascular surgery: A systematic review and network meta-analysis. Ann Med Surg (Lond). 2021;61:161-8.
98. Allotey JK, King AH, Kumins NH, Wong VL, Harth KC, Cho JS, et al. Systematic review of hemostatic agents used in vascular surgery. J Vasc Surg. 2020.
99. Chen YS, Loh EW, Shen SC, Su YH, Tam KW. Efficacy of Fibrin Sealant in Reducing Complication Risk After Bariatric Surgery: a Systematic Review and Meta-analysis. Obes Surg. 2021;31(3):1158-67.
100. Rechtin M, Broccoli N, Krishnan DG, Phero JA. Review Use of Tisseel, a Fibrin Sealant, for Particulate Graft Stabilization. J Oral Maxillofac Surg. 2020;78(10):e2-e5.
101. Clark RAF. Fibrin and Wound Healing. Annals of the New York Academy of Sciences. 2001;936(1):355-67.
102. Okada M, Blombäck B, Chang MD, Horowitz B. Fibronectin and fibrin gel structure. Journal of Biological Chemistry. 1985;260(3):1811-20.
103. Corbett SA, Lee L, Wilson CL, Schwarzbauer JE. Covalent cross-linking of fibronectin to fibrin is required for maximal cell adhesion to a fibronectin-fibrin matrix. J Biol Chem. 1997;272(40):24999-5005.

104. Chantre CO, Campbell PH, Golecki HM, Buganza AT, Capulli AK, Deravi LF, et al. Production-scale fibronectin nanofibers promote wound closure and tissue repair in a dermal mouse model. Biomaterials. 2018;166:96-108.
105. Qiu Z, Kwon AH, Kamiyama Y. Effects of plasma fibronectin on the healing of full-thickness skin wounds in streptozotocin-induced diabetic rats. J Surg Res. 2007;138(1):64-70.
106. Hamed S, Ullmann Y, Egozi D, Daod E, Hellou E, Ashkar M, et al. Fibronectin potentiates topical erythropoietin-induced wound repair in diabetic mice. J Invest Dermatol. 2011;131(6):1365-74.
107. Kwon AH, Qiu Z, Hirao Y. Topical Application of Plasma Fibronectin in Full-Thickness Skin Wound Healing in Rats. Experimental Biology and Medicine. 2007;232(7):935-41.
108. Johnson MB, Pang B, Gardner DJ, Niknam-Benia S, Soundarajan V, Bramos A, et al. Topical Fibronectin Improves Wound Healing of Irradiated Skin. Scientific Reports. 2017;7(1):3876.
109. Mosher DF. Physiology of fibronectin. Annu Rev Med. 1984;35:561-75.
110. Hynes RO, Yamada KM. Fibronectins: multifunctional modular glycoproteins. Journal of Cell Biology. 1982;95(2):369-77.
111. Ariëns RA, Lai TS, Weisel JW, Greenberg CS, Grant PJ. Role of factor XIII in fibrin clot formation and effects of genetic polymorphisms. Blood. 2002;100(3):743-54.
112. Kalappurakkal JM, Anilkumar AA, Patra C, van Zanten TS, Sheetz MP, Mayor S. Integrin Mechano-chemical Signaling Generates Plasma Membrane Nanodomains that Promote Cell Spreading. Cell. 2019;177(7):1738-56.e23.
113. Slater JH, Frey W. Nanopatterning of fibronectin and the influence of integrin clustering on endothelial cell spreading and proliferation. J Biomed Mater Res A. 2008;87(1):176-95.
114. McKelvey K, Jackson CJ, Xue M. Activated protein C: A regulator of human skin epidermal keratinocyte function. World Journal of Biological Chemistry. 2014;5(2):169-79.
115. Park S, Gonzalez DG, Guirao B, Boucher JD, Cockburn K, Marsh ED, et al. Tissue-scale coordination of cellular behaviour promotes epidermal wound repair in live mice. Nat Cell Biol. 2017;19(2):155-63.
116. Edwards S, Axe S. The 10 ‘R's of safe multidisciplinary drug administration. Nurse Prescribing. 2015;13(8):398-406.
117. Pierce JMT, Taylor R. Validation of the mathematics in the anaesthetic impact calculator, a smartphone app for the calculation the CO2e of inhalational anaesthesia. Anaesthesia. 2020;75(1):136-8.
118. Russell WMS. The principles of humane experimental technique [by] W.M.S. Russell and R.L. Burch. Burch RL, editor. London: Methuen; 1959.

ANEXOS

Anexo 1

UNICAMP

CEUA/UNICAMP

CERTIFICADO

Certificamos que a proposta intitulada **Avaliação do efeito do complexo fibrinogênio/fibronectina sobre a cicatrização de feridas em animais diabéticos**, registrada com o nº **4467-1/2017**, sob a responsabilidade de **Profa. Dra. Eliana Pereira de Araujo e Carlos Poblete Jara**, que envolve a produção, manutenção ou utilização de animais pertencentes ao filo *Chordata*, subfilo *Vertebrata* (exceto o homem) para fins de pesquisa científica (ou ensino), encontra-se de acordo com os preceitos da **LEI Nº 11.794, DE 8 DE OUTUBRO DE 2008**, que estabelece procedimentos para o uso científico de animais, do **DECRETO Nº 6.899, DE 15 DE JULHO DE 2009**, e com as normas editadas pelo **Conselho Nacional de Controle da Experimentação Animal (CONCEA), tendo sido** aprovada pela **Comissão de Ética no Uso de Animais** da **Universidade Estadual de Campinas - CEUA/UNICAMP,** em **29 de março de 2017**.

Finalidade:	**( ) Ensino (X) Pesquisa Científica**
Vigência do projeto:	**01/02/2017-01/02/2021**
Vigência da autorização para manipulação animal:	**29/03/2017-01/02/2021**
Espécie / linhagem/ raça:	**Camundongo isogênico / C57BL/6J**
No. de animais:	**192**
Peso / Idade:	**09 semanas / 21g**
Sexo:	**machos**
Origem:	**CEMIB/UNICAMP**

A aprovação pela CEUA/UNICAMP não dispensa autorização prévia junto ao **IBAMA**, **SISBIO** ou **CIBio** e é **restrita** a protocolos desenvolvidos em biotérios e laboratórios da Universidade Estadual de Campinas.

Campinas, 29 de março de 2017.

Profa. Dra. Liana Maria Cardoso Verinaud
Presidente

Fátima Alonso
Secretária Executiva

IMPORTANTE: Pedimos atenção ao prazo para envio do relatório final de atividades referente a este protocolo: até 30 dias após o encerramento de sua vigência. O formulário encontra-se disponível na página da CEUA/UNICAMP, área do pesquisador responsável. A não apresentação de relatório no prazo estabelecido impedirá que novos protocolos sejam submetidos.

Anexo 2

SIGMA-ALDRICH®

sigma-aldrich.com

3050 Spruce Street, Saint Louis, MO 63103, USA
Website: www.sigmaaldrich.com
Email USA: techserv@sial.com
Outside USA: eurtechserv@sial.com

Certificate of Analysis

Product Name:
Fibrinogen from human plasma - 50-70% protein (≥80% of protein is clottable)

Product Number:	**F3879**
Batch Number:	**SLBZ2294**
Brand:	SIGMA
CAS Number:	9001-32-5
MDL Number:	MFCD00131060
Storage Temperature:	Store at -20 °C
Quality Release Date:	06 NOV 2018
Recommended Retest Date:	NOV 2023

Test	Specification	Result
Appearance (Color)	White to Off White	White
Appearance (Form)	Powder	Powder
Solubility (Color)	Colorless to Light Yellow	Almost Colorless
Solubility (Turbidity) 10 mg/mL, 0.9% NaCl	Clear to Hazy	Slightly Hazy
Water (by Karl Fischer)	≤ 10 %	7 %
% Protein (Biuret)	50 - 70	60
% Clottable protein	≥ 80	93
Tested For Infectious Agents	Tested	Tested
Human Source Testing (Source)	Tested	Tested
HBSAG	Negative	Negative
HCV	Negative	Negative
HIV-1/HIV-2	Negative	Negative

Rodney Burbach, Manager
Analytical Services
St. Louis, Missouri US